INVESTIGATION OF THE WAVY CHANNEL COLD PLATE THERMAL PERFORMANCE

CHIN YU HONG

A project report submitted in partial fulfilment of the requirements for the award of Bachelor of Engineering (Honours) Mechanical Engineering

Lee Kong Chian Faculty of Engineering and Science
Universiti Tunku Abdul Rahman

JAN 2019

DECLARATION

I hereby declare that this project report is based on my original work except for citations and quotations which have been duly acknowledged. I also declare that it has not been previously and concurrently submitted for any other degree or award at UTAR or other institutions.

Signature : _____

Name : CHIN YU HONG

ID No. : 14UEB03749

Date : _____

APPROVAL FOR SUBMISSION

I certify that this project report entitled **"INVESTIGATION OF THE WAVY CHANNEL COLD PLATE THERMAL PERFORMANCE"** was prepared by **CHIN YU HONG** has met the required standard for submission in partial fulfilment of the requirements for the award of Bachelor of Bachelor of Engineering (Honours) Mechanical Engineering at Universiti Tunku Abdul Rahman.

Approved by,

Signature : _____

Supervisor : DR. BERNARD SAW LIP HUAT

Date : _____

ACKNOWLEDGEMENTS

I would like to express my special gratitude of thanks to the University for providing the platform and facilities required to carry out this Final Year Project. I would also like to appreciate the constructive guidance, advices, insight and expertise provided by my supervisor, Dr. Bernard Saw Lip Huat, the lab officers, workshop officers as well as my academic seniors which have assisted the effort in conducting this Project. Lastly, I thank my parents for their understanding and support throughout the completion of this Project.

ABSTRACT

Liquid cold plate helps dissipate excess heat from electronic devices during operation, thus prevents overheating of the devices. This project was conducted by first carrying out literature reviews on the relevant topic. Based on the reviews, it was found that the larger the contact area between the coolant and the heat source, the more heat will be removed. Also, recirculation flow of coolant will improve the heat removal performance as well. Thus, from the Part 1 of the project, the design concept of wavy channels cold plate with secondary branches have been selected. The contours were attached from A-1 to A-4. In the Part 2 of the project, Computer-Aided Design modelling (SOLIDWORKS) and fluid flow simulation (ANSYS CFX) were then being carried out back and forth to obtain the cold plate design with the optimised thermal performance. In order to have a more structured modelling and simulation process, the Taguchi Method was applied to narrow down the number of possible designs. The spreadsheet created for the Method was attached in the Appendices section from A-5 to A-8. As for this project, the desired temperature difference of heat source across the cold plate design was set to be close to 5 ℃ under a fluid mass flow rate of 50 g/s. If the desired temperature difference value was met, that particular cold plate design would be chosen to undergo further flow simulations to determine the thermal performance of that design under different fluid mass flow rates of up to 100 g/s. Besides temperature difference, the pressure variation of fluid across the cold plate were studied to ensure that the drops would not damage the structure of the cold plate made of 6061 aluminium alloy. In fact, the pressure drops should be lower than the tensile yield strength of 276 MPa and Ultimate Yield Strength of 310 MPa for a 6061 Aluminium plate (ASM Aerospace Specification Metals Inc., 2018). In this project, an aluminium wavy channel cold plate (200 mm × 130 mm × 17 mm), with channels depth of 14 mm, added with 74 secondary channels, was designed to enhance the occurrence of flow recirculation and heat dissipation. The equal width of the wavy channels and the design of the inlet as well as outlet dividers help stabilise the drops in fluid pressure across the cold plate. Lastly, milling toolpaths of the finalised design was generated through MasterCAM before being transmitted to CNC milling machine for fabrication. After 31 days of machining, using 1.5 mm, 2 mm and 4 mm end mills, the prototype was produced and ready to be sent for documentation.

TABLE OF CONTENTS

LIST OF TABLES

LIST OF FIGURES

LIST OF SYMBOLS / ABBREVIATIONS

M	fluid mass flow rate, g/s
T	heat source-cold plate interface temperature, ℃
ΔT	variation of interface temperature, °C
T_{max}	maximum heat source-cold plate interface temperature, °C
T_{min}	minimum heat source-cold plate interface temperature, °C
P	average fluid pressure, Pa
ΔP	average fluid pressure drop, Pa
P_{in}	average fluid inlet pressure, Pa
P_{out}	average fluid outlet pressure, Pa

LIST OF APPENDICES

CHAPTER 1

INTRODUCTION

1.1 General Introduction

Thermal management involves the monitoring and controlling temperature of a system to provide it an ideal operating temperature. Thermal management process can be carried out by applying the knowledge from heat transfer such as conduction and convection, as well as the concept of thermodynamics. The performance of a complete thermal management process can be justified through its ability to bring the system temperature towards the set-point or any ideal operating temperature. There are a wide range of systems which involve thermal management process, including the air-conditioning system in a building, housing appliances that generate heat, vehicle engines, machineries, and electronic devices.

As a matter of fact, electronic devices have become the daily essential to every consumer in this modernised society. Hence, the heat dissipation of these devices should be taken care of so as to provide an acceptable level of user satisfaction. In order to provide an efficient removal of waste heat from the electronic devices, several cooling methods have been proposed and some of them are currently being adopted in the industry. These cooling methods function mainly based on conduction and convection, while applying different techniques or structures to complete the thermal management cycle. There are two ways to classify different methods of cooling, namely the modes of cooling and the types of heat transfer medium used. The modes of cooling are active cooling and passive cooling, while the heat transfer mediums can be either air or liquid, or both. Active cooling is carried out by creating fluid motion for heat transfer medium by external electrical or mechanical means, such as a fan and pump. Meanwhile, passive cooling occurs by natural means of conduction and convection of the fluid motion. Examples of cooling methods are thermoelectric cooling, forced air cooling, spray cooling, heat pipes, liquid cooling, and thermoacoustic cooling.

As mentioned above, thermal cooling methods can be classified through the medium of heat transfer used. When air cooling is applied, the heated air will rise and transfer to the colder side (ambient environment), thus reducing the temperature at the heat source (electronic device). In order to improve the rate of heat dissipation, forced

air cooling can be applied in which a fan or air pump is adopted to create a turbulent flow of the air. This will in turn increase the rate of heat transfer from the electronic device to the ambient environment.

On the other hand, liquid cooling technique can be applied to dissipate heat from the heat source. Principally, the liquid, acting as a coolant, will absorb heat from the electronic device and flow to a remote heat exchanger in which heat removal process takes place. The cold liquid will then return to the heat source and the heat dissipation cycle is repeated again. When a liquid cold plate is used, the cold liquid (water) would flow inside the cold plate through mini-channels, beneath the electronic device, and dissipate heat from the heat source. The coolant will then transfer the heat to a secondary heat exchanger and release it to the ambient environment. After the heat removal action, the lower temperature water would return to the cold plate, thus completing one heat dissipation cycle. As compared to air cooling, liquid cooling provides higher efficiency in transferring heat due to its naturally higher specific heat capacity, thermal conductivity and density than air. These properties of water allow liquid cooling to have a higher heat removal rate than air cooling.

Furthermore, an ideal selection of heat transfer medium should be matched with optimised geometries of the cold plate in order to enhance the thermal management performance of the system. The geometries that should be taken into account include the size and shape of the plate as well as the special features associated in the plate. In fact, size and shape of the cold plate should be able to cover the base area of the target electronic module. This is to maximise the area for heat dissipation process to take place between the heat source and coolant. Also, special features could be introduced to the interior of the cold plate to optimise the heat transfer process. These features include creating pin fins of different shapes which extrude from the base of the plate or by forming channels for the coolant to flow through in a certain parallel direction. These fins and channels help increase the effective surface area for heat absorption from the electronic device to the liquid coolant, thus improving the thermal management efficiency. Besides increasing the effective surface area for heat transfer, further improvements can still be done on the features mentioned by considering the flow condition of liquid coolant in these channels. Turbulence, for instance, can be induced to the liquid flow in the cold plate. This can be done by introducing numerous wavy channels for the liquid to flow through. As the water flow

along the troughs and crests, liquid flow is distorted in which turbulent flow occurs, flow velocity increases, and the rate of heat transfer is further enhanced.

As for this project, electronic devices or modules like the Insulated-gate Bipolar Transistors (IGBTs) and Metal Oxide Semiconductor Field-Effect Transistors (MOSFETs) were the main heat sources in which the study was to be based on. The study of the thermal management of the electronic devices mentioned was vital to prevent the devices from overheating while enabling them to operate under an optimal condition. Also, an advantageous thermal management system would help prevent over-consumption of electrical power, thus saving energy. Hence, the investigation of the thermal performance of a liquid cold plate with wavy channels was carried out in this project.

1.2 Importance of Study

It is known that a high operating temperature of electronic device will affect its performance. If this condition persist, overheating might happen and the lifespan of that specific device will eventually be shortened. Therefore, a thorough study on the thermal management of electronic devices like the Insulated-gate Bipolar Transistors (IGBTs) and Metal Oxide Semiconductor Field-Effect Transistors (MOSFETs) is important.

Hence, the result of this study in wavy channel liquid cold plate may shed light on an enhanced thermal management system for the electronic devices. Also, this study may provide a better understanding on the feasibility and sustainability of the heat dissipation technique using liquid cold plate.

1.3 Problem Statement

As predicted by Moore’s Law, the size of transistors and other electronic components will shrink every year with an increase in processing speed and power. This phenomenon has seen a significant reduction in size of electronic devices in the past, say, 20 years. Although it is welcomed in the market for a smaller size device due to its ease of handling, the resulted high operating temperature has also drawn attention from the manufacturers and users. If there is inadequate cooling of the electronic devices when they are running, overheating might happen, thus shortening the lifespan of the devices. As a result, high maintenance cost or replacement cost will need to be incurred for the devices.

Next, cooling methods can be classified through the medium of heat transfer used. The medium used can either be air or liquid. In fact, air cooling thermal management system has received much preference due to its ease in assembly and installation, as well as a light weight structure required. However, the limitations associated with air cooling were often overlooked by the industries and consumers. Firstly, the heat transfer rate of convective air cooling method is lower than that of liquid cooling. This is because the specific heat capacity of air at a certain temperature is typically lower than that of liquid (water). Also, the thermal conductivity of air is lower than that of water. These in turn result in a lower thermal management efficiency of air cooling as compared to liquid cooling. Furthermore, forced air cooling must operate with a fan or pump to accelerate the flow motion and set the flow direction of air when transferring heat. These additions will be equally disadvantageous in terms of cost and installation process. Besides that, heat transfer through convective air cooling might not be as uniform as that of liquid cooling. This is due to the fact that air particles can move more randomly in all directions as compared to water particles. This unsteady flow can affect the efficiency in heat transfer and create undesired aerodynamic noise.

Therefore, by identifying the two problems mentioned above, it is of interest to explore more aspects on the wavy channels liquid cooling system to justify its potential in thermal managing electronic devices.

1.4 Aims and Objectives

The main purpose for this project was to optimise the thermal performance of wavy channel cold plate through simulation. The specific objectives for this study were:

1. To investigate the thermal management performance of wavy channel cold plate under different liquid mass flow rate.
2. To develop the wavy channel cold plate prototype.

1.5 Scope and Limitation of the Study

Different cooling methods have been investigated in the industry to provide an optimised transferring of waste heat from the electronic devices to the ambient. As for this project, the subject of study was wavy channel liquid cold plate. Meanwhile, the scope of the study would be focused on optimising, modifying and fabricating the wavy channel cold plate prototype. The feasibility and sustainability of these

modifications could be justified through simulations under specific conditions. The medium of heat transfer used, for instance, was water. Also, the range of interest for the rate of water flow was set from 50 g/s to 100 g/s. At the same time, the maximum heat flux transferred from the electronic device was set at 1000 W. This heat flux value was set by considering the maximum heat that was able to be generated by the heater in the laboratory.

As for the cold plate itself, the material of choice was aluminium due to its capability in transferring heat and a lightweight physical property. The cold plate dimension of $length \times width \times height$ was set at $200\ \text{mm} \times 130\ \text{mm} \times 17\ \text{mm}$, with channels depth of 14 mm. If a 3 mm cover was to be included, the total height of the of the model would be 20 mm.

1.6 Contribution of the Study

Upon the completion of this project, a better understanding on the effect of different parameters and features of wavy channels cold plate on its thermal management performance would be achieved. Also, the significance of fluid mass flow rate and secondary flow or Dean vortices on the heat removal rate as well as fluid pressure drop would also be justified through the thorough simulation studies. Furthermore, this project helped discover the possibility, feasibility and machining workability of using a wavy channels cold plate as a heat removal equipment for electronic devices.

1.7 Outline of the Report

This report consists of a total of five chapters. In Chapter 1, a general introduction is given to describe the importance of heat dissipation for electronic devices and the techniques used. Also, the introduction section briefs about the usage of liquid cold plate in the heat removal process. The same Chapter also includes the importance of the study, problem statement, besides listing out aim and objectives, as well as the scope and limitations of this project. Furthermore, literature review on the relevant topics is carried out in Chapter 2. The topics covered include related researches on cold plates and channels cooling, as well as different cooling methods and mediums. In an addition, the effect of different geometries of a cold plate and wavy channels on heat removal performance is also reviewed in Chapter 2. The Chapter ends with reviews on researches related to fluidic diodes and a summary of the chapter. After literature review, Chapter 3 focuses mainly on the methodology of carrying out the

whole project. In fact, the methodology is illustrated in the form of flowchart for easier understanding. This Chapter will also describe the modelling and simulation processes, including the software used. Besides that, Chapter 3 demonstrates the correct procedures in prototype fabrication, including stock material selection, milling tools selection and cutting toolpaths generation, before ending with a brief summary. In the next chapter, the simulated results under different fluid mass flow rate will be tabulated and graphs will be plotted before carrying out in-detailed results analysis. Also, the parameters and features of the optimised wavy channels cold plate design will be tabulated in Chapter 4. After making sure the simulation results are all in place, results analysis is carried out before putting them into words in the Discussion section. This report ends with Chapter 5 in which a conclusion on the project is drawn. At the same instance, recommendations and possible improvements are included in Chapter 5 and it can be referred if similar project is to be carried out in the future.

CHAPTER 2

LITERATURE REVIEW

2.1 Introduction

This section serves as a compilation and an in-detailed review of the previous researches done by different authors of respective institute or organisation. The studies carried out include the characteristics of different cooling methods and cooling mediums available. Also, the investigations on different geometries of channels used for thermal cold plate and their effects on thermal management performance are highlighted in this chapter. In addition, specific sub-sections will be dedicated to the researches done on different aspects of wavy channels heat sinks and fluidic diodes. Furthermore, the importance, inadequacies and approaches applied in the previous studies will be reviewed.

2.2 Related Researches on Cold Plates and Channels Cooling

With regards to the global realisation of the importance of an efficient thermal management process, there have been an increasing number of researches being carried out to explore on the potential of applying thermal cold plates and channels cooling for the electronic or electrical systems. From these studies, different factors affecting the performance of the cold plates and channels have been discovered, and the optimum geometry as well as fluid flow conditions were determined.

Although the cold plate structures might look different from one system to the other, the concepts and working principles remain intact. In year 2011, Jarret and Kim I. Y. (2011) proposed to utilise cold plates for heat dissipation from the battery cells stack of an electric vehicle. The schematic illustration of the cold plate can be observed from Fig. 2.1 (Jarrett and Kim, 2011). In this study, the basic geometries of the cold plates were varied to determine their effects on heat transfer. Based on the analysis data, channel with the largest width would promote the best thermal management performance with the lowest average temperature and pressure drop across the plate. Other than the width of the channel, it was learnt from this research that the route, length and shape of the channel would also play a part in heat transfer. In addition, this research has also paved way for future studies on the relevant topic under a more complex operating condition.

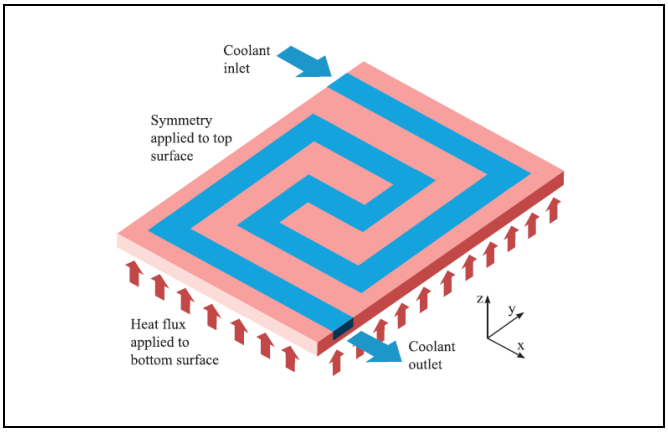

Figure 2.1: Schematic Illustration of Thermal Cold Plate (Jarrett and Kim, 2011).

About 5 years later, there was a different approach to cool the lithium-ion battery of an electric vehicle. In this research, strips (in blue) consisting of aluminium mini-channels were wrapped around three surfaces of the battery, as shown in Fig. 2.2 and Fig. 2.3 (Lan et al., 2016). The effects of channel configurations and coolant flow directions were investigated in detailed. Based on the validated results, it was found that the higher the number of channels per strip, the larger the surface area available for heat transfer. This in turn increased the rate of heat removal from the battery. Also, it was learnt that a unidirectional coolant flow in channels would promote better cooling performance than that of an alternating coolant flow direction.

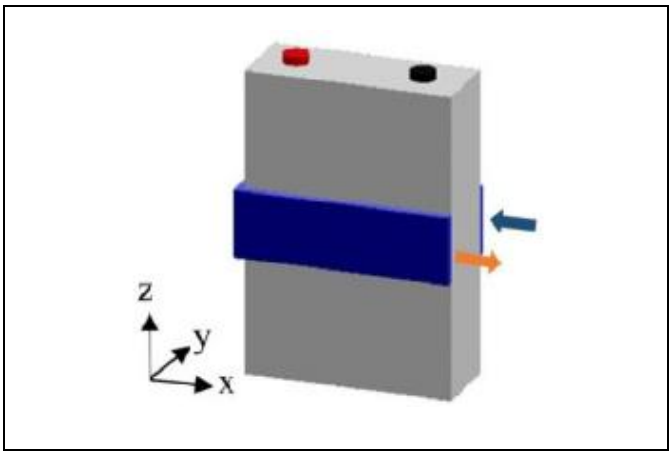

Figure 2.2: Single Strip of Mini-channels Wrapped Around Battery (Lan et al., 2016).

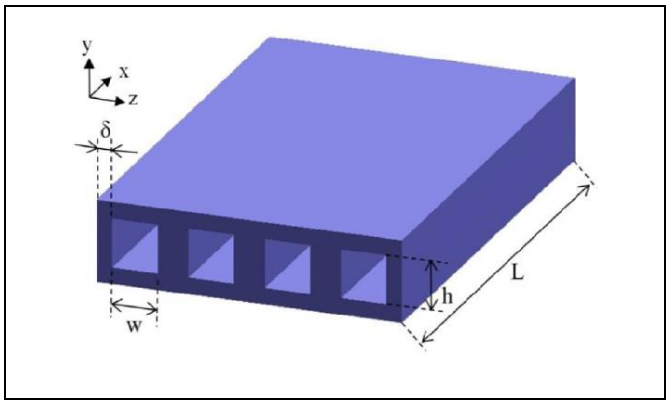

Figure 2.3: Details of a Strip with Four Mini-channels (Lan et al., 2016).

With the similar study objectives, Qian, Li and Rao (2016) have proposed to use cold plates with mini-channels in heat transfer of the lithium-ion battery. The cold plates would be placed in between the cells in the battery cells stacks. The arrangement of a stack of cells and cold plates as well as a piece of cold plate are shown in Fig. 2.4 and Fig. 2.5 (Qian, Li and Rao, 2016). The results obtained from this research conformed with that by Lan et al in 2016, in which the more the channels adopted in heat transfer, the higher the cooling rate. Also, coolant flowing through the channels in one direction from the electrodes side reduced the maximum temperature of the battery cells. In addition, it was found that the wider the channels, the slower the flow velocity flowing through the channels. This in turn reduced the pressure drop across the cold plates. These studies are highly commendable for providing important information on the optimum number and size of channels as well as the ideal coolant flow directions to generate an efficient thermal management system.

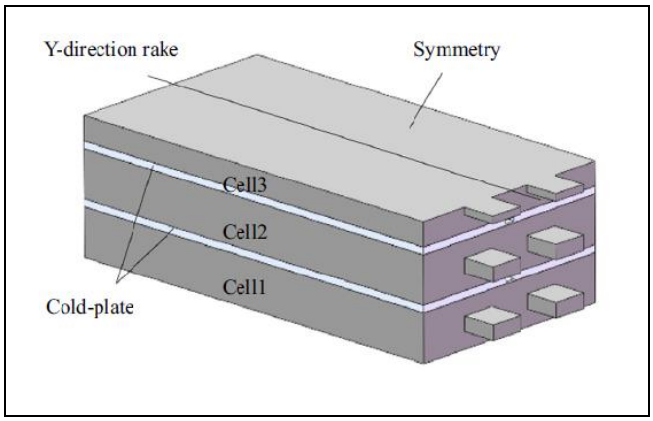

Figure 2.4: Arrangement of Battery Cells with Cold Plates (Qian, Li and Rao, 2016).

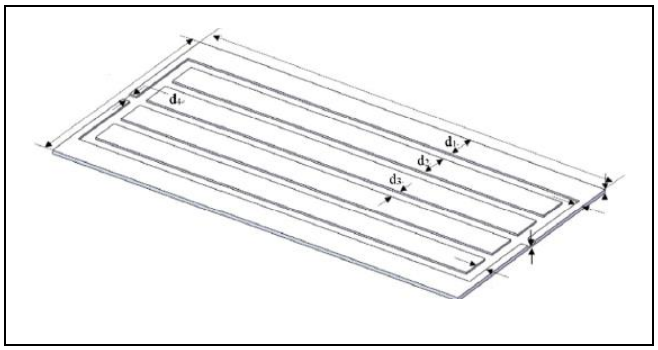

Figure 2.5: The Top Surface of a Single Piece of Cold Plate (Qian, Li and Rao, 2016).

2.3 Related Researches on Different Cooling Methods and Mediums Used

A number of researches have been carried out in the past to determine the suitable thermal management methods and medium that would provide an optimum heat dissipation performance. One of the heat transfer mediums that has been receiving major attentions in the industry is the nanofluid. Based on the comprehensive review completed by Salman et al, it was learnt that there were many researches done on the relevant topic. These researches included the nanofluid preparation techniques, the types and shapes of base materials involved as well as its flow properties under certain channel conditions (Salman et al., 2013). Although there was a great potential in enhancing heat transfer through the use of nanofluid, it was concluded by Salman et al. (2013) that the main challenges in making the nanaofluid marketable were the cost and time consumed for the preparation processes. Therefore, it is advisable to find an alternative medium to act as a coolant for the heat transfer of electronic devices.

There are many applications associated with water cooling method in the industry. Previously, four thermal management methods, namely air cooling, direct liquid cooling, indirect liquid cooling and fin cooling for lithium ion battery cells were investigated (Chen et al., 2016). The configurations of each of the cooling methods are shown in Fig. 2.6. Based on the results, the fin cooling would add the most weight to the battery cell while the addition of weight from direct cooling and indirect cooling methods were acceptable for an electric vehicle. Also, the results showed that the channels adopted in the indirect cooling would lengthen the pathway of coolant flow, thus enhancing the heat dissipation performance. It was concluded that the indirect cooling method was more practical due to the high risk in coolant leakage associated in direct cooling. Next, the research done by Li et al. (2018) have also demonstrated

the adoption of active water cooling system to enhance the heat transfer process from the battery pack in an electric vehicle.

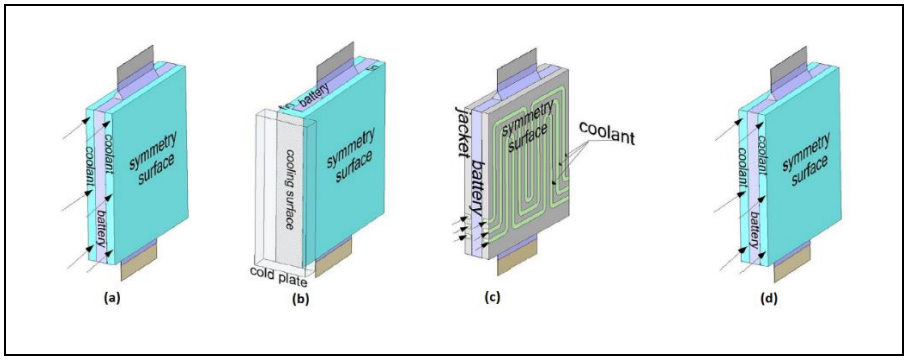

Figure 2.6: Configurations of (a) Air Cooling (b) Fin Cooling (c) Indirect Liquid Cooling (d) Direct Liquid Cooling (Chen et al., 2016).

Moreover, the novel self-cooling concept has been proposed for the thermal management system of electronic devices (Kiflemariam and Lin, 2015). Based on Fig. 2.7 shown, when heat is transferred from the heat source to the primary (microchannel) heat sink, the thermoelectric generator will convert the heat energy into electrical energy, which in turn operates the pump to run the coolant through the primary heat sink, in which the heat removal process takes place. From this system, it can be observed that the heat flux generated from the device and the coolant flow rate, as well as the ultimate thermal management performance, are inter-related with each other. Although this self-cooling method does not require human intervention, the large spatial design and the design complexity such as the various power outputs of pumps involved might be the obstacles that should be handled appropriately in order to commercialise the concept.

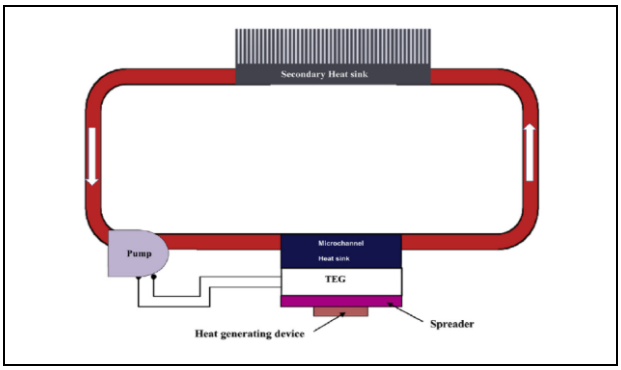

Figure 2.7: Illustrative Diagram of Self-Cooling System (Kiflemariam and Lin, 2015).

When water cooling method is applied in the thermal management system of electronic devices, care must be taken to prevent leakage of coolant which would potentially harm the devices and user. In order to tackle this issue, Kheirabadi and Groulx (2018) have proposed to replace the inlet and outlet connectors of a conventional liquid cooling method with a pair of heat exchanger plates, as shown in Fig. 2.8 (Kheirabadi and Groulx, 2018). The design was proposed to be utilised in the military applications. Based on the experimental results, the proposed design would increase the thermal resistance, hence reducing the heat transfer of the system. Therefore, it is dependent on each individual and application in order to justify the worthiness of the trade-off between the heat transfer and reliability of the system.

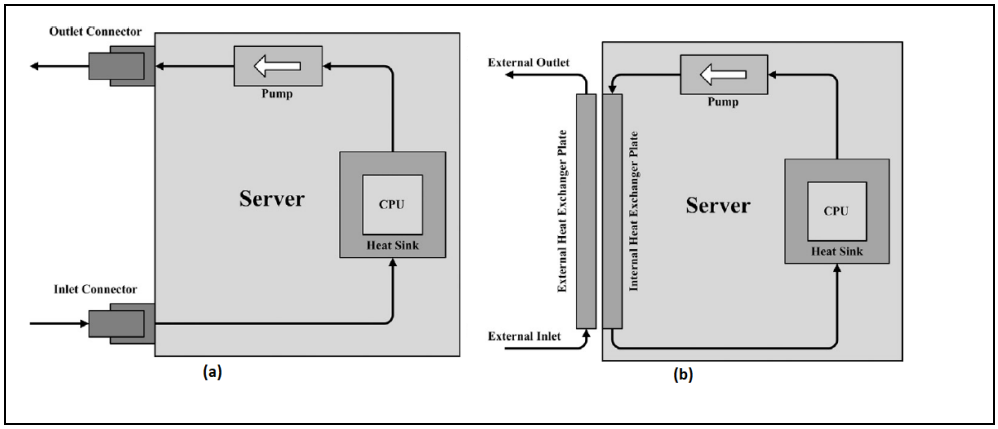

Figure 2.8: Diagram of (a) Conventional Water Cooling System (b) Thermal Contact Water Cooling System (Kheirabadi and Groulx, 2018).

2.4 Related Researches on Different Geometries in Cold Plate

Numerous researches have been done over the years to investigate the effect of different geometries in the cold plates on the performance of heat transfer. With regard to this topic, a research was carried out by Sui et al. in 2010 to study on the flow terminology of fluid and the associated heat transfer characteristic in a wavy microchannel heat sink. The wavy channel heat sink is shown in Fig. 2.9. Comparison was carried out among heat sinks with straight channels and wavy channels with different sinusoidal amplitude. Based on the study, it was deduced that the heat transfer rate would increase with the waviness of waveforms. In the same research, the authors have proposed to alter the amplitude and wavelength of the sinusoidal walls of the heat sinks along the fluid flow direction. This variation in waviness would produce a heat sink with higher local heat transfer efficiency in the event of heat points dissipations.

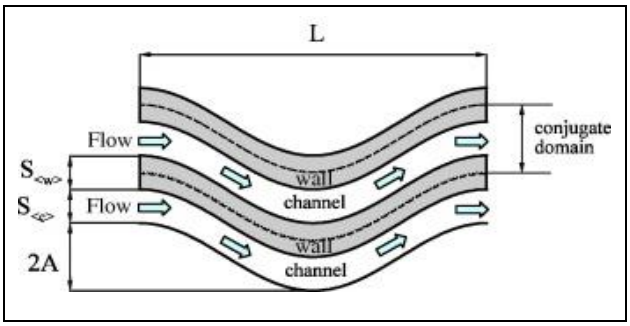

Figure 2.9: Dimensions of Two In-Phase Wavy-walls (Sui et al., 2010).

It was later justified by another research carried out by Mohammed, Gunnasegaran and Shuaib in 2011. In fact, the three researchers have proven that the heat sink with wavy wall channels would perform better in heat transfer as compared to the heat sink with straight wall channels. However, it was also discovered by the author that the cooling performance would only optimised within a certain range of waveforms amplitude, beyond which would result in bad heat dissipation performance. In this research, the dimensionless waveforms amplitude of $\alpha = 0.25$ would result in a heat transfer performance poorer than that in the conventional straight channels heat sink (Mohammed, Gunnasegaran and Shuaib, 2011).

Furthermore, Naqiuddin et al. (2018) have compiled a number of researches carried out in recent years. The geometries introduced in the articles included straight channels, wavy channels, pin fins, ribs, and dimples. Based on the overview of the articles, thermal performance of a cold plate can be improved through the generation of recirculation flow or Dean vortices, and wavy channels with increased wavy amplitudes can enhance this phenomenon. In addition, the rate of mixing of coolant can be increased further by introducing secondary branches on the channel walls, as shown in Fig. 2.10.

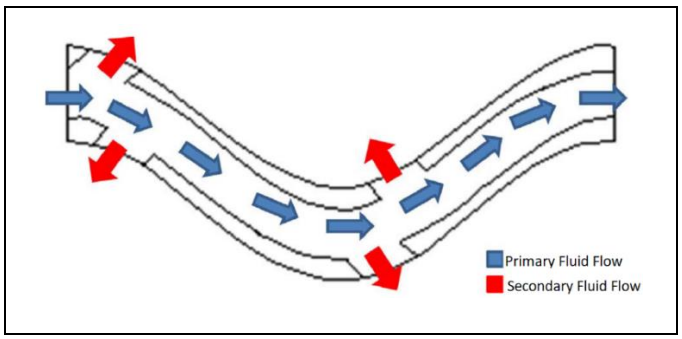

Figure 2.10: Secondary Branches Introduced in Wavy Channels (Naqiuddin et al., 2018).

Moreover, Ghani, Kamaruzaman and Sidik (2017) have proposed a novel geometric design by introducing a combination of sinusoidal cavities and rectangular ribs in the heat sink channels. The proposed design is shown in Fig. 2.11 below. By comparison, a sinusoidal-cavities rectangular-ribs heat sink have showed an increase in the generation of Dean vortices. Another enhancement that should be highlighted was that the hybrid design has showed a sharp decrease in pressure drop despite the flow distortions generated by the rectangular ribs. This decrease was due to the large fluid motion area promoted by the sinusoidal cavities (Ghani, Kamaruzaman and Sidik, 2017).

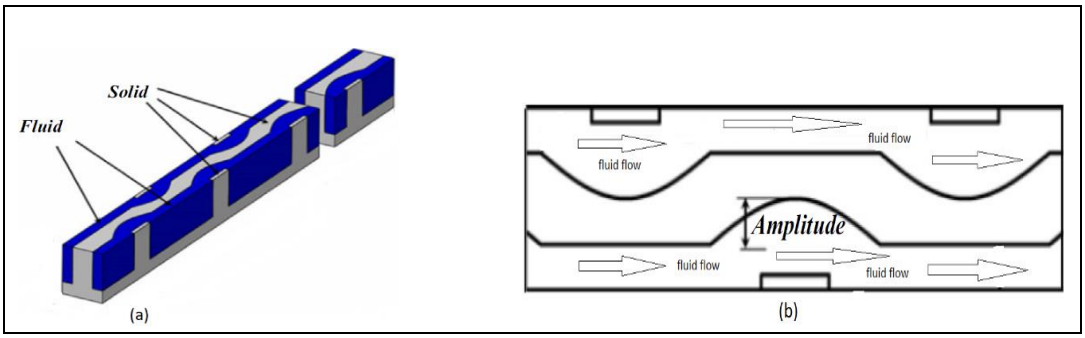

Figure 2.11: Illustrative Diagrams of Hybrid Heat Sink Channel Design (Ghani, Kamaruzaman and Sidik, 2017).

Besides that, Xia et al. (2015) investigated effect of the locations of inlet and outlet, header shapes and channel re-entrant cavity shapes on the coolant flow and thermal management performance of heat sinks. For the first section of this research, three types of inlet and outlet locations were introduced, as shown in Fig. 2.12 (Xia et al., 2015). Based on the numerical results, the I-type inlet/outlet locations created a better flow distribution in the channels as compared to that of Z-type. Therefore, the coolant in the I-type heat sink would achieve velocity uniformity, thus enhancing the overall heat transfer of the heat sink. In addition, it was found that the header shapes of the cold plate also play a role in coolant flow uniformity. With reference to the three header shapes shown in Fig. 2.13, the rectangular header shape produced the best result in fluid motion velocity distribution in the channels due to the most uniform branching of fluid from the inlet header into the channels and outlet. In the last section of the research, it was found that the channels with offset fan-shaped cross-section and the channels with triangular cross-section promoted better heat transfer mechanism than

that with a rectangular-shaped cross-section. This happened due to the formation of flow disturbance and an enhanced mixing of coolant.

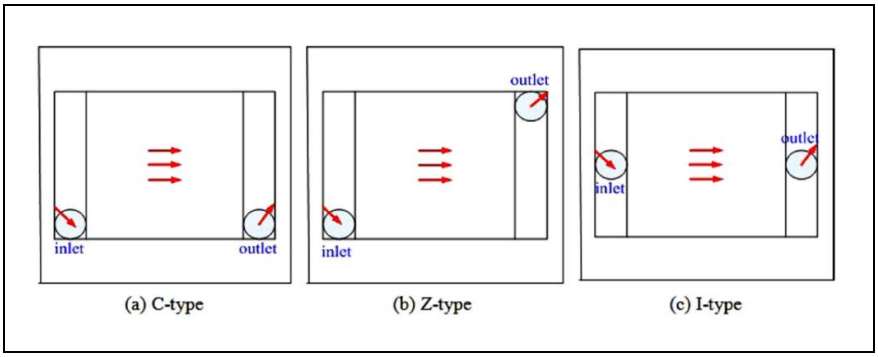

Figure 2.12: Different Inlet and Outlet Locations Proposed for the Heat Sink (Xia et al., 2015).

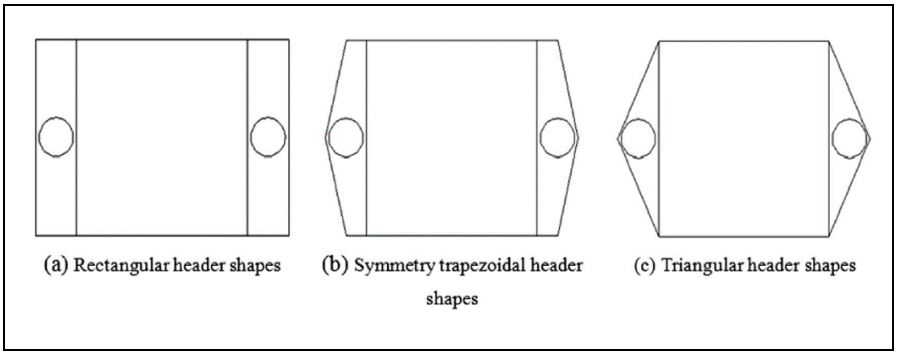

Figure 2.13: Different Header Shapes Proposed for the Heat Sink (Xia et al., 2015).

Other than the study carried out by Xia et al. (2015), other investigations have also been executed to enhance flow distribution and flow velocity uniformity. Gong, Zhao and Huang (2015), for instance, have proposed to apply metal foam at the inlet header of heat sinks. The simulation figures are shown in Fig. 2.14 below. According to the simulated data, it was discovered that the metal foam adopted did play a significant role in distributing the coolant evenly into each channel. In fact, only a negligible area of wake region is noticed at the inlet header in Fig. 2.14(a) as compared to the large wake region at the inlet header observed in Fig 2.14(b) (Gong, Zhao and Huang, 2015). The uniformity in flow distribution implicated that the temperature field across the heat sink channels was dispersed evenly as well.

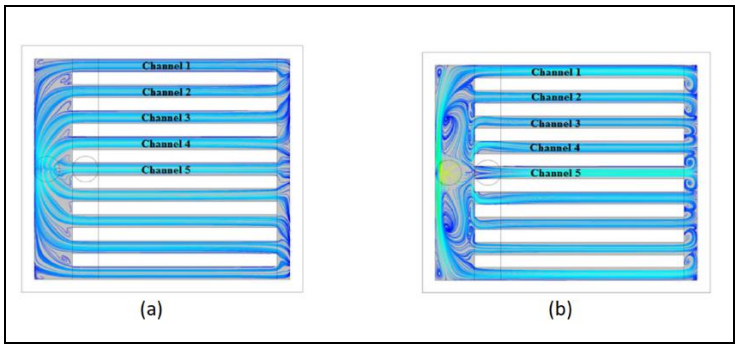

Figure 2.14: Flow Characteristics for Heat Sink (a) With Metal Foam (b) Without Metal Foam (Gong, Zhao and Huang, 2015).

2.5 Related Researches on Heat Transfer Through Wavy Channels

When studying through the researches and journals composed in recent years, it was noticed that most of the researchers were focusing on optimising the geometrical parameters of the cold plate and fluidic channels to maximise its cooling ability. As a matter of fact, the adoption of wavy channels in heat sink is an engineering trend that should be noticed in the field of heat transfer. Therefore, it is a wise move to study about it in-depth in this section.

2.5.1 Different Geometrical Profiles of Wavy Channels

The thermal management performance in wavy channels is dependence on several factors, namely the geometrical properties of the channels and the flow properties of coolant. Given a typical wavy channel heat sink, Akbarzadeh, Rashidi and Esfahani (2017) explored in-depth on the possibilities of manipulating the corrugation profiles of the wavy walls in an effort to improve the heat transfer of the cold plate. Throughout this study, a comprehensive comparison in terms of entropy generation, heat transfer, and pressure drop among three corrugation profiles, namely sinusoidal, trapezoidal and triangular shapes was carried out through numerical simulation. Then, the results were compared with an ordinary straight channel heat sink. Fig. 2.15 illustrates the configurations of the corrugation profiles and a straight channel heat sink. With water flowing under Reynolds number ranging from 400 to 1400, it was found that the trapezoidal shape produced the largest recirculation region in the downstream direction. This would promote the highest rate of coolant mixing in the channel. Also, it was observed that the trapezoidal shape resulted in the largest pressure drop while triangular shape had the smallest drop in pressure across the channel. In addition, thermal irreversibility, or thermal entropy generation was investigated through this

study. Based on the numerical results, it was discovered that the thermal entropy generation has an inverse relationship with Reynolds number for all channel configurations. In relation to that, the triangular shape wavy channel generated the highest value of thermal entropy, followed by the sinusoidal shape and lastly, the trapezoidal shape channel. Hence, trapezoidal shape with the least thermal irreversibility would provide the best heat transfer performance. After considering the results from all the aspects mentioned for this study, it was recommended to use a sinusoidal wall in developing a cold plate channel due to its low thermal irreversibility, high thermal performance and an acceptable range of pressure drop (Akbarzadeh, Rashidi and Esfahani, 2017).

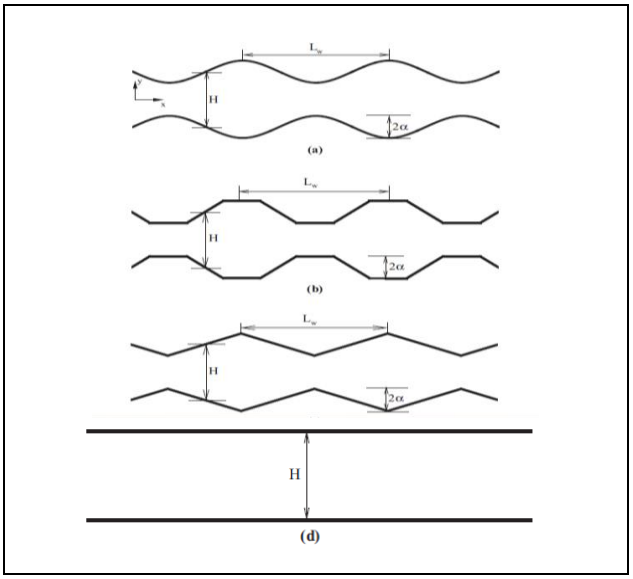

Figure 2.15: Cold Plate Channel Profiles (a) Sinusoidal (b) Trapezoidal (c) Triangular (d) Straight Channel (Akbarzadeh, Rashidi and Esfahani, 2017).

In year 2016, a numerical study was carried out to compare the thermal management characteristics of symmetric sinusoidal wavy-walled channels and asymmetric sinusoidal wavy-walled channels (Ramgadia and Saha, 2016). The responding variables for this study were the flow structures and thermal performance resulted from phase shift angles of $\varphi = 0°, 90°, and\ 180°$ between two opposite wavy walls, as shown in Fig. 2.16. Among the phase angles of interest, the asymmetric configuration of $\varphi = 0°$ generated the highest Nusselt number, signifying the best convective heat transfer performance. Also, asymmetric configurations promoted higher relative strength of shear stress than that of a symmetric wall channel. Thus, higher transport

momentum between fluid of dissimilar temperatures were observed for asymmetric walls channels. However, the main drawbacks of channel with wavy wall of $\varphi = 0°$ were the high friction factor and pressure drop. Therefore, relevant steps must be carried out in future study to compensate the undesired penalties.

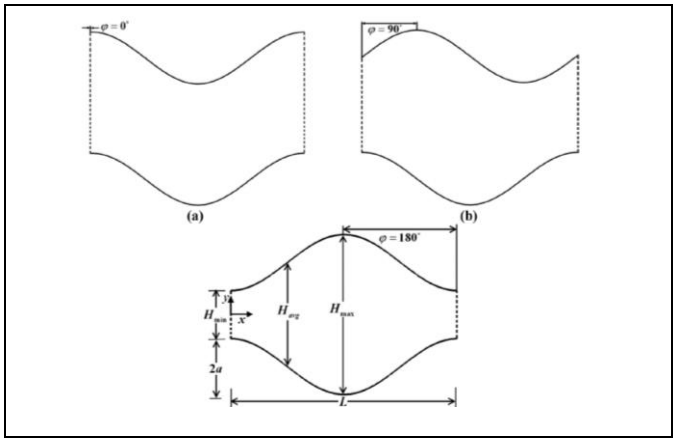

Figure 2.16: Phase Shift Angles Between Two Opposite Wavy Walls (Ramgadia and Saha, 2016).

Besides that, Lin et al. (2017) had proposed to enhance the formation of flow vortices by having a wavy microchannel heat sink with varying wavelengths, λ and amplitudes, A along the coolant flow direction as shown in Fig. 2.17. In this research, a straight channel heat sink and an original wavy channel heat sink were put in place as an indication of cooling performance of the proposed designs. The thermal resistance and the bottom wall temperature distribution of the three designs were compared. Through numerical results, it was noticed that the mixing of coolant and the heat transfer between liquid and wavy walls of the proposed designs were greatly improved as compared to the other two original structure. In fact, with fixed pumping power, the thermal resistance, R and the maximum bottom wall temperature difference, ΔT_b were reduced significantly when the amplitude of the corrugated walls was increased or wavelength was decreased along the downstream direction. Also, the thermal work of the heat sink had improved with an elevation in the wavelength difference and the amplitude difference between two adjacent wave units, as shown in Fig. 2.18. Based on the two observations mentioned, it can be deduced that an enhancement in the formation of vortices can aid in the mixing of coolant while increasing the rate of heat transfer between the coolant and channel walls. These in turn enhance the heat transfer characteristics of the wavy channel heat sink.

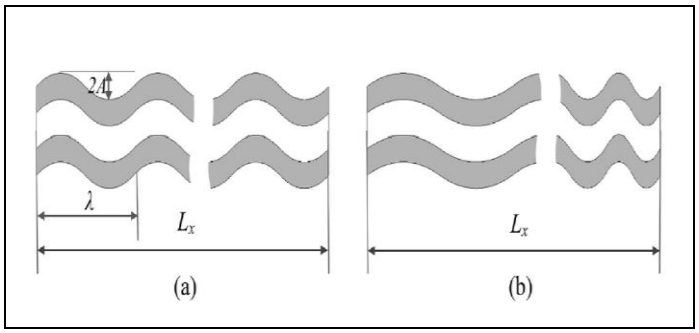

Figure 2.17: Wavy Channel with (a) Constant Wavelength (b) Changing Wavelength (Lin et al., 2017).

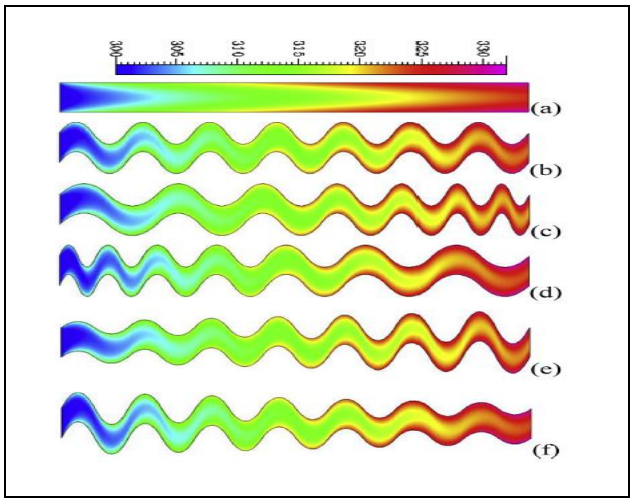

Figure 2.18: Temperature Contours of Coolant along Different Channel Configurations (Lin et al., 2017).

Other than these, the effects of amplitude of waviness and Reynolds Number on thermal management in a wavy passage had been investigated with the geometrical properties shown in Fig. 2.19 (Ramgadia and Saha, 2012). Throughout this study, numerical simulation of fully developed flow was executed to study on the effects mentioned. The amplitude of waviness was determined by the ratio H_{min}/H_{max}, in which the higher the amplitude of waviness, the lower the H_{min}/H_{max} ratio. Based on the simulated result, a high amplitude of waviness would result in a high rate of heat transfer, with a drawback of large pressure drop. In addition, the effect of Reynolds number on thermal performance of wavy passage was also investigated. It was found that under steady coolant flow region, the Thermal Performance Factor (TPF) would decrease with a rise in Reynolds number. Meanwhile, with an unsteady flow of coolant, the TPF would increase with Reynolds number.

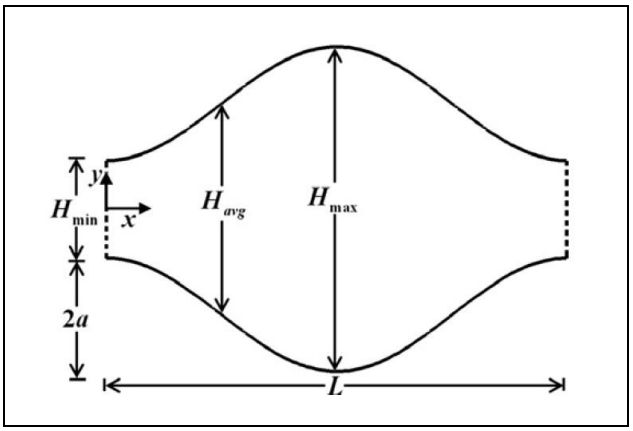

Figure 2.19: Schematic Diagram of the Sinusoidal Wavy Channel (Ramgadia and Saha, 2012).

Besides altering the wavelength, amplitude and profile of the waveforms, secondary channels or branches can also be introduced to aid in the flow of coolant. This concept was proposed by a group of researchers from Singapore and India. In 2016, Chiam et al. have simulated and experimented the concept by introducing allowing secondary flow to occur through the wavy walls. As shown in Fig. 2.20, the thermal performance of three models with different amplitude to wavelength aspect ratios (A/λ) was studied. Based on the results, both of the branched designs (Design (B) and Design (C))have resulted in a better heat transfer characteristic than the conventional wavy channel (Design (A)) (Chiam et al., 2016). However, though the secondary flows of fluid would increase the rate of fluid mixing and disrupt fluid boundary layers, it could also permit high pressure drops across the channels, an event which was undesirable. This phenomenon leads us to the next sub-section, which will be focusing on the pressure drops across wavy channels and the methods proposed to reduce it.

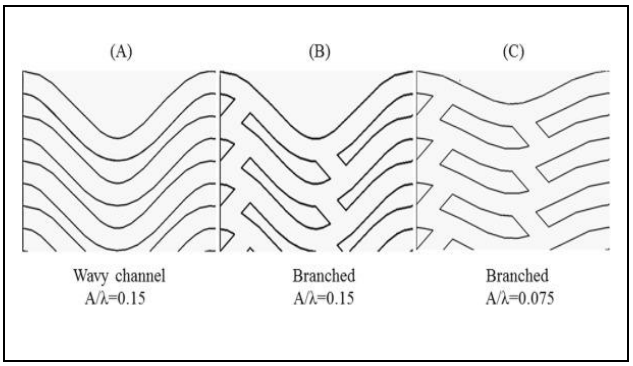

Figure 2.20: Three Designs of Interest for the Study (Chiam et al., 2016).

2.5.2 Method Proposed to Reduce Pressure Drop Across Wavy Channel

As a continuation from the last sentence of the previous sub-section, the increase in pressure drop resulted from the introduction of secondary branches was observed from the simulation results. In fact, when the $aspect\ ratio = 0.15$ model with secondary channels was applied, the pressure drops across the channels undermined the cooling enhancement by the secondary flows. For such a case, the speed of fluid flow must be low to retain the advantages of introducing secondary branches. On the other hand, the heat transfer improvements resulted from the secondary flows could also be retained when the amplitude of waveforms was reduced to aspect ratio of 0.075.

Moreover, the research carried out in 2010 have suggested that the pressure drop resulted from the wavy walls was insignificant as compared to the improvement in its cooling performance (Sui et al., 2010). It was later confirmed by Mohammed, Gunnasegaran and Shuaib in the same year. However, it was also shown in the same research that the pressure drop increased with the amplitude of waveforms and Reynolds number. The result was plotted in Fig. 2.21. Also, the wall shear stress encountered along the wavy walls would rise with an increase in amplitude ratio. When the magnitude of pressure drop reached a significant value, the overall heat transfer performance would eventually be override. Therefore, these researches have provided an idea in which decreasing the waveforms amplitude would help reduce pressure drops.

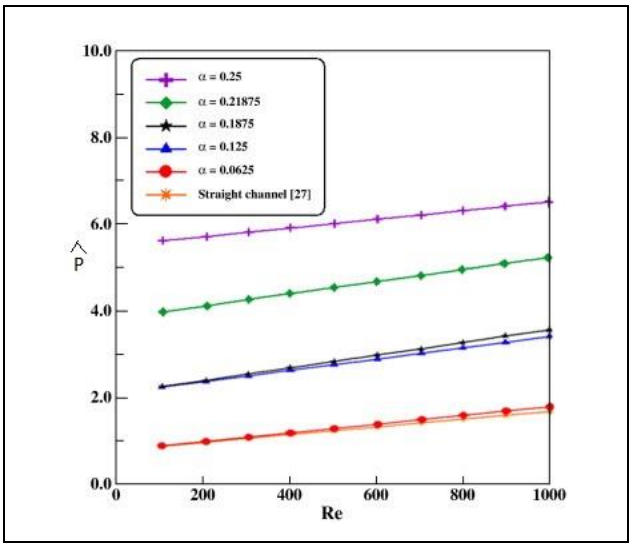

Figure 2.21: Graph of Pressure Drop Variations Against Reynolds Number for Wavy and Straight Channels (Mohammed, Gunnasegaran and Shuaib, 2011).

It should be clear now that having a higher wave amplitude for the wavy walls would generate a large coolant recirculation region, thus enhancing the heat transfer rate. However, this method is usually accompanied by an increase in pressure drop, which is undesirable for the endurance of the heat sink structure itself. In regard to that issue, Harikrishnan and Tiwari (2018) have proposed to introduce different degree of skewness, Φ to the wavy structures, expecting to enhance the thermal performance with relatively less increase in pressure drop. Using ANSYS Fluent 16.1, and Reynolds number of $Re = 3000$, a numerical study was carried out to investigate the effect of skewness angle in a wavy channel on thermodynamics. Based on the numerical results, it was found that when the skewness angle increased, Nusselt number would increase with a decrease in friction factor as compared to an un-skewed wavy channel. This eventually resulted in an improvement in the Thermal Performance Factor (TPF). However, the increase in TPF was only observed up to a certain degree of skewness angle and amplitude, beyond which would result in an increase in entropy generation and decrease in Nusselt number. As concluded from this research, with reference to Fig. 2.22, the combination of wavy amplitude $0.2H$ with skewness angle, $\Phi = 45°$ would produce the highest TPF with a relatively low pressure drop.

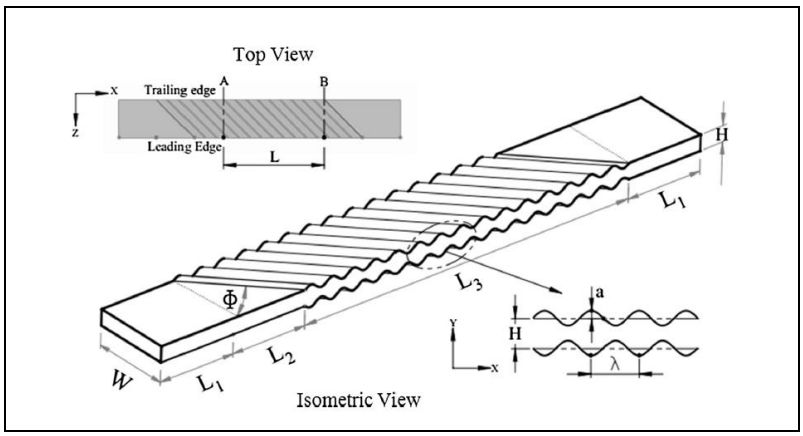

Figure 2.22: Illustrations of Skewed Wavy Channel Heat Sink (Harikrishnan and Tiwari, 2018)**.**

2.5.3 Proposal to Develop Wavy Channel with Silicon Materials

Lu et al. (2017) had proposed to use a silicon porous fins instead of an ordinary aluminium in developing the wavy channel cold plate. The basic structures of the porous fins cold plate are illustrated in Fig. 2.23. Based on the numerical results, the application of silicon porous fins as the base material of wavy channels would reduce

the pressure drop while improving heat transfer between the coolant and the wavy walls. According to the researchers, permeation effect and slip effect of the coolant had played a major part in minimising the pressure drop of the liquid flow. In addition, the concept was also tested with different geometries of wavy channels and similar results were obtained for all cases. This indicated that the porous fin design is accompanied with high feasibility.

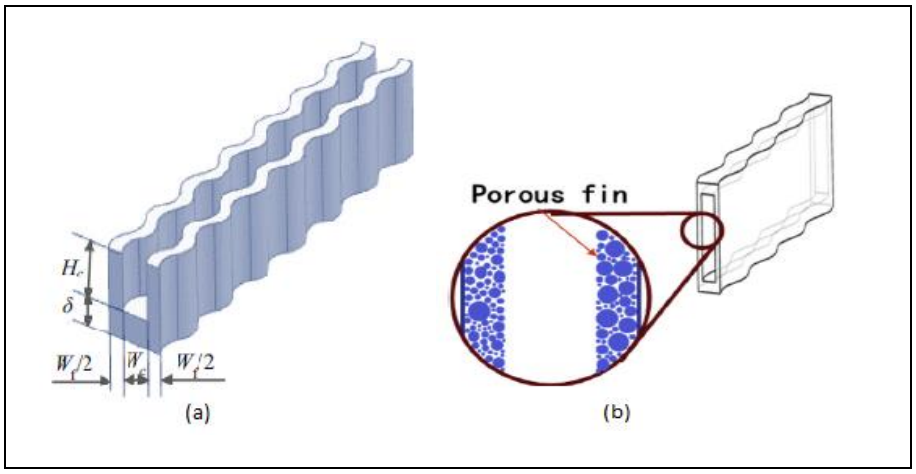

Figure 2.23: Illustrative Diagram of (a) A Single Channel of Wavy Channel Heat Sink and (b) Wavy Channel Heat Sink with Porous Fins (Lu et al., 2017)**.**

Similarly, Rostami, Abbassi and Saffar-Avval (2015) used silicon as the base material to develop the wavy channel. The purpose of this research was to investigate the thermal management performance of silicon wavy channels cold plate with a straight channel design. Also, the optimum geometry for the wavy channels was determined. Based on the research data, the heat transfer performance of the silicon wavy channels plate was superior over that of the silicon straight channels design (Rostami, Abbassi and Saffar-Avval, 2015). This result showed that the wavy channels would always produce the better heat dissipation performance than that of straight channels regardless of the material used.

2.6 Related Researches on Fluidic Diodes

The researches and reports filed back in the 60's up to the current years have been reviewed and studied thoroughly in order to gain a better understanding on the operating principle of fluidic diode. Also, the invention, innovation and development of the flow element throughout the years have been observed. As defined in the

reviewed patent reports, a fluidic diode is known as a flow element which allows fluid to flow in one direction while prohibiting the flow in the opposite direction (Bermel (1968), Wieme (1972), Kobsa (1992), Reed (1993), Yoder et al. (2011)). This element is able to provide an enormous reliability in solving the backflow problem in a fluidic system due to it having no moving parts.

2.6.1. Different Configurations of Fluidic Diodes

Fluidic diode can assume different configurations as long as the operating principle retains. This can be observed through the different invention from late 60's to early 90's, as shown in Fig. 2.24. By reviewing another research, three other types of fluidic diode designs were learnt, namely the vortex diode, tesla diode, and diaphragm diode, as shown in Fig. 2.25 (Khabarova, Podzerko and Spiridonov, 2017). The enlarged diagram of a Tesla diode, invented in 1920, is shown in Fig. 2.23 (Reed, 1993). Based on this diagram, reversing channels were adopted along the plate. As indicated by the arrows, the fluid was flowing in the opposite direction. When the reversed flow occurred in the channels, it would be directed to coincide with the incoming flow, thus cancelling out or minimising the undesired flow effect. This indirectly resulted in more head loss observed for the reversed flow as compared to that of the forward flow (Reed, 1993). In short, different orifices and channel shapes had been introduced in the past to direct a unidirectional flow of fluid in channels.

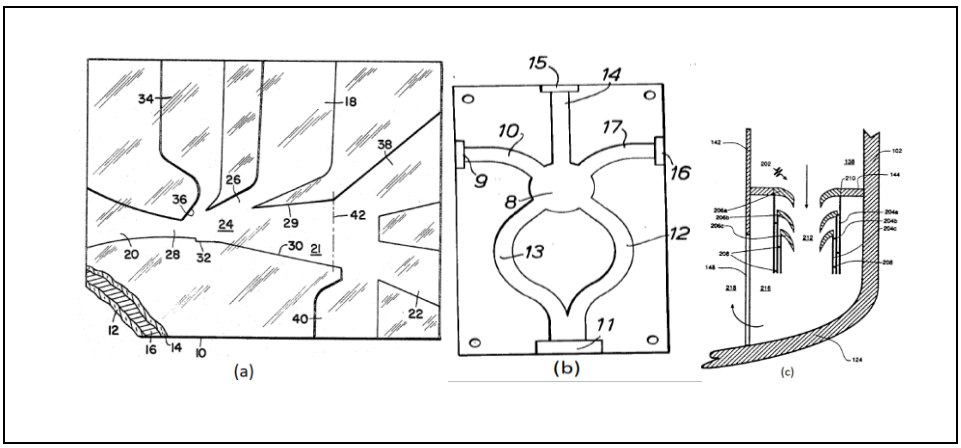

Figure 2.24: Different Configurations of Fluidic Diodes Patented (Bermel (1968), Wieme (1972), and Kobsa (1992)).

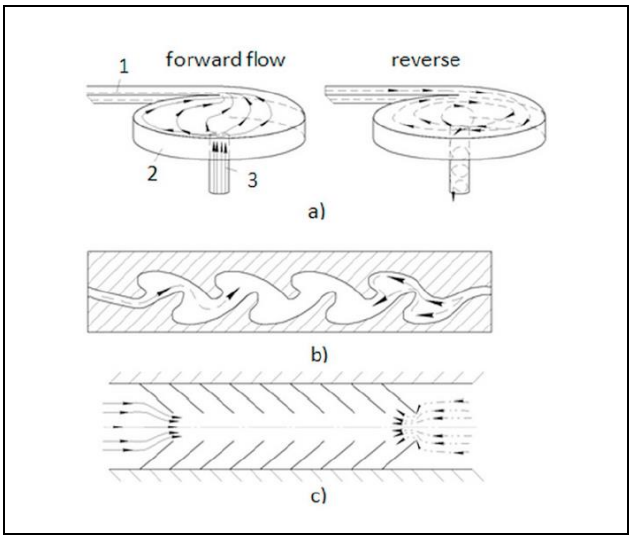

Figure 2.25: (a) Vortex Diodes (b) Tesla Diode (c) Diaphragm Diode (Khabarova, Podzerko and Spiridonov, 2017).

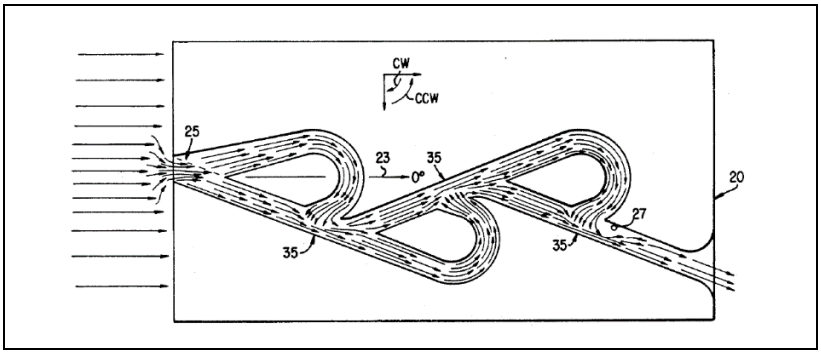

Figure 2.26: Reversed Fluid Flow in Tesla Diode (Reed, 1993).

2.6.2. Role of Fluidic Diode in Reducing Pressure Loss Along Fluid Channels

As reviewed from the previous sub-sections, it was found that a thermal cold plate with wavy channels would always be accompanied by a significant pressure drop. Therefore, an additional flow element will need to be adopted to the heat sink to ensure an anisotropic flow direction for the coolant so as to reduce the hydraulic shocks received by the cold plate. According to the reviewed report by Kobsa (1992) which was later confirmed in the research done by Burnett, Caso and Tang (2010), a fluidic diode is able to take on the tasks mentioned above. In fact, a parameter, namely diodicity was used to qualify the fluidic diode's performance. According to Burnett, Caso and Tang (2010), diodicity can be understood as "the ratio of the pressure differential in the direction of high flow resistance to the pressure differential in the direction of low flow resistance".

By reviewing the paper by Khabarova, Podzerko and Spiridonov (2017), the effect of Reynolds number on hydraulic resistance in a vortex diode was studied. Based on the experimental results, it was shown that the diodicity of vortex diode only achieved stability after the air flow exceeded Reynolds number of 3000. Although air was used as the coolant medium instead of water, this research has proven that fluidic diode is able to provide an effective way to reduce the pressure drop across the cold plate channels as long as it is operating under an ideal range of Reynolds numbers.

2.6.3. Applications of the Working Principle of Fluid Diodes

The concept of fluidic diode is also applied in many other systems. For example, in a comprehensive research, a layer of super-hydrophobic coating was applied on one side of a porous substrate (Mates et al., 2014). As shown in Fig. 2.27, fluid would only pass through the substrate in one direction without facing much hindrance. In the opposite direction, however, there will be a high magnitude of flow pressure preventing the passing through of fluid. The rate and direction of fluid flow can be adjusted easily by changing the porosity of the substrate and the coating properties.

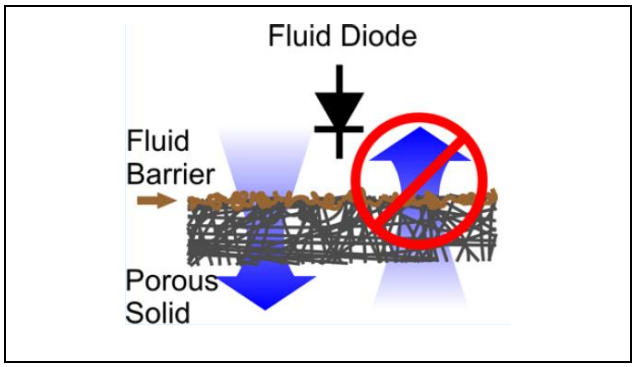

Figure 2.27: Illustrative Diagram of Flow Condition Across the Substrate (Mates et al., 2014).

Besides that, the fluidic diode concept has also helped in the development of topological liquid diode in micro-scale (Li et al., 2017). With reference to the topological structure shown in Fig. 2.28, liquid droplet will flow without obstacle towards the leading edge of the cavities, while preventing the flow of the fluid in the reverse direction through pinning. Although the two applications mentioned above are not related to thermal cold plates, these researches serve as a major milestone in the development of fluidic diodes to reduce the pressure drops in a fluid flow condition.

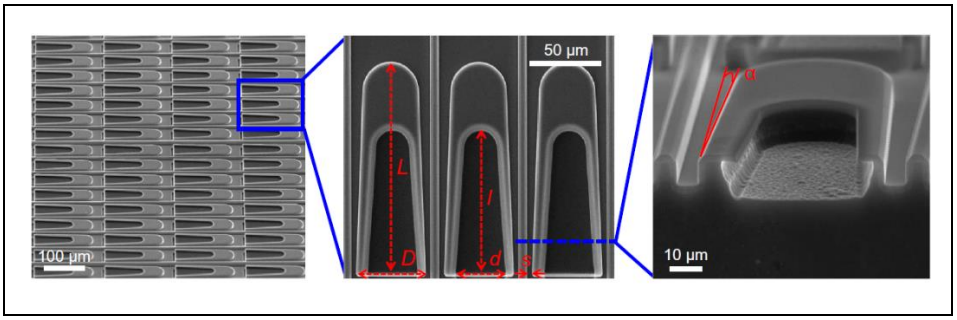

Figure 2.28: Microscopic View of the Topological Liquid Diodes (Li et al., 2017).

2.7 Summary on the Reviews

After reviewing the journals and patents produced in the past, it was found that most of the researches were carried out by using liquid (water) as the cooling medium instead of air when cold plates were used. This was due to the fact that water has higher specific heat capacity and thermal conductivity than that of air. Also, water was used over nanofluids due to the high cost and complex preparing procedures of nanofluids. In addition, reviews were also done to determine the methods used to prevent leakage of liquid during heat transfer process.

Besides that, further study on the journals revealed that the thermal management performance in a cold plate was affected by the total surface area available for heat transfer, formation of dean vortices, rate of mixing of liquid, flow velocity of liquid and the pressure drop along the channels. In relation to that, cold plates with channels of different geometries were proposed. These included the introduction of rectangular ribs along the channels, manipulation of inlet and outlet locations, as well as changing header shapes for the heat sink. Next, the addition of metal foams at the inlet section and its effect were determined in the journal reviewed. The review on different geometrical properties have led to the realisation of the potential of adopting wavy channels in a cold plate. As a consequence, wavy channels were taken as the base for different modifications to be done on it. These changes consisted the application of different corrugated profiles, phase shift angles, profile amplitudes and wavelengths. Also, one of the researches showed that the introduction of secondary branches in the channels walls would increase the mixing of liquid. Nevertheless, the significant pressure drop and non-uniformity of flow velocity due to the increase in liquid mixing should not be taken lightly as it would cause damage on the structure of the cold plate in a long run. These problems were tackled by

researchers through the application of an optimum angle of skewness and through the usage of porous fin materials such as silicon.

Lastly, the reviews were also done on the patented designs of and related journals on fluidic diodes in order to determine the potential of applying the similar working principle into the cooling mechanism of electronic devices. Based on the studies, it was found that the concept of applying fluidic diode prevented liquid backflow effectively, which would in turn minimise hydraulic shocks, or pressure drops, in the channels. Nonetheless, the feasibility of this concept has been justified through its applications in different fields related to fluid flow.

In short, these literature reviews provided a clear guidance in designing the methodology and work plan for this project. It would also ensure that effective steps should be carried out to complete the following investigations, so as to achieve the objectives of this project.

CHAPTER 3

METHODOLOGY AND WORK PLAN

3.1 Introduction

An aluminium wavy channel liquid cold plate with improved characteristics was introduced in this project to further enhance the thermal management performance for electronic devices. In order to achieve the proposed objectives, this section provides a clear guideline on the planning of, and methods used for the thermal management of electronic devices using wavy channels cold plate.

Before any simulation and fabrication works were executed, the project was started off by drawing the cold plate design through computer-aided design using SOLIDWORKS software. In relation to that, the dimension of the cold plate that would be fabricated for this project would be $length \times width \times height$ of $200\ \text{mm} \times 130\ \text{mm} \times 17\ \text{mm}$, with another cover of $3\ \text{mm}$ thick on top of the cold plate. In other words, the total height of the cold plate structure would be 20 mm including cover during actual use. Also, the material used for the cold plate was 6061 aluminium alloy.

Next, the designed model was transferred to another software for computational fluid dynamics (CFD) simulation. The software tool used for the task was ANSYS version 18.1, Fluid Flow CFX. As for this process, several flow parameters were applied to simulate the operating condition of the cold plate. As far as the investigation was concerned, the rate of flow of coolant (water) pumped into the channels would be in the range of $50\ \text{g/s}$ to $100\ \text{g/s}$, with a maximum heat flux of 1000 W transferred from device. In this process, it was expected that several changes and amendments in cold plate design would be made based on the simulated results.
After an optimised cold plate design has been selected, MasterCAM (an external add-on of SOLIDWORKS) was used to generate NC Codes for CNC machining. Lastly, the G-Codes and M-Codes were transmitted into the CNC milling machine to fabricate the cold plate model.

3.2 Methodology

In order to track the progress of the project, the actual pace in proceeding the work would be compared with the milestone achieved and the planned schedule. In fact, the project flowchart shown in Fig 3.1 served as an important visual aid for the purpose

mentioned. The flowchart provided a clear guidance as to how and where the project would be headed to after each task was completed.

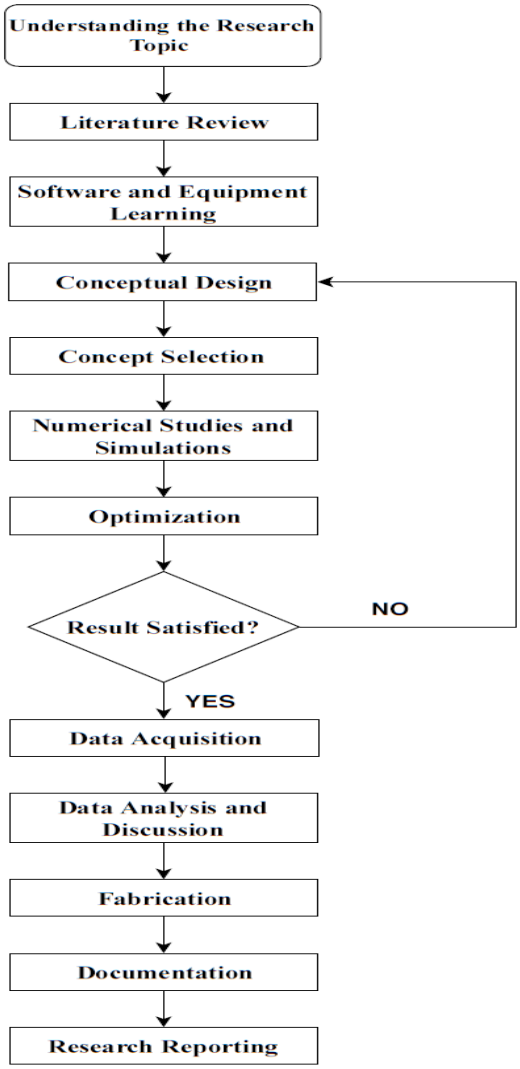

Figure 3.1: Flowchart of the Project.

3.3 Modelling and Simulation

3.3.1 SOLIDWORKS

Prior to designing the detailed features, the general dimension and geometry parameters of the model had already been decided. Next, the detailed designs such as the channels width and shape were modelled using a computer-aided design software called SOLIDWORKS 2017. Initially, SOLIDWORKS Part was used to design both the cold plate and the heat source separately. For the cold plate, the “Top Plane” was used to sketch the base of the plate, before extruding it to the desired height using the

Extruded Boss/Base feature. Furthermore, sketches were also done on different planes to draw the outline for the final model. To make the 2D sketches into 3D model, several features were applied. These features included the Extruded Boss, Extruded Cut, Swept Cut, Fillet and Hole Specification. Another note to be taken was the way to form wavy shape for the channels. As for this project, the wavy shape was formed through the expression of mathematical functions. This method allowed changes on the wavelength and amplitude to be made with ease. Also, the secondary channels were sketched using the linear sketch pattern so that the distance between each secondary channel would be equal. Moreover, the hole on both sides of the plate were formed using Dowel Hole type with ANSI Inch Standard. The hole size was set at ¼ inch. As for the heat source, it was drawn with the same face area as the cold plate, with 3 mm thickness, in a separate SOLIDWORKS Part file. Lastly, the two parts were imported into the SOLIDWORKS Assembly and mated together, before saving it as a Parasolid (*.x_t) file.

3.3.2 ANSYS Fluid Flow (CFX)

At the pre-simulation stage, solid modelling was completed and the conceptual design was transferred to ANSYS Fluid Flow (CFX) for computational fluidic performance simulation. The geometry was imported by browsing and selecting the desired parasolid file. In the Geometry window, it was noticed that only two parts were listed, namely the cold plate and the heat source. In order to study the fluid, it was necessary to convert the cavities or channels into volumes. This was done through two steps. Firstly, surfaces were created through the edge of the inlet and outlet. Next, the Fills feature was applied to fill everything between both selected surfaces (inlet and outlet), so that the software would be able to read the fluid as a volumetric structure. This Geometry was then updated to the ANSYS Workbench before proceeding for meshing.

In the Mesh window, each of the parts of concern was named accordingly using the “Named Selection” feature. These parts are the heat source, the cold plate itself, the fluid, inlet and outlet. Next, meshing was done on the model by considering the desired sensitivity and accuracy of the simulated results. The sizing of the mesh was done under the size function of “Proximity and Curvature” with relevance center set as “Coarse” and span angle center set as “Fine”. Initial settings were also done for minimum size of 0.1 m, proximity minimum size of 0.1 m, maximum tetrahedral size of 10 m, and maximum face size of 5 m. In an addition, the Inflation feature was also

adopted to provide a more realistic fluid condition. As the last step for this section, mesh would be generated.

In the Setup window, the boundary conditions and initial conditions were calibrated to simulate the real working environment. For the cold plate, the material used was aluminium, with initial temperature of $T = 30$ ℃. At the same time, the walls of the cold plate were assumed to be adiabatic. Also, two interfaces were formed between the cold plate with fluid and with heat source. Besides that, water with continuous fluid morphology was the subject of concern for this project. The water was assumed to be at atmospheric pressure, flowing along smooth walls of the channels. Moreover, the inlet fluid mass flow rate, M and inlet static temperature, T were set at 50 g/s and 30 ℃, respectively. Meanwhile, the relative pressure at the outlet was at 0 Pa. Beyond the cold plate and fluid, the specifications of heat source were also set up. The material used was aluminium and it was assumed to have a continuous solid morphology. Besides that, interface was formed between the heat source and the cold plate. In relation to that, surfaces other than the interface was taken as adiabatic. Also, a subdomain was created to simulate the heat of 1000 W being transferred from the heat source to the cold plate. At the final stage of the set up procedures, the number of iterations were calibrated at the Solver Control section. In fact, the minimum and maximum iterations were set as 1 and 200, respectively. After setting up the conditions, the model was ready to be sent for simulation.

In the Solution window, the simulation would commence upon clicking the "Start Run" button. The time taken for the simulation process might vary according to design complexity as well as the number of nodes generated during meshing. Through the simulation process, the maximum and minimum temperature readings at the heat source-cold plate interface would be obtained. Besides that, the average fluid pressure readings at the inlet and outlet would also be determined through the ANSYS Fluid Flow (CFX) software. These results were shown numerically and illustrated in contours. With the results obtained, the temperature differences, ΔT at the heat source-cold plate interface and fluid pressure drops, ΔP at both sides of the liquid cold plate were to be calculated using Eq. 3.1 and Eq. 3.2, respectively.

$$\Delta T = T_{max} - T_{min} \quad (3.1)$$

where

ΔT = Variation of temperature at heat source-cold plate interface, °C

T_{max} = Maximum temperature at heat source-cold plate interface, °C

T_{min} = Minimum temperature at heat source-cold plate interface, °C

$$\Delta P = P_{in} - P_{out} \quad (3.2)$$

where

ΔP = Fluid pressure drop across the cold plate, Pa

P_{in} = Average fluid inlet pressure, Pa

P_{out} = Average outlet pressure, Pa

At the post-simulation stage, the thermal management performance of the liquid cold plate was justified based on the temperature uniformity and pressure drop across the channels of the plate under different water flow rate. In fact, a heat source-cold plate interface's temperature variation of 5 ℃ or less, as well as a pressure drop lower than the tensile yield strength and Ultimate Yield Strength for a 6061 Aluminium plate would signify a good design. By applying the Taguchi Method, it was expected that changes and amendments would need to be done for a few times on the cold plate model in order to achieve an optimised design. After the design has been finalised, a computer-aided manufacturing (CAM) software was used to generate G-Codes before proceeding to prototype fabrication using CNC milling machine.

3.4 Prototype Fabrication

3.4.1 Stock Material

The stock material chosen to be fabricate into the designed wavy channel cold plate was the 6061 aluminium alloy block. The stock material purchased from the supplier was in the size of 202 mm × 132 mm × 20 mm, as shown in Fig. 3.2. There were several factors that influenced the aluminium alloy selection process. Firstly, the 6061 class aluminium alloy was readily available in the market, thus reducing the price of the stock and resulting in a lower cost of cold plate product. Furthermore, the material

properties of the 6061 aluminium alloy including high strength, toughness and durability, would enhance the life cycle of the product. Also, its high workability would ease the CNC milling processes using mill tools of different diameters. Lastly, its excellence resistance towards corrosion and high thermal conductivity would make the end product a high quality thermal cold plate performing its heat removal function. After receiving the stock material, it was then proceeded for facing and squaring processes to obtain the desired material dimension for the cold plate.

Figure 3.2: Picture of 6061 Aluminium Alloy Block Purchased.

3.4.2 Facing and Squaring

As mentioned in the previous sub-subsection, the 6061 aluminium block purchased was in the dimension of $202\ \text{mm} \times 132\ \text{mm} \times 20\ \text{mm}$. In order to achieve the desired design of $200\ \text{mm} \times 130\ \text{mm} \times 17\ \text{mm}$, facing and squaring were carried out. The face milling process aimed to produce totally flat horizontal surfaces besides creating a block thickness of 17 mm. Meanwhile, the squaring process was performed to obtain the desired length (200 mm) and width (130 mm) of the cold plate. It was vital to ensure that all the surfaces were flat so that there would be no misalignment when the block was being clamped on the vice for CNC machining in the next step. Both the manual milling machine used and the squaring process are shown in Fig. 3.3 and Fig. 3.4, respectively. The tool used for both processes was 20 mm end mill.

Figure 3.3: Milling Machine Used For Facing and Squaring.

Figure 3.4: Squaring Process Using a 20 mm End Mill.

3.4.3 Toolpaths Generation

After an optimised wavy cold plate design is obtained through fluid flow simulations, a computer-aided manufacturing (CAM) software was used to create, design, simulate and generate toolpaths so as to automate the manufacturing process. The CAM software used for this project was the MasterCAM for SOLIDWORKS.

In the software, it was required to select the machine that would be used to fabricate the cold plate after loading in the chosen design from SOLIDWORKS. Due to the shape, size of and the designed features on the product, it was a straightforward decision to select the mill machines. Next, stock setup was carried out by defining the dimensions and origin of the actual stock material that would be sent for CNC Milling

processes. As for this project, the X, Y, and Z dimensions of the stock material were set to be exactly the same as the size of the cold plate (200 mm × 130 mm × 17 mm). The reason for this was that the stock material purchased earlier had already been faced and squared to the exact dimension of the design material using the manual milling machine. Meanwhile, the origin was set at the top left corner of the stock to ease calculations when generating toolpaths.

The different toolpath choices available in the software included facing, contour, pocket and drill. As for the inlet divider, an open pocket toolpath was generated using 4 mm flat end mill going down a depth of 14 mm in 1 mm per step, with a simulated milling duration of 22 hours and 24 minutes. Meanwhile, the toolpath for the outlet divider was created manually due to the simplicity in milling the shape, which were mainly formed by straight lines and simple curves. Next, the toolpath for the wavy channels were created through ramping contour toolpaths with 2 mm end mill going down 1 mm per step until the final depth of 14 mm. Through simulation, the milling process for the wavy channels would take a total of 945 hours and 45 minutes. The simulated milling process for the wavy channels using MasterCAM Simulator is shown in the screenshot in Fig. 3.5. Lastly, the toolpath for the secondary channels were again generated through ramping contour with a 1.5 mm end mill going down a depth of 14 mm. However, the depth per step was set at 0.5 mm, considering the small mill tool size. This milling process was expected to take 6 hours and 46 minutes until completion. The screenshot of the toolpaths generated are summarised in the left portion of the MasterCAM interface that are attached in the Appendices section from A-21 to A-23.

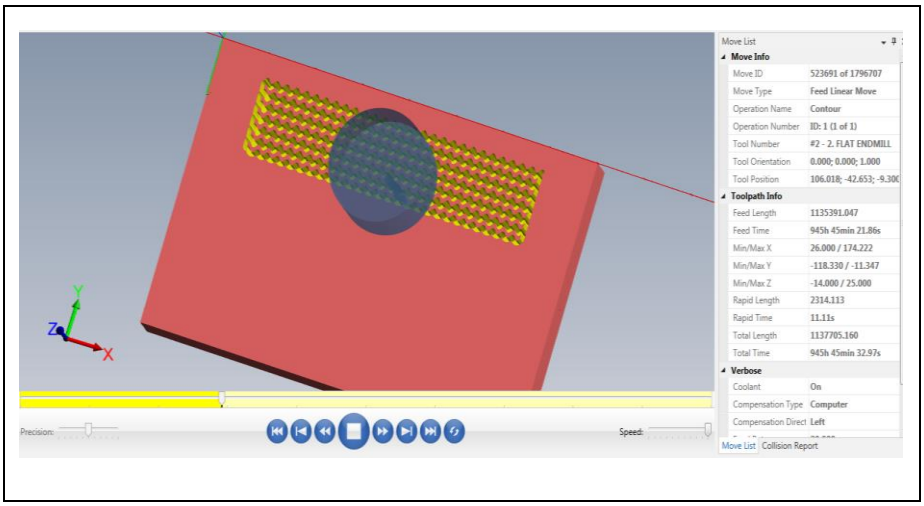

Figure 3.5: CAM Simulation of Milling Process For Wavy Channels.

On a side note, the feed rate of the mill tools cutting in the Z-direction was set at 10 mm per minute (F10) while going in 20 mm per minute (F20) in the X and Y-axis directions. After being created and simulated, the toolpaths for each part of the design were then converted into several programmes in the form of G-Codes and M-Codes. Prior to transmitting the codes to the CNC milling machine, however, it was necessary to do some modifications on the generated programmes so as to simplify the codes and reduce the overall milling process duration.

3.4.4 Cutting Tools

As mentioned in the previous section, the mill tools chosen to perform the CNC milling process were flat end mills with different diameters of 4 mm, 2 mm, and 1.5 mm. In fact, the inlet divider would be fabricated using the 4 mm end mill, which was readily available in the workshop. Meanwhile, the outlet divider with maximum channels gap of 3 mm was fabricated using 2 mm end mill. Similarly, the wavy channels with channels gap of 3 mm were milled using 2 mm end mill. Lastly, 1.5 mm end mill was used to fabricate the secondary channels with gap of 1.80 mm. The usage of smaller diameter end mills allowed smaller channels and wider channels to be milled simultaneously. Also, the 1.5 mm and 2 mm end mills were more widely available in the market. For the 1.5 mm end mill, it has a 2.3 mm cutting length, 16 mm neck length, 50 mm total length with 4 mm shank diameter. Meanwhile, the 2 mm end mill has a 3 mm cutting length, 16 mm neck length, 50 mm total length with 4 mm shank diameter. Both the 1.5 mm and 2 mm end mills have two flutes, which increased the cutting rate and better prevented chips from clogging and adding chips load onto the cutting edge. The 1.5 mm, 2 mm and 4 mm end mills used for this project were of long series in which the neck length was long enough for cutting 14 mm depth channels. The cutting tools are shown Fig. 3.6.

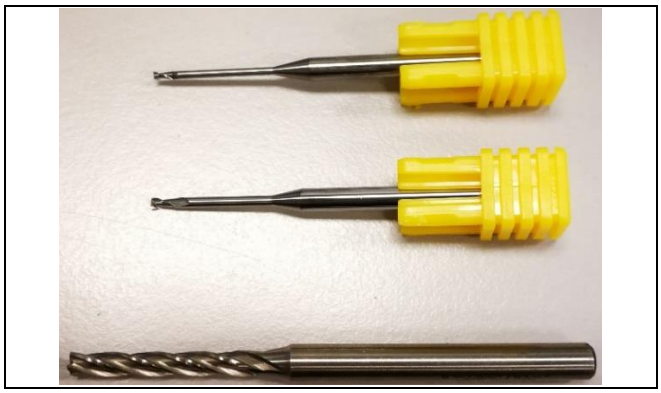

Figure 3.6: The 1.5 mm, 2 mm and 4 mm End Mills From Top To Bottom.

3.4.5 CNC Milling Machine

After getting all the cutting tools in place, the CNC milling process began. The CNC milling machine was used to fabricate the inlet and outlet dividers, the wavy channels as well as the secondary channels by reading the NC Codes generated through MasterCAM. There were different modes on the control panel, including Home, Edit, Auto, Manual Data Input (MDI) and Rapid. The Home mode was applied when it was required to send the tools and the work-table to their home positions in all three axes. The control knob was turned to Edit mode when one would like to edit the G-codes that had been transmitted into the machine. Next, the Auto mode allowed the machine to read and perform the programme according to the NC codes block-by-block. Furthermore, the MDI mode allowed one to manually key in the G-codes into the machine. This would be an ideal mode option to be applied when the codes are short and simple as the user would not have to transmit them through laptop, but keying in the codes directly on the display panel. Lastly, the Rapid mode was used to move the cutting tool in Z-axis direction while the work-table in both X and Y directions according to the selected moving speed. Besides selecting the operation mode, the control panel also allowed user to adjust the feed rate and spindle speed manually. The V-40 Leadwell CNC milling machine used for this project is shown in Fig. 3.7.

Figure 3.7: Leadwell V-40 Model CNC Milling Machine Used For The Project.

As for this project, after obtaining the desired aluminium block dimension through facing and squaring, the block was then being clamped to a CNC milling machine using precision vice. The alignment of the precision vice was adjusted so that the jaw of the vice is aligned with the X and Y-axes, with the aid of a dial indicator. The set up process was proceeded by setting the absolute origin of the aluminium block on the precision vice. In fact, an edge finder was used to acquire the X and Y coordinates of the machine that met with the origin of the stock material. Meanwhile, the Z coordinate of the machine was determined by placing a 0.1 mm feeler gauge on the top surface of the block until the tip of the end mill touched the gauge. The meeting point was taken to be equivalent to Z= 0 mm of the stock material.

After that, the NC Codes generated through MasterCAM was being transferred from a laptop to the CNC Machine using a software called NCnet Lite 7 with the aid of the RS232 driver. After final checking of the codes on the display panel, the machine was switched to Auto mode to run the milling process. The steps were repeated for each depth step and for each channel. As for this project, the inlet and outlet dividers were milled first, before proceeding for the wavy channels and ended with secondary channels contour ramping.

When operating the CNC milling machine, there were several precaution steps that should be taken into account. Firstly, it was essential to switch on the coolant during the milling operation to prevent premature breaking due to excessive temperature at the point of cut. Also, the flushing of coolant on the tool and material would prevent the aluminium chips from being clogged on the tools or in the narrow channels. The flushing of coolant on the cutting tool and material is shown in Fig. 3.8 below. Other than this, it was vital to always keep an eye on the motion of the cutting

pathway and the feed rate as well as the spindle speed of the cutting tools during operation. This would ensure that any motion that went rogue could be stopped immediately, thus preventing damage caused on the material. Also, the feed rate control knob would be adjusted from time to time, depending on the position and motion of the cutting tools, to prevent tool breakage as well as allowing faster cutting feed when cutting simpler channels.

Figure 3.8: Coolant Was Switched On During Milling Operation.

3.5 Summary

The designs of wavy channels cold plate were modelled using SOLIDWORKS and the operating conditions were simulated through ANSYS CFX. These two steps were repeated back and forth to obtain the desired heat removal performance of the cold plate. In order to have a more structured modelling and simulation process, the Taguchi Method was applied to narrow down and reduce the number of possible designs for simulations. The spreadsheet created for the Method was attached in the Appendices section from A-5 to A-8. Next, computer-aided manufacturing was carried out to generate the toolpaths and NC codes so as to turn the optimised conceptual design into a physical product. At the same time, a slightly oversized 6061 aluminium block was purchased before converting the block into the stock material for the cold plate through facing and squaring. Also, end mills of 1.5 mm and 2 mm diameters were purchased as it was not readily available in the workshop. Two-flutes end mills were chosen to allow better chips removal rate within the small channels gap. After making sure that all materials and equipment were set up in place, the NC codes generated were transferred into the CNC milling machine through a programme transmission driver. Lastly, the correct procedures of operating the CNC milling machine were carried out and repeated for each channels and depth step to produce the prototype.

CHAPTER 4

RESULTS AND DISCUSSIONS

4.1 Introduction

As mentioned in Chapter 3, fluid flow simulations were carried out using ANSYS CFX to test the heat removal performance of the cold plate under different fluid mass flow rate. Through simulation, the maximum and minimum heat source-cold plate interface temperatures. Also, the average fluid pressure readings at the inlet and outlet were acquired. The variations in heat source-cold plate interface temperature and pressure drop were then calculated using Eq. 3.1 and Eq. 3.2. The two variation readings were studied and investigated correspondingly with the design of the cold plate. In fact, the variation of the interface temperature with fluid mass flow rate of 50 g/s had to be as close to 5 ℃ as possible to prevent damaging the heat source (electronic devices). Also, the pressure drop of fluid across the cold plate should be lower than the tensile yield strength (276 MPa) and Ultimate Yield Strength (310 MPa) for a 6061 Aluminium plate. If the targets were not met, this process would be repeated back and forth with the aid of the Taguchi Method until an optimised cold plate design was obtained.

For the Part 1 of this project, simulation has been carried out to investigate the thermal management performance of a conventional wavy channels cold plate and a wavy channels cold plate with secondary branches under fluid mass flow rate of 50 g/s. The simplified results were tabulated in Chapter 4. Based on the results, the fundamental cold plate design concept has been selected, before proceeding to the second part of this project. Also, the temperature contours for both design concepts were attached in Appendix A.

The design concept selected was a wavy channels cold plate with secondary branches, due to its superior heat removal performance. Thus, in the Part 2 of this project, a number of wavy channels cold plates with secondary flow had been simulated using ANSYS CFX with fluid mass flow rate of 50 g/s to obtain the optimised design. All of these designs were varied in terms of wavelength, channels width, and the number of secondary branches. The Excel spreadsheets of all the simulation runs that had been carried out were attached in this report as appendices from A-5 to A-8. In Chapter 4, the results for each simulation run in Part 2 of this project would be simplified in a Table for comparison purpose in the next sub-section.

Next, the model with the lowest temperature variation would be chosen as the optimised and finalised design. The thermal performance of the finalised cold plate design would then be verified under fluid mass flow rate of 60 g/s, 70 g/s, 80 g/s, 90 g/s and 100 g/s. At the same instance, graphs of heat source-cold plate interface temperature variations and fluid pressure drops against fluid mass flow rate were plotted to better illustrate the performance of the wavy channels cold plate. Lastly, the parameters of the optimised cold plate design would be tabulated and explained before proceeding to prototype fabrication process.

4.2 Simulation Results

4.2.1 Simulation Results for Part 1

Different design concepts had been simulated and studied during the first part of this project. The concepts simulated were a conventional wavy channels cold plate and a wavy channels cold plate with secondary branches. With fluid mass flow rate of 50 g/s, the simulated results have been recorded as shown below. The maximum and minimum temperature at the heat source-cold plate interface as well as the average fluid pressure at the inlet and outlet were recorded. Next, temperature variations and pressure drops were determined by applying Eq. 3.1 and Eq. 3.2.

Table 4.1: Simulations Results for Project Part 1.

	Heat Source-Cold Plate Interface Temperature (℃)			Average Fluid Pressure (Pa)		
Design Concept	Minimum	Maximum	ΔT	Inlet	Outlet	ΔP
Without Secondary Branches	35.654	43.983	8.3	2805.99	18.0799	2787.910
With Secondary Branches	35.300	42.790	7.5	3271.22	8.3482	3262.872

4.2.2 Overall Simulation Runs for Part 2

After selecting the fundamental design concept from Part 1, the project Part 2 began by carrying out simulation runs with fluid mass flow rate of 50 g/s to test the thermal performance of different designs modelled from the concept. Through Taguchi Method, the scope of designs to be considered had been narrowed down. Similar to the Part 1 of this project, the temperature and pressure readings were recorded. Next, temperature variations and pressure drops were also calculated. The simulation result

for each run is shown in Table 4.2, with the temperature difference rounded up to two decimal places while pressure drops were rounded up to three decimal places for comparison purpose. Meanwhile, the detailed features and parameters for each run design were attached in Appendices from A-5 to A-8.

Table 4.2: Project Part 2 Simulations Results with the Aid of Taguchi Method.

	Interface Temperature (℃)			Average Fluid Pressure (Pa)		
Design	Minimum	Maximum	ΔT	Inlet	Outlet	ΔP
1	34.632	40.318	5.69	4080.88	125.019	3955.861
2	34.717	40.033	5.32	3565.48	113.103	3452.377
3	34.643	40.44	5.80	3334.14	92.9443	3241.196
4	34.856	41.858	7.00	3993.08	93.9833	3899.097
5	34.858	41.112	6.25	3560.01	122.238	3437.772
6	34.854	40.74	5.89	3284.4	95.3247	3189.075
7	35.321	45.328	10.01	3995.51	89.1868	3906.323
8	35.135	42.408	7.27	3236.9	119.375	3117.525
9	35.24	44.311	9.07	3469.27	94.1388	3375.131
10	35.128	42.793	7.67	3172.6	97.0093	3075.591
11	35.182	42.868	7.69	3911.04	90.7183	3820.322
12	34.873	41.92	7.05	3484.23	108.446	3375.784
13	34.926	41.293	6.37	3228.79	91.635	3137.155
14	34.962	41.609	6.65	3993.39	124.778	3868.612
15	34.694	40.91	6.22	3498.68	94.2911	3404.389
16	35.151	42.73	7.58	3241.44	94.4183	3147.022
17	35.197	42.982	7.79	3963.62	115.101	3848.519
18	34.871	42.329	7.46	3515.02	104.33	3410.690
19	35.131	42.724	7.59	3478.88	93.3918	3385.488
20	34.852	42.396	7.54	3239.42	126.665	3112.755
21	34.952	42.334	7.38	3897.91	139.791	3758.119
22	35.45	43.652	8.20	3471.41	100.691	3370.719
23	35.182	44.954	9.77	3213.84	91.2407	3122.599
24	35.187	42.981	7.79	3894.72	136.983	3757.737
25	35.3	43.166	7.87	3422.36	86.6851	3335.675
26	35.004	43.258	8.25	3187.99	92.8463	3095.144
27	35.066	42.536	7.47	3936.98	92.2223	3844.758

Through the first round of ANSYS fluid flow simulation, it was found that the cold plate of Design 2 has the most ideal result. It has a heat source-cold plate interface temperature of 5.32 ℃ with pressure drop of 3452.377 Pa. This design was then taken as the fundamental to be modified through modelling software so as to come out with an optimised cold plate model. Thus, a number of versions were derived from Design 2 and were simulated using ANSYS CFX with the same fluid mass flow rate of 50 g/s. The simulated result is shown in Table 4.3.

Table 4.3: Simulations Results of Models Derived from Design 2.

	Heat source-Cold plate Interface Temperature (℃)			Average Fluid Pressure (Pa)		
Design	Minimum	Maximum	ΔT	Inlet	Outlet	ΔP
Design 2 (V2)	34.635	39.946	5.31	3654.65	124.791	3529.859
Design 2 (V3)	34.475	39.843	5.37	3796.16	80.9693	3715.191
Design 2 (V4)	34.475	39.835	5.36	3752.27	90.3114	3661.959
Design 2 (V5)	34.608	39.987	5.38	3642.12	119.518	3522.602
Design 2 (V6)	34.606	40.528	5.92	3400.2	119.964	3280.236
Design 2 (V7)	34.654	40.52	5.87	3216.67	78.8853	3137.785
Design 2 (V8)	34.62	40.642	6.02	3234.32	76.0403	3158.280
Design 2 (V9)	34.614	40.002	5.39	3518.94	100.142	3418.798
Design 2 (V10)	34.541	40.02	5.48	3483.16	102.474	3380.686
Design 2 (V11)	34.639	39.949	5.31	3616.7	96.0746	3520.625
Design 2 (V12)	34.551	39.97	5.42	3626.67	92.9585	3533.712

4.2.3 Simulation Results of the Optimised Design

In this sub-section, ANSYS CFX simulation was again carried out on the chosen cold plate design (Design 2 (V2)) with fluid mass flow rate of 60 g/s, 70 g/s, 80 g/s, 90 g/s and 100 g/s. Through simulation, the minimum and maximum temperatures at the heat source-cold plate interface were obtained. The results for each mass flow rate were recorded in Table 4.4. Furthermore, the temperature differences between the maximum and minimum temperatures were calculated by applying Eq. 3.1, before rounding up to one decimal place for documentation purpose. Besides that, a graph of Temperature Difference against Mass Flow Rate was plotted for better illustration, as shown in Fig. 4.1.

Table 4.4: Variation of Temperature at Heat Source-Cold Plate Interface for Different Fluid Mass Flow Rate for the Optimised Cold Plate Design.

Fluid Mass Flow Rate (g/s)	**Heat Source-Cold Plate Interface Temperature** (℃)		
	Minimum, T_{min}	**Maximum,** T_{max}	**Difference,** ΔT
50	34.635	39.946	5.3
60	34.269	38.930	4.7
70	33.981	38.228	4.2
80	33.751	37.670	3.9
90	33.562	37.233	3.7
100	33.401	36.901	3.5

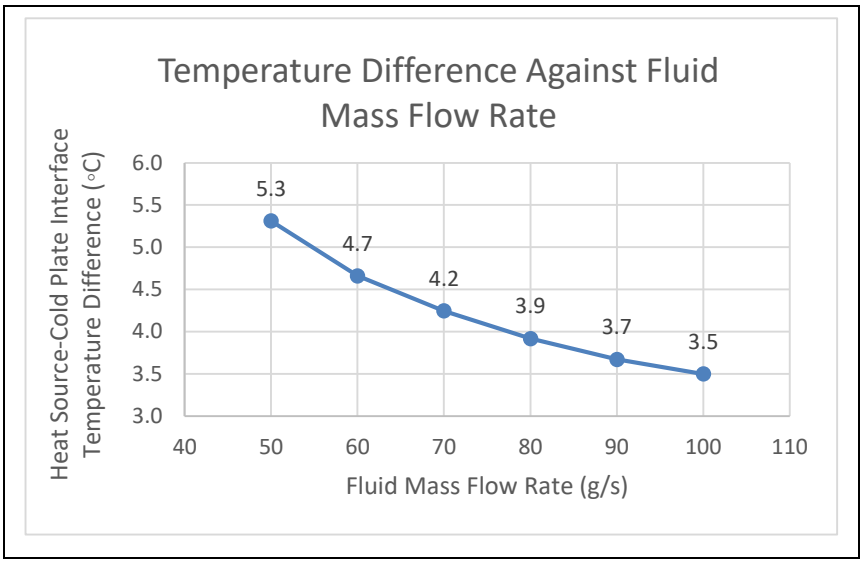

Figure 4.1: Graph of Temperature Difference at Heat Source-Cold Plate Interface Against Fluid Mass Flow Rate for the Optimised Cold Plate Design.

Next, the results acquisition process was proceeded by determining the fluidic pressure readings across the cold plate for the same range of fluid mass flow rate. Through simulation, the average fluidic pressure readings at the inlet and outlet of the cold plate were obtained. The results for each mass flow rate were recorded in Table 4.5. Moreover, the average fluidic pressure drops between the inlet and outlet were calculated by applying Eq. 3.2. Also, a graph of Pressure Drops against Fluid Mass Flow Rate was plotted for better illustration, as shown in Fig. 4.2.

Table 4.5: Average Pressure Readings of Fluid (Water) in the Cold Plate for Different Fluid Mass Flow Rate for the Optimised Cold Plate Design.

Fluid Mass Flow Rate (g/s)	Average Pressure of Fluid (Pa)		
	Inlet, P_{in}	Outlet, P_{out}	Pressure Drop, ΔP
50	3654.650	124.791	3529.859
60	5170.710	194.900	4975.810
70	6861.92	257.713	6604.207
80	8828.640	337.480	8491.160
90	11148.000	434.783	10713.220
100	13509.100	536.640	12972.460

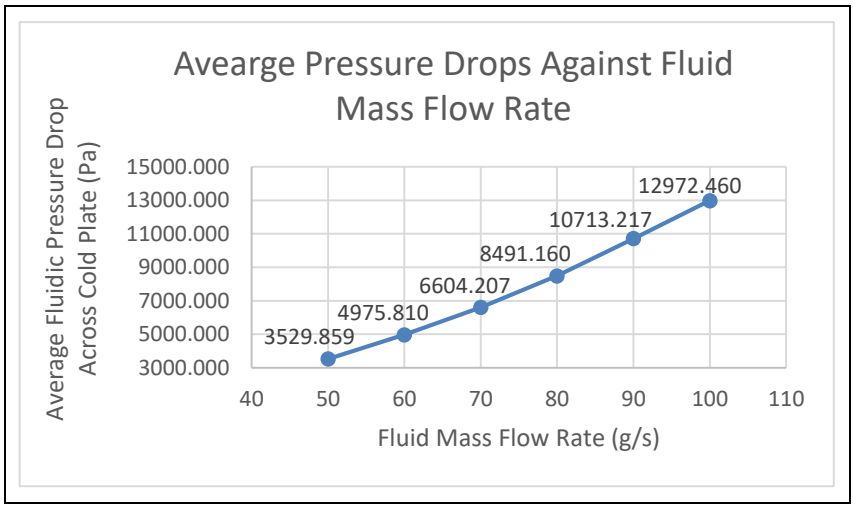

Figure 4.2: Graph of Pressure Drops Across Cold Plate Against Fluid Mass Flow Rate for the Optimised Cold Plate Design.

Sample calculation for temperature difference and pressure drop at fluid mass flow rate of 50 g/s,

∴ Temperature Difference at Heat Source-Cold Plate Interface,

$$\Delta T = T_{max} - T_{min}$$
$$= 39.946\ ℃ - 34.635\ ℃$$
$$= 5.311\ ℃$$
$$= 5.3\ ℃$$

∴ Average Pressure Drops of Fluid Across Cold Plate,

$$\Delta P = P_{in} - P_{out}$$
$$= 3654.650\ \text{Pa} - 124.791\ \text{Pa}$$
$$= 3529.859\ \text{Pa}$$

Based on the tabulated results, the temperature difference across the heat source-cold plate interface for each fluid mass flow rate was found to be either close to or lower than 5 ℃. Also, the highest pressure drop among the mass flow rates simulated was 12972.46 Pa, which was much lower than the tensile yield strength of 276 MPa and Ultimate Yield Strength of 310 MPa for a 6061 Aluminium plate. Therefore, this justified that this particular liquid cold plate design should be chose as the finalised design. The detailed features of this design is shown in Table 4.6 below. Also, the top view of the CAD model obtained from SOLIDWORKS is shown in Fig. 4.3. For in-

detailed illustration, the engineering drawing of the finalised design is attached in Appendix D.

Table 4.6: Detailed Features of the Finalised Wavy Channels Cold Plate Design.

Features	Values
Number of Wavy Channels	21
Wavy Channels Width	3 mm
Wavelength	$5\pi/3$ (5.24 mm)
Waveforms on One Channel	27 complete waveforms
Number of Secondary Channels	74
Secondary Channels Width	1.8 mm
Inlet Divider	6.5 mm
Outlet Divider	2.5 mm – 3 mm
Inlet and Outlet Diameter	6.35 mm

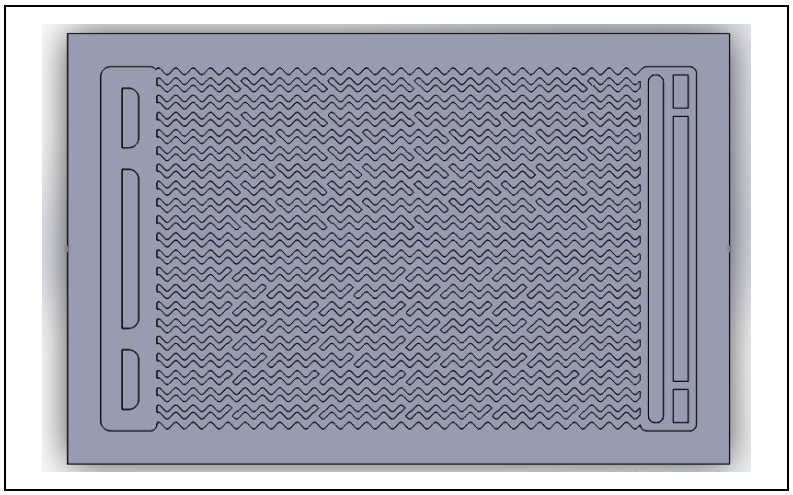

Figure 4.3: Optimised Wavy Channels Cold Plate Design (Top View).

4.3 Prototype Fabrication

After the wavy channels cold plate design was finalised, computer-aided manufacturing procedures were carried out on that model through MasterCAM. At the same time, facing and squaring were performed on the 6061 aluminium block to obtain the exact size of the desired stock material. Next, the NC Codes generated were transmitted to the CNC milling machine for fabrication. End mills of 1.5 mm, 2 mm and 4 mm were used to cut different parts of the 3-D model with channels depth of 14 mm. Due to the shorter toolpaths, the inlet and outlet dividers as well as the secondary channels took shorter duration to be fabricated than the wavy channels. After 31 days of CNC milling process, the fabrication of the wavy channels cold plate with secondary flow was completed as shown in Fig. 4.4 and in Appendix E. Lastly, the project was ready for research reporting and documentation.

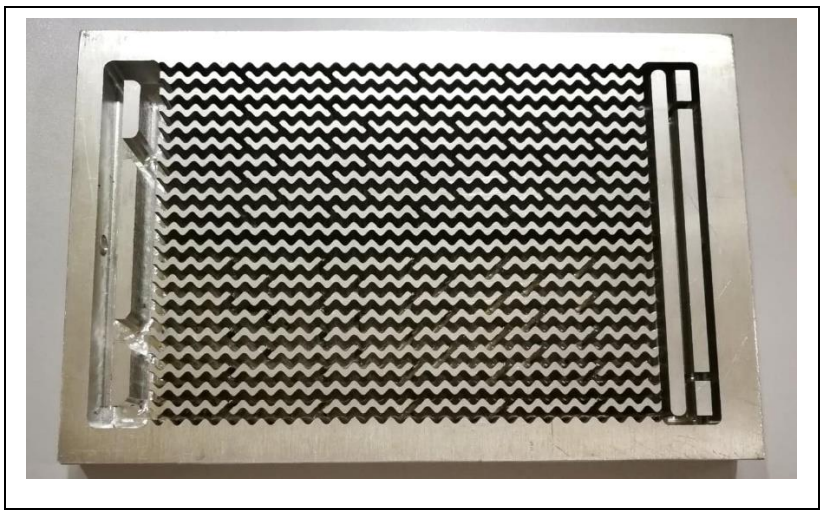

Figure 4.4: Fabricated Wavy Channels Cold Plate Prototype (Top View).

4.4 Discussion

As mentioned earlier, the objectives of this project were to optimise the thermal performance of wavy channels cold plate and to fabricate the cold plate prototype. Therefore, simulation procedures were carried out to investigate the heat removal performance and to figure out the enhanced design. As such, the temperature distribution at the heat source-cold plate interface was an ideal indicator on the heat dissipation efficiency of the cold plate. In fact, the smaller the temperature difference at that interface, the better the design, since a large variation in temperature will adversely impact the normal operation of the heat source (electronic device). As for this project, temperature variation of 5 ℃ or lower was set as the threshold for a cold plate model to be considered as an ideal design.

Based on the simulation results portrayed in Table 4.1, the first part of the project had justified that a wavy channels cold plate with secondary branches have better thermal management performance than a conventional wavy channel cold plate. In fact, the tabulated results showed that with secondary branches, the temperature variation at the interface between heat source and cold plate were lower (7.5 ℃) as compared to that of the conventional design concept (8.3 ℃). The increase in heat removal rate was due to the introduction of secondary fluid flow in the channels, thus enhancing the rate of liquid mixing. On the other hand, the increase rate of secondary fluid flow would also increase the rate of disruption of fluid boundary layer. As a result, the design concept with secondary branches have higher fluid pressure drop (3262.872 Pa) across the cold plate than that without the secondary branches (2787.910 Pa). However, the fluid pressure drops were all well below the tensile yield strength of a 6061 aluminium plate. Therefore, after comparing the temperature and pressure variations of both design concept, the wavy channels with secondary branches was selected as the fundamental design concept to kick-start the Part 2 of the project.

Based on the simulation results portrayed in Table 4.2, the first round of simulation in Part 2 have shown that the Design 2 has the lowest heat source-cold plate interface temperature difference recorded at 5.32 ℃. Also, the pressure drop was determined to be 3452.377 Pa. Meanwhile, Design 7 has the highest temperature variation of 10.01 ℃ among all the design at the same interface with fluid pressure drop of 3906.323 Pa. When comparing both of these designs with extreme temperature values, with reference to A-5, it was found that Design 7 has wider wavy channels at the middle of the plate than that of Design 2. Also, the wavy channels in Design 7 has

longer wavelength, thus lesser waveforms per channel than Design 2. Furthermore, the number of secondary channels of Design 7 was lesser than that in Design 2. These features have caused the lesser occurrence of liquid mixing and secondary flow of fluid across the channels in Design 7, which eventually reduced the rate of heat transfer between the liquid and cold plate. Hence, with features totally opposite from that in Design 7, the Design 2 model with the lowest temperature variation was taken as the best design for the Stage 1 of fluid flow simulation. Design 2 model was then taken as the benchmark for further improvement during modelling and simulation in Stage 2.

Modifications were made based on the fundamental of Design 2 and several versions of Design 2 were then being modelled. Based on the readings shown in Table 4.3, the Version 2 and Version 11 of Design 2 have resulted in the lowest interface temperature variation values, with both recorded at 5.31 ℃. As for this project, Version 2 of Design 2 was chosen over Version 11 as the optimised wavy channels cold plate design. This was due to the fact that the maximum interface temperature of Version 11 was slightly higher than Version 2. Besides that, the more persuasive reason was the feasibility in machining process. In fact, the milling process of Version 11 would likely to take longer duration since it has an inlet divider made up of 7 mm and 8 mm channels, as shown in Appendices A-6. This would in turn require longer and more complicated milling toolpaths. Meanwhile, the model of Design 2 Version 2 only has a single width value for the inlet divider, which was 6.50 mm.

Hence, the Version 2 of Design 2 for the wavy channels cold plate was chosen as the optimised design for this project. Its thermal performance was then verified through simulation under fluid mass flow rate from 50 g/s to 100 g/s. With reference to Table 4.4, the highest maximum interface temperature reading was found to be 39.946 ℃, which occurred when the coolant flew through in 50 g/s. Meanwhile, the lowest maximum interface temperature of the system was found to be 36.901 ℃, which occurred when the fluid mass flow rate was set at 100 g/s. Furthermore, it was observed that the temperature difference was all lower than 5 ℃, except for the fluid mass flow rate of 50 g/s. In relation to that, the tabulated result shows that the temperature variation would decrease exponentially when fluid mass flow rate increased. This was due to the fact that when flow rate increases, Reynolds number would increase, which in turn increases the rate of heat transfer. Therefore, it can be said that the thermal

performance of the wavy channels cold plate is enhanced when the fluid is flowing across the model at higher flow rate.

Besides investigating the temperature variation at the heat source-cold plate interface, the second indicator on cold plate performance was the pressure drops of coolant across the model. As a matter of fact, the lower the pressure drops of water across the cold plate, the more feasible is the design, since a large pressure drops might damage the structure of the channels in a long run. In order to determine pressure drops across the cold plate, the average fluid pressure at the inlet and outlet of the cold plate must be obtained. During the data acquisition process, it was vital to ensure that the pressure readings were not higher than the typical tensile yield strength (276 MPa) and ultimate yield strength (310 MPa) of a 6061 aluminium block. This would prevent pressure drops of fluid from damaging the structure of thin channels within the cold plate. Based on the results in Table 4.5, the maximum average fluid inlet and outlet pressure of the system were 13509.100 Pa and 536.640 Pa, respectively. Both of which have occurred at a fluid mass flow rate of 100 g/s. This resulted in the highest pressure drop of the system of 12972.460 Pa. By observing the pressure drops with respect to the fluid mass flow rate across the cold plate, it was shown that when the fluid mass flow rate increased, the average pressure drops increased almost linearly. One contributing factor was the disruption of boundary layers due to increased rate of liquid mixing, especially when secondary channels were also present. As a result, the wall shear stress along the channel walls increased with significant pressure drop. Therefore, it was recommended to apply lower coolant mass flow rate when operating the cold plate to avoid high pressure drops and damaging the model.

After verifying the cold plate design through temperature variation and pressure drop readings under different fluid mass flow rates, the model was then considered to be optimised and finalised. The features and parameters comprised in the cold plate design were documented. With reference to Table 4.6, the cold plate was made up of 21 wavy channels with channels width of 3 mm. The wavelength for the channels was 5.24 mm, which was modelled from the function equation of $y = \sin 1.2x$. This formed a total of 27 waveforms per channel. When comparing with the other designs listed in Table 4.2 and Table 4.3, with reference to A-5 and A-6, the finalised design with short wavelength has the best thermal performance. This was due to the waveform design which promoted a large contact area between the coolant and the channels wall which would increase the surface area for heat transfer to occur as

well as generating Dean vortices to the fluid. However, the wavelength was not to be too short that it might retain the fluid and stall the fluid flow in the channels which would in turn affect the heat removal performance.

Furthermore, secondary flow was promoted in the system through the introduction of secondary channels. A total of 74 secondary channels with 1.8 mm width were formed. This allowed the coolant to flow from one channel to the next halfway, and mix with the main channels coolant. The mixing of coolant from one channel to that in the next would form Dean vortices which improve the rate of heat transfer.

Moreover, inlet and outlet dividers were introduced at both ends of the plate to direct the flow of fluid into and out of the cold plate. The dividers were made up of channels of different width. The inlet divider, for instance, have channels width of 6.5 mm. By comparing the simulation results with the other designs listed in Table 4.2 and Table 4.3, with reference to A-5 and A-6, it was found that when the inlet divider width was decreased, the maximum heat source-cold plate interface temperature would increase. This in turn increased the temperature variation readings, which was undesirable for normal operation of electronic devices. On the other hand, the outlet divider was made up of channels of 2.5 mm and 3.0 mm. This section of the cold plate was designed to increase the time and surface area in which the fluid was in contact with the cold plate wall, which would further enhance the heat transfer to the fluid before flowing out of the cold plate. Lastly, the inlet and outlet were tapered hole and the diameter had been set in advance at 6.35 mm (0.25 inch). Pipes will be connected to the tapered hole to channel the water in and out of the cold plate under different mass flow rate. As the final step, toolpaths were generated for the model for CNC milling procedure. The fabrication process took a total of 31 days to be completed using 1.5 mm, 2 mm and 4 mm end mills.

4.5 Summary

From the Part 1 of the project, it was deduced that the introduction of secondary flows would improve the thermal management performance of a conventional wavy channels cold pate. Thus, it was chosen as the fundamental design concept to begin with in the Part 2 of the project. The temperature contours of both the design concepts from Part 1 were attached in Appendix A. With the aid of Taguchi method, a number of wavy channels cold plate designs had been modelled and simulated through fluid flow

analysis to determine the thermal performance of each design in heat removal operation for electronic devices. The fluid mass flow rate for the first stage of simulations were set at 50 g/s. During simulation, the readings that were of interest for this project were the temperature variation at heat source-cold plate interface and the pressure drop of fluid across the cold plate. In fact, the temperature variation should be close to or below 5 ℃ to prevent thermal shock to the electronic device. Also, pressure drop across the cold plate should be lower than the tensile yield strength (276 MPa) and ultimate yield strength (310 MPa) of a 6061 aluminium block. Through the first round of simulation, the most ideal design was chosen to undergo the second round of modelling and simulation. As a result, the optimised wavy channels cold plate design was generated. The simulation results were all tabulated in separated Tables the previous subsections and have been attached in Appendices section. Next, the optimised design underwent verification process through fluid flow analysis under different fluid mass flow rate. The simulation results were tabulated in the Results section. Also, the simulation contours of the optimised design were attached in Appendix C. Based on the recorded results, the temperature variation would decrease almost exponentially when the fluid mass flow rate increased in steps from 50 g/s to 100 g/s. This phenomenon was attributed to the increased rate of liquid mixing and heat transfer when fluid flow through the channels at higher flow rate. The liquid mixing was further enhanced through the introduction of secondary channels in the cold plate which promoted the occurrence of secondary flow or dean vortices. However, the optimised thermal performance of the chosen cold plate design was also accompanied by an increase in fluid pressure drop. In fact, the pressure drop increased almost linearly when the optimised design was simulated with increasing fluid mass flow rate. One contributing factor was the disruption of boundary layers due to increased rate of liquid mixing. As a result, the wall shear stress along the channel walls increased with significant pressure drop. After obtaining the finalised cold plate design with its features and parameters documented, milling toolpaths for the model was generated, before proceeding to prototype fabrication. CNC milling machine was operated for a total of 31 days to create the prototype for this project.

CHAPTER 5

CONCLUSIONS AND RECOMMENDATIONS

5.1 Conclusions

In the Part 2 of the project, the point of focus was to optimise the wavy channels cold plate design based on the literature and researches reviewed in Part 1. A number of cold plate concepts have been modelled and simulated through fluid flow analysis at fluid mass flow rate of 50 g/s, before choosing the most ideal design. A temperature variation across the length of heat source-cold plate interface of close to or below 5 ℃ was an indicator of a good design. Also, the fluid pressure drop should not be higher than the tensile yield strength and ultimate yield strength of a 6061 aluminium block. Through thorough simulation and optimisation processes, the most ideal wavy channels cold plate design was numerically verified under different fluid mass flow rate. Based on the simulation results on the optimised design, it was found that the temperature variations was recorded as 5.3 ℃ at flow mass rate of 50 g/s. Meanwhile, the reading was all lower than 5 ℃ when fluid mass flow rate was increased from 60 g/s to 100 g/s, as shown in Chapter 4. In fact, the temperature difference across the heat source-cold plate interface decreased when fluid mass flow rate increased. This was due to the increased frequency of liquid mixing, thus improved rate of heat transfer. On the other hand, the pressure drops of fluid across the cold plate channels was found to be increasing when the fluid mass flow rate was increased. This could be attributed to the increase in boundary layer disruptions, hence increasing the wall shear stress along the channels wall. After the cold plate design has been finalised, the associated features were documented in Chapter 4. In short, the model was made up of 21 wavy channels with wavelength of 5.24 mm. Also, 74 secondary channels with 1.8 mm width were introduce to further promote secondary flow and mixing of fluid. Moreover, inlet and outlet dividers of different widths were created to direct the flow of fluid while stabilising fluid pressure drops across the cold plate. Lastly, the wavy channels cold plate prototype was fabricated using CNC milling machine with end mills of 1.5 mm, 2 mm and 4 mm. In a nutshell, the correct procedures in carrying out the optimisation process were conducted and a prototype was milled based on the

finalised wavy channels cold plate design. Hence, the aims and objectives set for this project have been achieved.

5.2 Recommendations for future work

After conducting this project, it was found that there are several recommendations that can be applied if the effort is to be proceeded for future work. Firstly, the prototype fabricated can be sent for experimental testing. This is due to the fact that an ideal condition was assumed during the fluid flow analysis and simulation procedure. In actual case, however, thermal resistance exists at the interface between the heat source and cold plate and that will definitely affect heat transfer between these surfaces. Through experiments, the actual heat removal performance of the wavy channels cold plate can be obtained before determining the percentage errors involved. Furthermore, if experimental work is to be carried out, it is recommended to do a National Pipe Thread (NPT) tapping at both the inlet and outlet of the liquid cold plate. NPT tapping allows the connection between pipes and cold plate to be sealed tightly. This will thus prevent any kind of fluidic leakage during experimental testing. Moreover, a test rig is recommended to be constructed to hold the liquid cold plate for experimental works. In fact, a test rig can also be used during normal operation when cooling an electronic device. This is because the test rig is able to hold the model securely in place and prevent any kind of imbalance, especially when the fluid mass flow rate is high in the liquid cold plate channels. Besides that, it should be noticed that the simulation conducted in this project has included a cover of 3 mm thickness on top of the 17 mm thickness liquid cold plate. Therefore, in actual practice, the fabricated prototype of 17 mm thickness should be covered by a 3 mm aluminium plate to prevent the fluid flowing in channels from coming in contact with the electronic device (heat source). This measure will also retain a thermal performance that is as close to that simulated as possible.

REFERENCES

Akbarzadeh, M., Rashidi, S. and Esfahani, J.A., 2017. Influences of corrugation profiles on entropy generation, heat transfer, pressure drop, and performance in a wavy channel. *Applied Thermal Engineering*, [online] 116, pp.278–291. Available at: <https://www-sciencedirect-com.libezp2.utar.edu.my/science/article/pii/S1359431116319603> [Accessed 24 Jun. 2018].

ASM Aerospace Specification Metals Inc., 2018. *ASM Material Data Sheet*. [online] Available at: <http://asm.matweb.com/search/SpecificMaterial.asp?bassnum=ma6061t6> [Accessed 2 Nov. 2018].

Bermel, Thomas W. (Corning, N.Y.., 1968. *FLUIDIC DIODE*. 3,480,030.

Chen, D., Jiang, J., Kim, G.-H., Yang, C. and Pesaran, A., 2016. Comparison of different cooling methods for lithium ion battery cells. *Applied Thermal Engineering*, [online] 94, pp.846–854. Available at: <https://www-sciencedirect-com.libezp2.utar.edu.my/science/article/pii/S1359431115010613> [Accessed 1 Jul. 2018].

Chiam, Z.L., Lee, P.S., Singh, P.K. and Mou, N., 2016. Investigation of fluid flow and heat transfer in wavy micro-channels with alternating secondary branches. *International Journal of Heat and Mass Transfer*, [online] 101, pp.1316–1330. Available at: <https://www-sciencedirect-com.libezp2.utar.edu.my/science/article/pii/S0017931016306093> [Accessed 23 Aug. 2018].

Ghani, I.A., Kamaruzaman, N. and Sidik, N.A.C., 2017. Heat transfer augmentation in a microchannel heat sink with sinusoidal cavities and rectangular ribs. *International Journal of Heat and Mass Transfer*, [online] 108, pp.1969–1981. Available at: <https://www-sciencedirect-com.libezp2.utar.edu.my/science/article/pii/S0017931016337644> [Accessed 3 Jul. 2018].

Gong, L., Zhao, J. and Huang, S., 2015. Numerical study on layout of micro-channel heat sink for thermal management of electronic devices. *Applied Thermal Engineering*, [online] 88, pp.480–490. Available at: <https://www-sciencedirect-com.libezp2.utar.edu.my/science/article/pii/S1359431114008205> [Accessed 3 Jul. 2018].

Harikrishnan, S. and Tiwari, S., 2018. Effect of skewness on flow and heat transfer characteristics of a wavy channel. *International Journal of Heat and Mass Transfer*, [online] 120, pp.956–969. Available at: <https://www-sciencedirect-com.libezp2.utar.edu.my/science/article/pii/S0017931017341509> [Accessed 24 Jun. 2018].

Jarrett, A. and Kim, I.Y., 2011. Design optimization of electric vehicle battery cooling plates for thermal performance. *Journal of Power Sources*, [online] 196(23), pp.10359–10368. Available at: <https://www-sciencedirect-com.libezp2.utar.edu.my/science/article/pii/S0378775311013279> [Accessed 29 Jun. 2018].

Khabarova, D.F., Podzerko, A.V. and Spiridonov, E.K., 2017. Experimental Investigation of Fluidic Diodes. *Procedia Engineering*, [online] 206, pp.93–98. Available at: <https://www-sciencedirect-com.libezp2.utar.edu.my/science/article/pii/S1877705817351263> [Accessed 1 Jul. 2018].

Kheirabadi, A.C. and Groulx, D., 2018. Experimental evaluation of a thermal contact liquid cooling system for server electronics. *Applied Thermal Engineering*, [online] 129, pp.1010–1025. Available at: <https://www-sciencedirect-com.libezp2.utar.edu.my/science/article/pii/S1359431117354030> [Accessed 1 Jul. 2018].

Kiflemariam, R. and Lin, C.-X., 2015. Numerical simulation of integrated liquid cooling and thermoelectric generation for self-cooling of electronic devices. *International Journal of Thermal Sciences*, [online] 94, pp.193–203. Available at: <https://www-sciencedirect-com.libezp2.utar.edu.my/science/article/pii/S1290072915000708> [Accessed 1 Jul. 2018].

Kobsa, Irvin R. (San Jone, C., 1992. *FORCED-CIRCULATION REACTOR WITH FLUIDC-DODE-ENHANCEO NATURAL CIRCULATION*. 5,303,275.

Lan, C., Xu, J., Qiao, Y. and Ma, Y., 2016. Thermal management for high power lithium-ion battery by minichannel aluminum tubes. *Applied Thermal Engineering*, [online] 101, pp.284–292. Available at: <https://www-sciencedirect-com.libezp2.utar.edu.my/science/article/pii/S1359431116302137> [Accessed 29 Jun. 2018].

Li, J., Zhou, X., Li, J., Che, L., Yao, J., McHale, G., Chaudhury, M.K. and Wang, Z., 2017. Topological liquid diode. *Science Advances*, [online] 3(10), p.eaao3530. Available at: <http://advances.sciencemag.org/lookup/doi/10.1126/sciadv.aao3530> [Accessed 1 Jul. 2018].

Lin, L., Zhao, J., Lu, G., Wang, X.-D. and Yan, W.-M., 2017. Heat transfer enhancement in microchannel heat sink by wavy channel with changing wavelength/amplitude. *International Journal of Thermal Sciences*, [online] 118, pp.423–434. Available at: <https://www-sciencedirect-com.libezp2.utar.edu.my/science/article/pii/S129007291631612X> [Accessed 24 Jun. 2018].

Lu, G., Zhao, J., Lin, L., Wang, X.-D. and Yan, W.-M., 2017. A new scheme for reducing pressure drop and thermal resistance simultaneously in microchannel heat sinks with wavy porous fins. *International Journal of Heat and Mass Transfer*, [online] 111, pp.1071–1078. Available at: <https://www-sciencedirect-

com.libezp2.utar.edu.my/science/article/pii/S0017931017309043> [Accessed 24 Jun. 2018].

Mates, J.E., Schutzius, T.M., Qin, J., Waldroup, D.E. and Megaridis, C.M., 2014. The Fluid Diode: Tunable Unidirectional Flow through Porous Substrates. *ACS Applied Materials & Interfaces*, [online] 6(15), pp.12837–12843. Available at: <http://pubs.acs.org/doi/10.1021/am5028204> [Accessed 1 Jul. 2018].

Mohammed, H.A., Gunnasegaran, P. and Shuaib, N.H., 2011. Numerical simulation of heat transfer enhancement in wavy microchannel heat sink. *International Communications in Heat and Mass Transfer*, [online] 38(1), pp.63–68. Available at: <https://www-sciencedirect-com.libezp2.utar.edu.my/science/article/pii/S0735193310002460> [Accessed 23 Aug. 2018].

Naqiuddin, N.H., Saw, L.H., Yew, M.C., Yusof, F., Ng, T.C. and Yew, M.K., 2018. Overview of micro-channel design for high heat flux application. *Renewable and Sustainable Energy Reviews*, [online] 82, pp.901–914. Available at: <https://www-sciencedirect-com.libezp2.utar.edu.my/science/article/pii/S1364032117313709> [Accessed 3 Jul. 2018].

Qian, Z., Li, Y. and Rao, Z., 2016. Thermal performance of lithium-ion battery thermal management system by using mini-channel cooling. *Energy Conversion and Management*, [online] 126, pp.622–631. Available at: <https://www-sciencedirect-com.libezp2.utar.edu.my/science/article/pii/S0196890416307373> [Accessed 29 Jun. 2018].

Ramgadia, A.G. and Saha, A.K., 2012. Fully developed flow and heat transfer characteristics in a wavy passage: Effect of amplitude of waviness and Reynolds number. *International Journal of Heat and Mass Transfer*, [online] 55(9–10), pp.2494–2509. Available at: <https://www-sciencedirect-com.libezp2.utar.edu.my/science/article/pii/S0017931012000117> [Accessed 24 Jun. 2018].

Ramgadia, A.G. and Saha, A.K., 2016. Numerical study of fully developed unsteady flow and heat transfer in asymmetric wavy channels. *International Journal of Heat and Mass Transfer*, [online] 102, pp.98–112. Available at: <https://www-sciencedirect-com.libezp2.utar.edu.my/science/article/pii/S0017931015301277> [Accessed 24 Jun. 2018].

Reed, J.L., 1993. *FLUIDIC RECTIFIER*. 5,265,636.

Rostami, J., Abbassi, A. and Saffar-Avval, M., 2015. Optimization of conjugate heat transfer in wavy walls microchannels. *Applied Thermal Engineering*, [online] 82, pp.318–328. Available at: <https://www-sciencedirect-com.libezp2.utar.edu.my/science/article/pii/S135943111500201X> [Accessed 24 Jun. 2018].

Salman, B.H., Mohammed, H.A., Munisamy, K.M. and Kherbeet, A.S., 2013. Characteristics of heat transfer and fluid flow in microtube and microchannel using conventional fluids and nanofluids: A review. *Renewable and Sustainable Energy Reviews*, [online] 28, pp.848–880. Available at: <https://www-sciencedirect-com.libezp2.utar.edu.my/science/article/pii/S1364032113005522> [Accessed 1 Jul. 2018].

Sui, Y., Teo, C.J., Lee, P.S., Chew, Y.T. and Shu, C., 2010. Fluid flow and heat transfer in wavy microchannels. *International Journal of Heat and Mass Transfer*, [online] 53(13–14), pp.2760–2772. Available at: <https://www-sciencedirect-com.libezp2.utar.edu.my/science/article/pii/S0017931010000979> [Accessed 23 Aug. 2018].

Wieme, Andre (Zwevegem, B., 1972. *FLUIDIC DIODE*. 3,654,946.

Xia, G.D., Jiang, J., Wang, J., Zhai, Y.L. and Ma, D.D., 2015. Effects of different geometric structures on fluid flow and heat transfer performance in microchannel heat sinks. *International Journal of Heat and Mass Transfer*, [online] 80, pp.439–447. Available at: <https://www-sciencedirect-com.libezp2.utar.edu.my/science/article/pii/S0017931014008400> [Accessed 3 Jul. 2018].

Yoder, G.L.J., 2011. *Vortex Diode Analysis and Testing for Fluoride Salt-Cooled High-Temperature Reactors*. Tennessee.

APPENDICES

APPENDIX A: Temperature Contours for Project Part 1

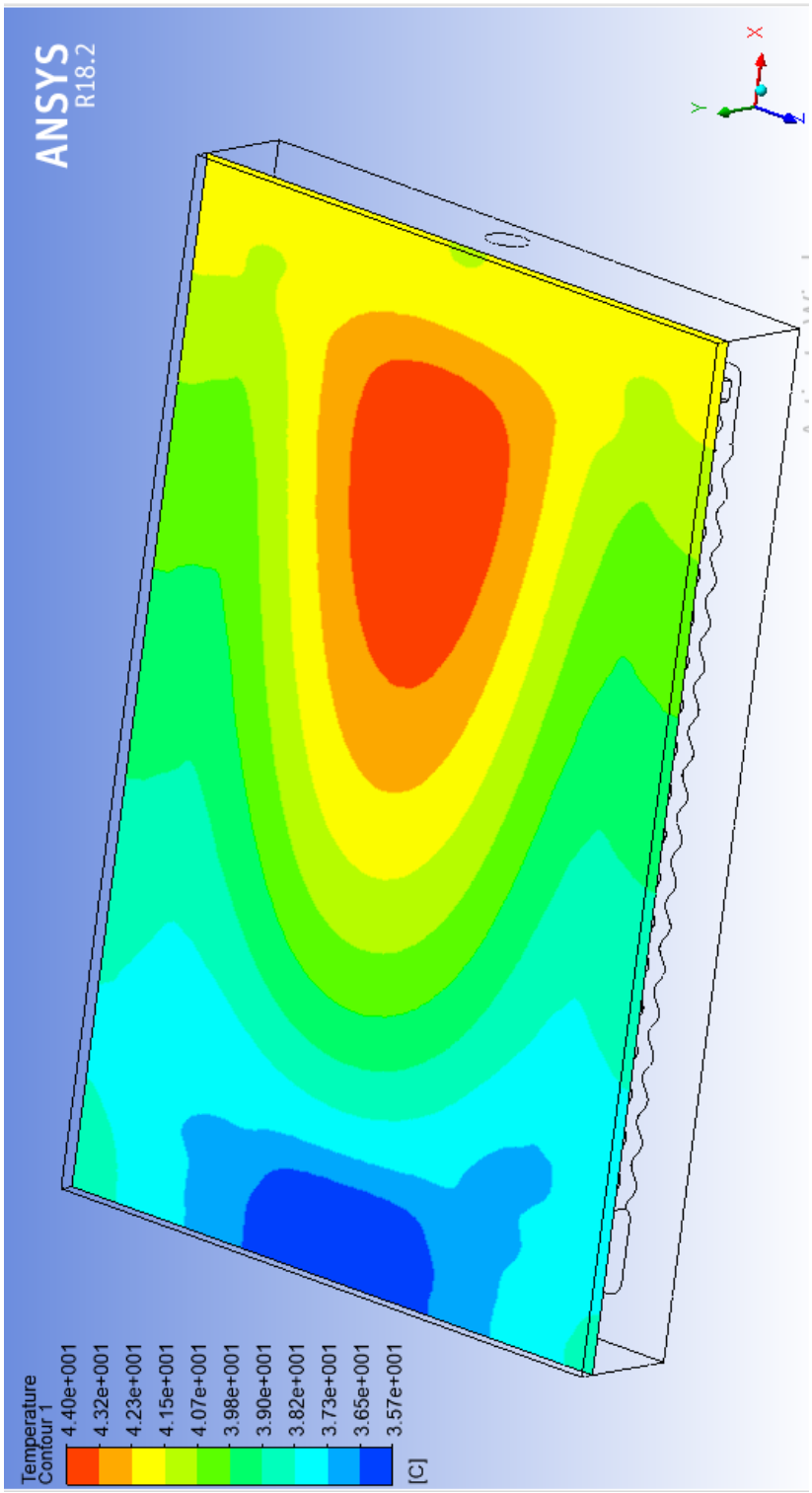

Figure A-1: Temperature Contours at the Heat Source-Cold Plate Interface for Wavy Channels Cold Plate Without Secondary Branches at Fluid Mass Flow Rate of 50 g/s.

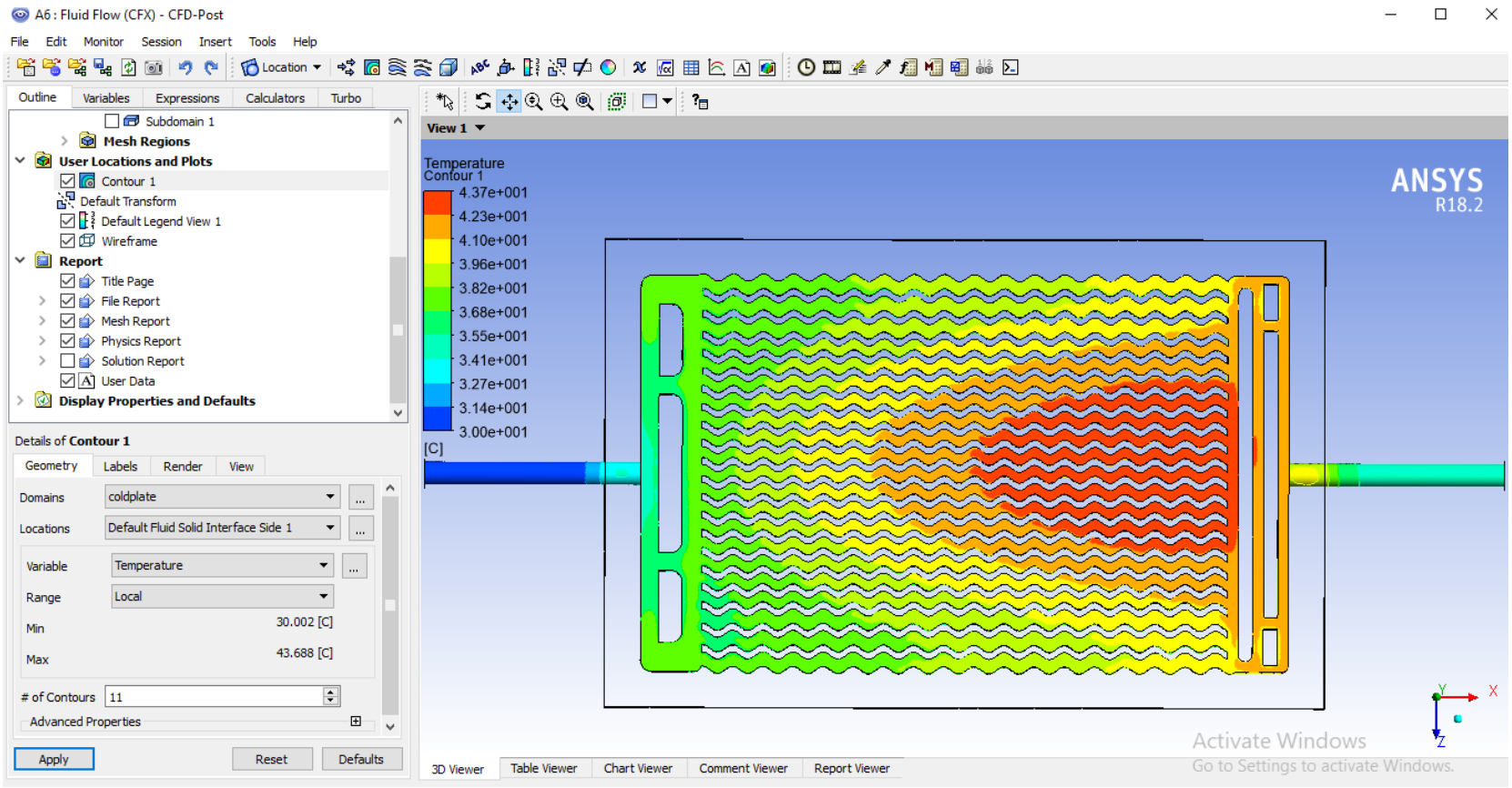

Figure A-2: Temperature Contour at the Fluid-Cold Plate Interface for Design Concept Without Secondary Branches at Fluid Mass Flow Rate of 50 g/s.

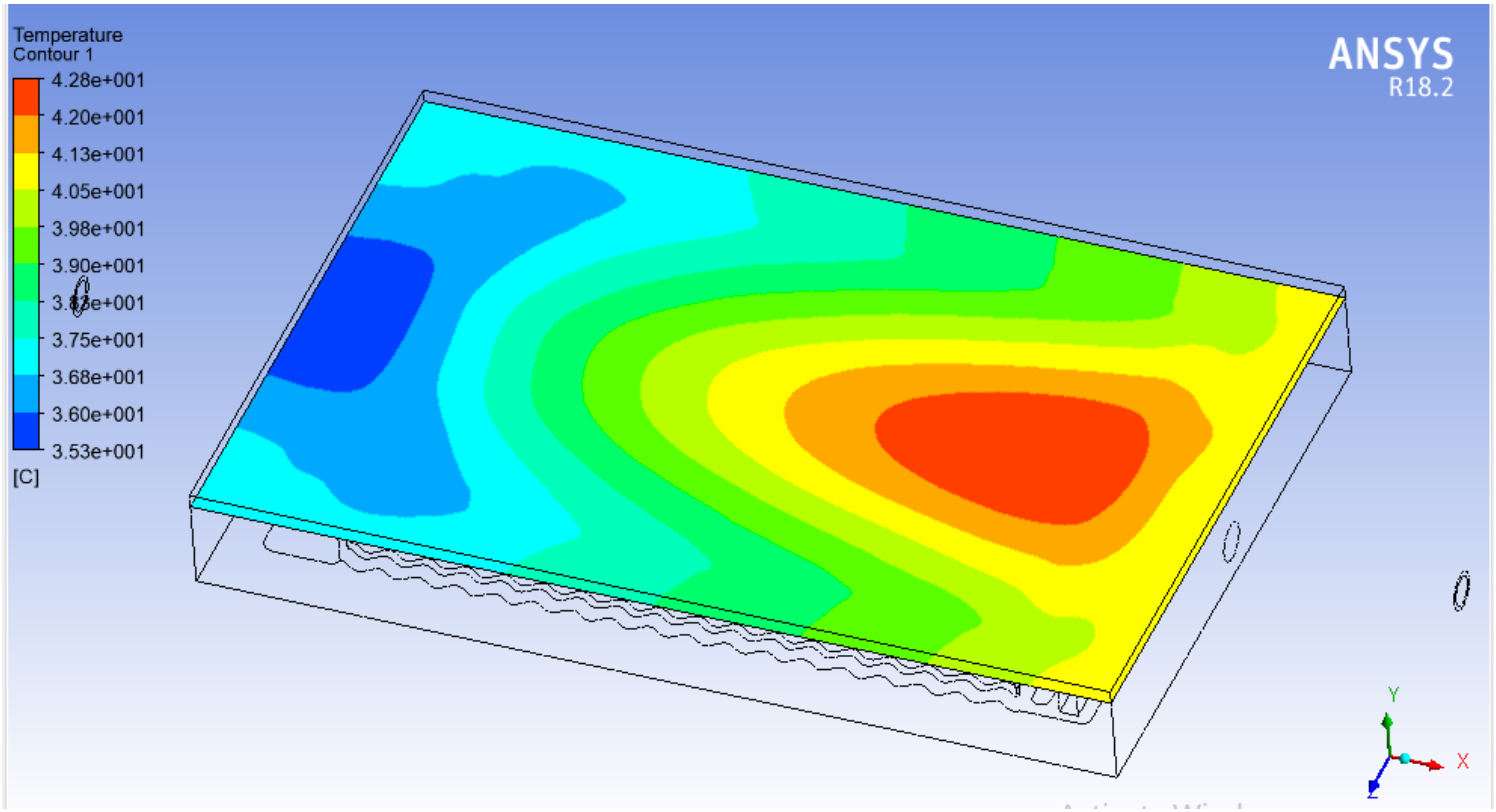

Figure A-3: Temperature Contours at the Heat Source-Cold Plate Interface for Wavy Channels Cold Plate With Secondary Branches at Fluid Mass Flow Rate of 50 g/s.

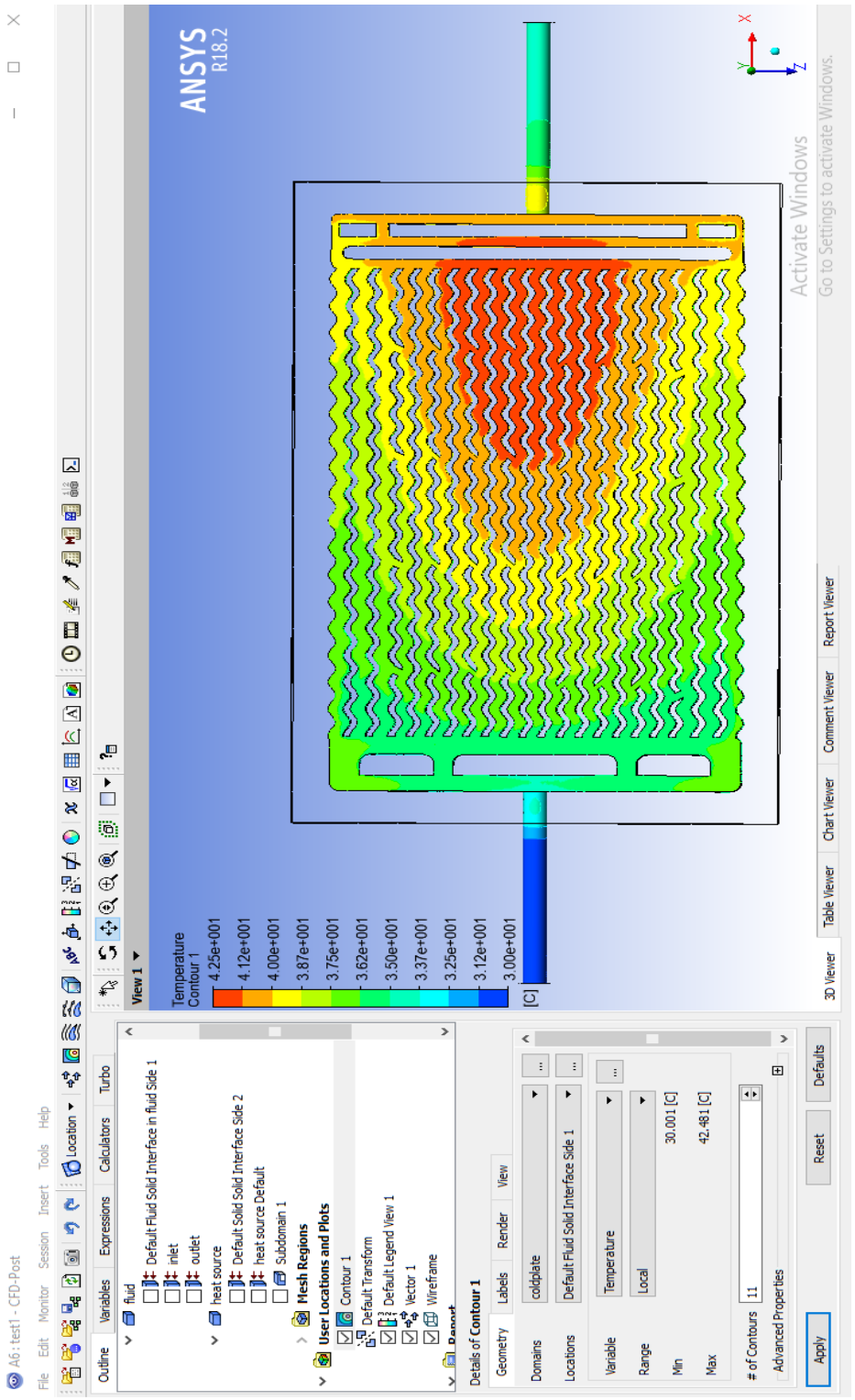

Figure A-4: Temperature Contour at the Fluid-Cold Plate Interface for Design Concept With Secondary Branches at Fluid Mass Flow Rate of 50 g/s.

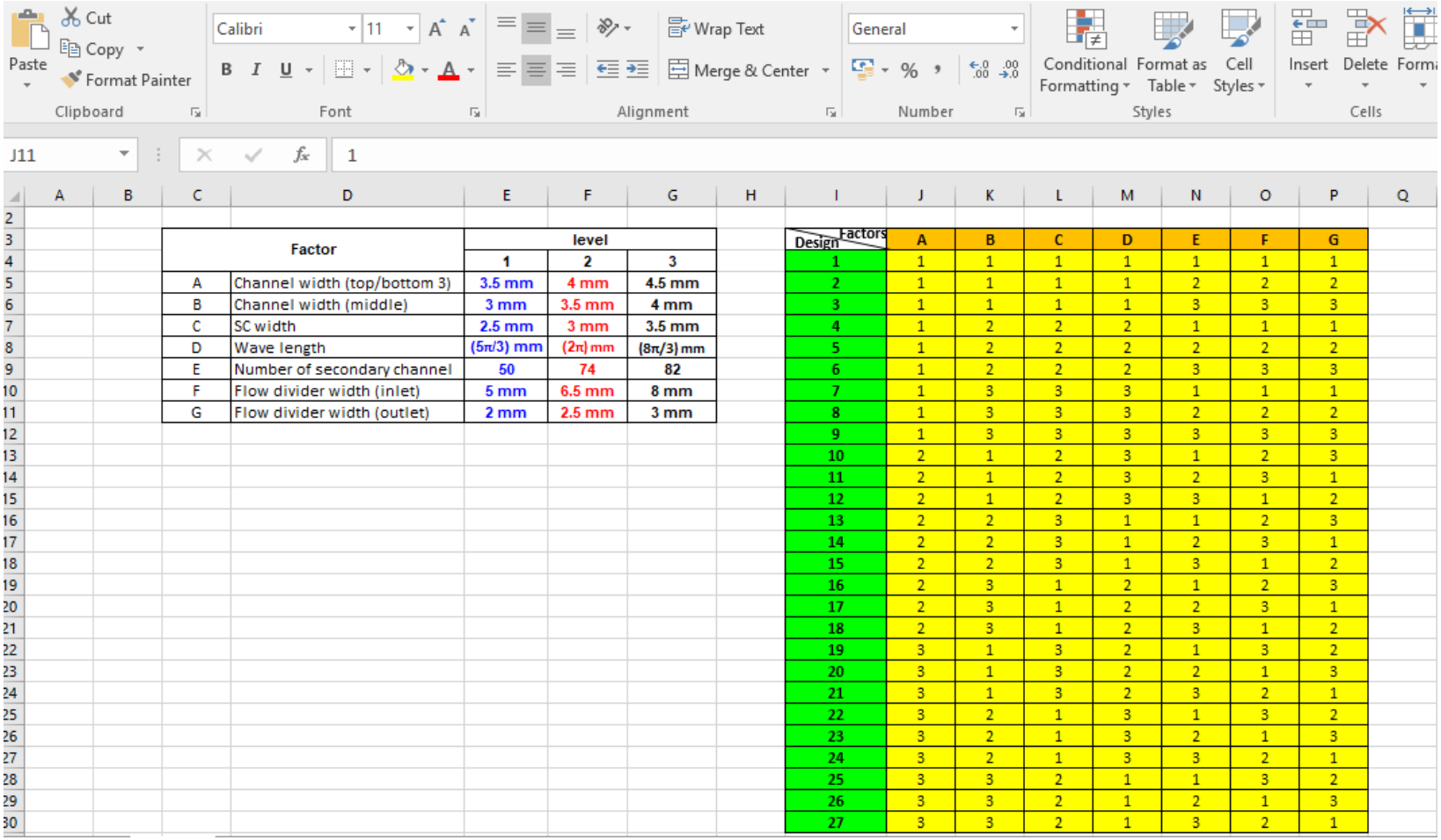

Factor		level		
		1	2	3
A	Channel width (top/bottom 3)	3.5 mm	4 mm	4.5 mm
B	Channel width (middle)	3 mm	3.5 mm	4 mm
C	SC width	2.5 mm	3 mm	3.5 mm
D	Wave length	(5π/3) mm	(2π) mm	(8π/3) mm
E	Number of secondary channel	50	74	82
F	Flow divider width (inlet)	5 mm	6.5 mm	8 mm
G	Flow divider width (outlet)	2 mm	2.5 mm	3 mm

Design \ Factors	A	B	C	D	E	F	G
1	1	1	1	1	1	1	1
2	1	1	1	1	2	2	2
3	1	1	1	1	3	3	3
4	1	2	2	2	1	1	1
5	1	2	2	2	2	2	2
6	1	2	2	2	3	3	3
7	1	3	3	3	1	1	1
8	1	3	3	3	2	2	2
9	1	3	3	3	3	3	3
10	2	1	2	3	1	2	3
11	2	1	2	3	2	3	1
12	2	1	2	3	3	1	2
13	2	2	3	1	1	2	3
14	2	2	3	1	2	3	1
15	2	2	3	1	3	1	2
16	2	3	1	2	1	2	3
17	2	3	1	2	2	3	1
18	2	3	1	2	3	1	2
19	3	1	3	2	1	3	2
20	3	1	3	2	2	1	3
21	3	1	3	2	3	2	1
22	3	2	1	3	1	3	2
23	3	2	1	3	2	1	3
24	3	2	1	3	3	2	1
25	3	3	2	1	1	3	2
26	3	3	2	1	2	1	3
27	3	3	2	1	3	2	1

Figure A-5: Taguchi Method Was Applied to Narrow Down the Scope for Fluid Flow Simulation Runs. Features for Each Run Was Recorded in the Spreadsheet.

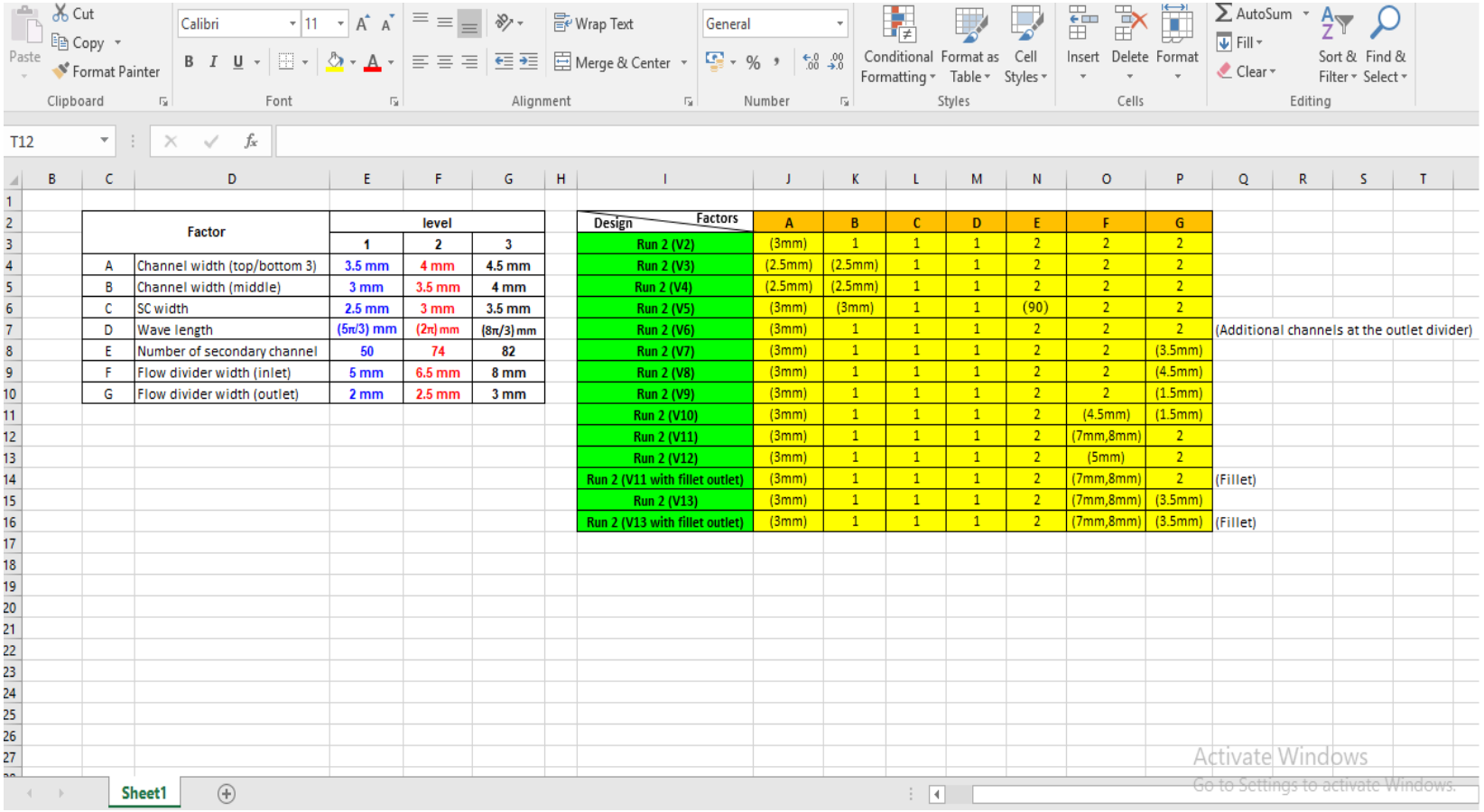

Factor		level		
		1	2	3
A	Channel width (top/bottom 3)	3.5 mm	4 mm	4.5 mm
B	Channel width (middle)	3 mm	3.5 mm	4 mm
C	SC width	2.5 mm	3 mm	3.5 mm
D	Wave length	(5π/3) mm	(2π) mm	(8π/3) mm
E	Number of secondary channel	50	74	82
F	Flow divider width (inlet)	5 mm	6.5 mm	8 mm
G	Flow divider width (outlet)	2 mm	2.5 mm	3 mm

Design \ Factors	A	B	C	D	E	F	G	
Run 2 (V2)	(3mm)	1	1	1	2	2	2	
Run 2 (V3)	(2.5mm)	(2.5mm)	1	1	2	2	2	
Run 2 (V4)	(2.5mm)	(2.5mm)	1	1	2	2	2	
Run 2 (V5)	(3mm)	(3mm)	1	1	(90)	2	2	
Run 2 (V6)	(3mm)	1	1	1	2	2	2	(Additional channels at the outlet divider)
Run 2 (V7)	(3mm)	1	1	1	2	2	(3.5mm)	
Run 2 (V8)	(3mm)	1	1	1	2	2	(4.5mm)	
Run 2 (V9)	(3mm)	1	1	1	2	2	(1.5mm)	
Run 2 (V10)	(3mm)	1	1	1	2	(4.5mm)	(1.5mm)	
Run 2 (V11)	(3mm)	1	1	1	2	(7mm,8mm)	2	
Run 2 (V12)	(3mm)	1	1	1	2	(5mm)	2	
Run 2 (V11 with fillet outlet)	(3mm)	1	1	1	2	(7mm,8mm)	2	(Fillet)
Run 2 (V13)	(3mm)	1	1	1	2	(7mm,8mm)	(3.5mm)	
Run 2 (V13 with fillet outlet)	(3mm)	1	1	1	2	(7mm,8mm)	(3.5mm)	(Fillet)

Figure A-6: The Second Part of the Simulation Runs Focused on Manipulating the Features of Design 2 in Different Versions (V), Since the Result from Design 2 Was the Closest to the Targeted Temperature Value.

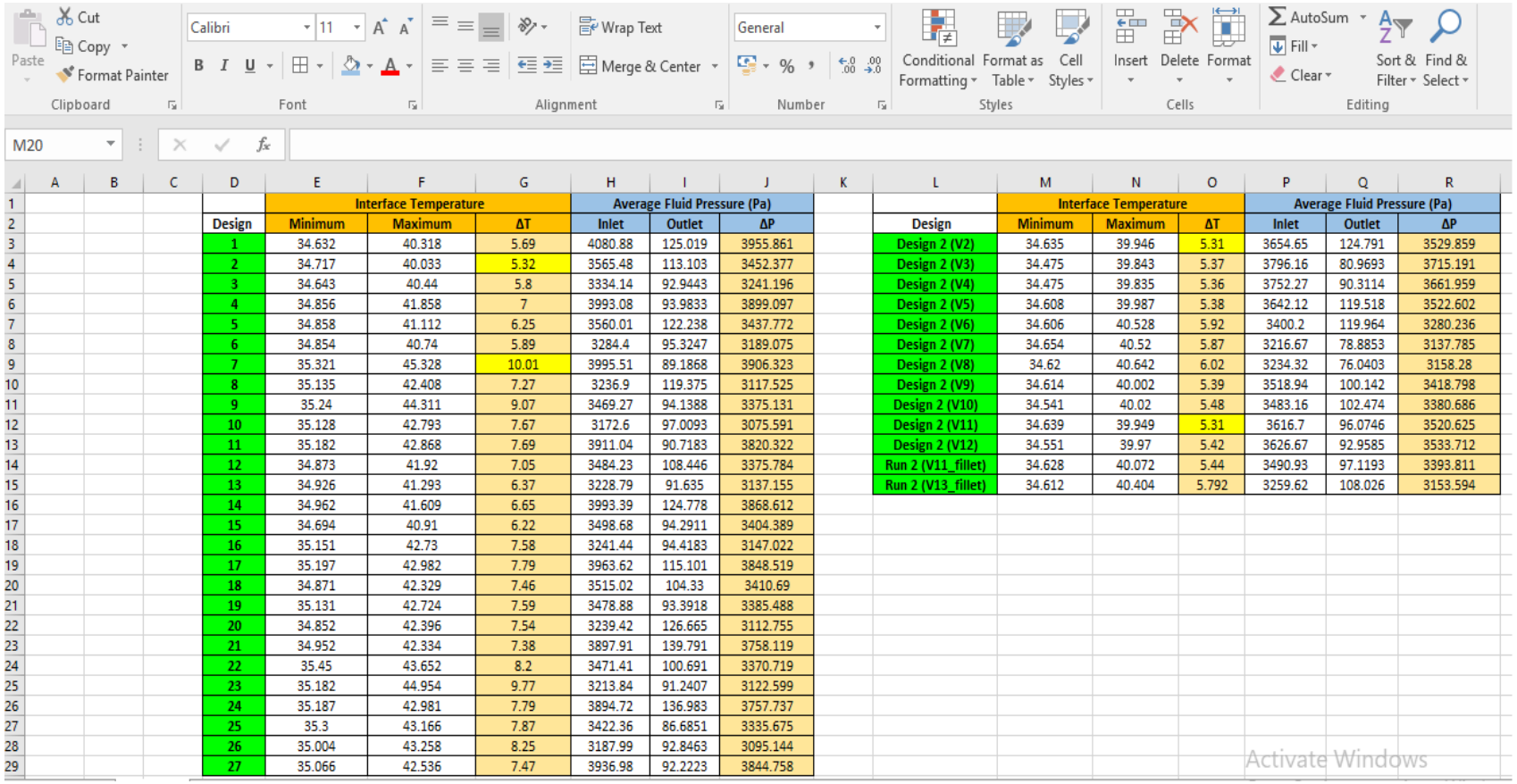

Design	Interface Temperature			Average Fluid Pressure (Pa)		
	Minimum	Maximum	ΔT	Inlet	Outlet	ΔP
1	34.632	40.318	5.69	4080.88	125.019	3955.861
2	34.717	40.033	5.32	3565.48	113.103	3452.377
3	34.643	40.44	5.8	3334.14	92.9443	3241.196
4	34.856	41.858	7	3993.08	93.9833	3899.097
5	34.858	41.112	6.25	3560.01	122.238	3437.772
6	34.854	40.74	5.89	3284.4	95.3247	3189.075
7	35.321	45.328	10.01	3995.51	89.1868	3906.323
8	35.135	42.408	7.27	3236.9	119.375	3117.525
9	35.24	44.311	9.07	3469.27	94.1388	3375.131
10	35.128	42.793	7.67	3172.6	97.0093	3075.591
11	35.182	42.868	7.69	3911.04	90.7183	3820.322
12	34.873	41.92	7.05	3484.23	108.446	3375.784
13	34.926	41.293	6.37	3228.79	91.635	3137.155
14	34.962	41.609	6.65	3993.39	124.778	3868.612
15	34.694	40.91	6.22	3498.68	94.2911	3404.389
16	35.151	42.73	7.58	3241.44	94.4183	3147.022
17	35.197	42.982	7.79	3963.62	115.101	3848.519
18	34.871	42.329	7.46	3515.02	104.33	3410.69
19	35.131	42.724	7.59	3478.88	93.3918	3385.488
20	34.852	42.396	7.54	3239.42	126.665	3112.755
21	34.952	42.334	7.38	3897.91	139.791	3758.119
22	35.45	43.652	8.2	3471.41	100.691	3370.719
23	35.182	44.954	9.77	3213.84	91.2407	3122.599
24	35.187	42.981	7.79	3894.72	136.983	3757.737
25	35.3	43.166	7.87	3422.36	86.6851	3335.675
26	35.004	43.258	8.25	3187.99	92.8463	3095.144
27	35.066	42.536	7.47	3936.98	92.2223	3844.758

Design	Interface Temperature			Average Fluid Pressure (Pa)		
	Minimum	Maximum	ΔT	Inlet	Outlet	ΔP
Design 2 (V2)	34.635	39.946	5.31	3654.65	124.791	3529.859
Design 2 (V3)	34.475	39.843	5.37	3796.16	80.9693	3715.191
Design 2 (V4)	34.475	39.835	5.36	3752.27	90.3114	3661.959
Design 2 (V5)	34.608	39.987	5.38	3642.12	119.518	3522.602
Design 2 (V6)	34.606	40.528	5.92	3400.2	119.964	3280.236
Design 2 (V7)	34.654	40.52	5.87	3216.67	78.8853	3137.785
Design 2 (V8)	34.62	40.642	6.02	3234.32	76.0403	3158.28
Design 2 (V9)	34.614	40.002	5.39	3518.94	100.142	3418.798
Design 2 (V10)	34.541	40.02	5.48	3483.16	102.474	3380.686
Design 2 (V11)	34.639	39.949	5.31	3616.7	96.0746	3520.625
Design 2 (V12)	34.551	39.97	5.42	3626.67	92.9585	3533.712
Run 2 (V11_fillet)	34.628	40.072	5.44	3490.93	97.1193	3393.811
Run 2 (V13_fillet)	34.612	40.404	5.792	3259.62	108.026	3153.594

Figure A-7: Simulation Results with Fluid Mass Flow Rate of 50 g/s Were Recorded in the Spreadsheet. Design 2 (V2) was then Chosen as the Finalised Design.

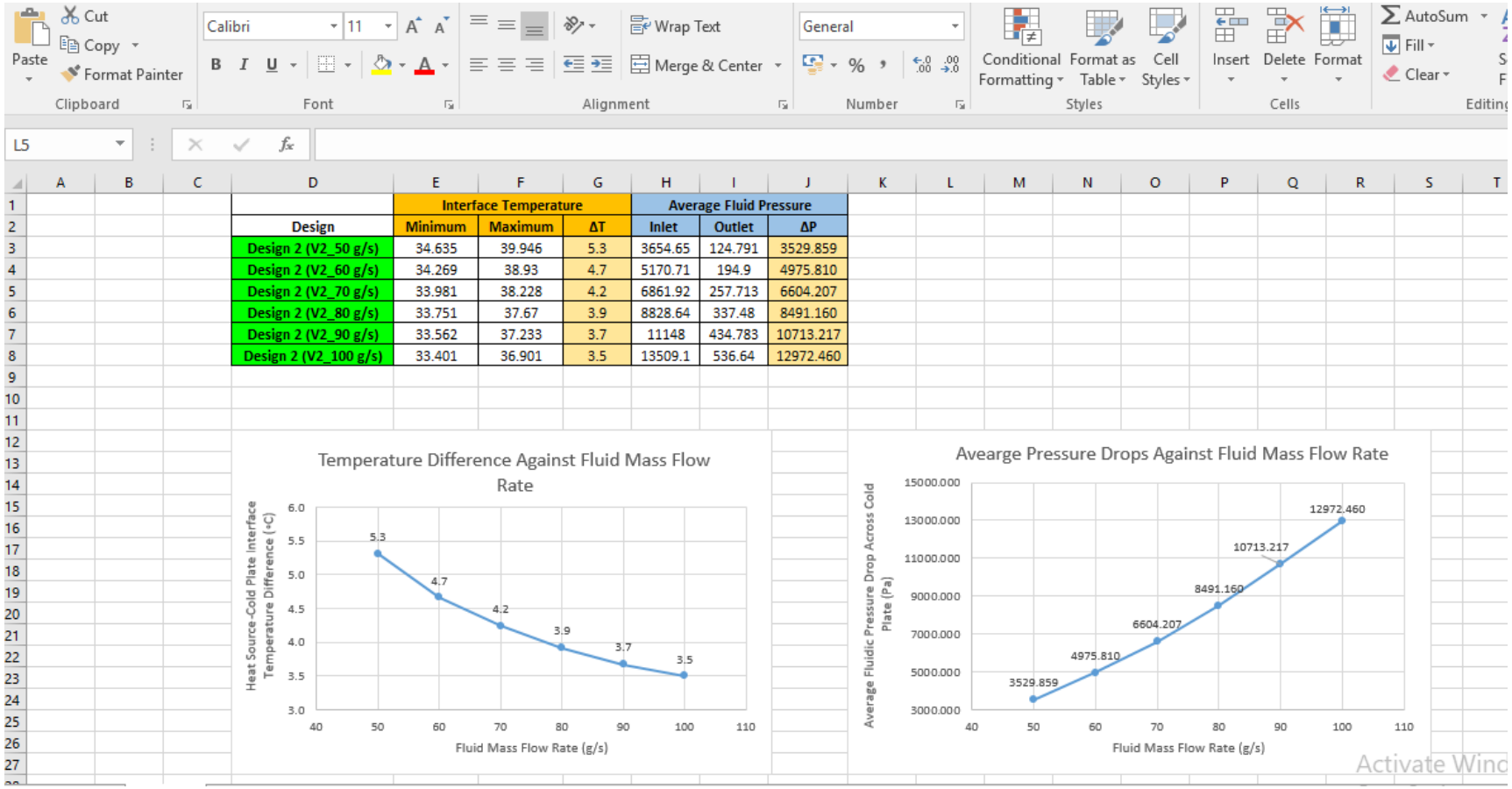

Design	Interface Temperature			Average Fluid Pressure		
	Minimum	Maximum	ΔT	Inlet	Outlet	ΔP
Design 2 (V2_50 g/s)	34.635	39.946	5.3	3654.65	124.791	3529.859
Design 2 (V2_60 g/s)	34.269	38.93	4.7	5170.71	194.9	4975.810
Design 2 (V2_70 g/s)	33.981	38.228	4.2	6861.92	257.713	6604.207
Design 2 (V2_80 g/s)	33.751	37.67	3.9	8828.64	337.48	8491.160
Design 2 (V2_90 g/s)	33.562	37.233	3.7	11148	434.783	10713.217
Design 2 (V2_100 g/s)	33.401	36.901	3.5	13509.1	536.64	12972.460

Figure A-8: Simulation Results on the Chosen Design with Various Fluid Mass Flow Rates for Verification Purpose.

APPENDIX C: Temperature Contours for Project Part 2

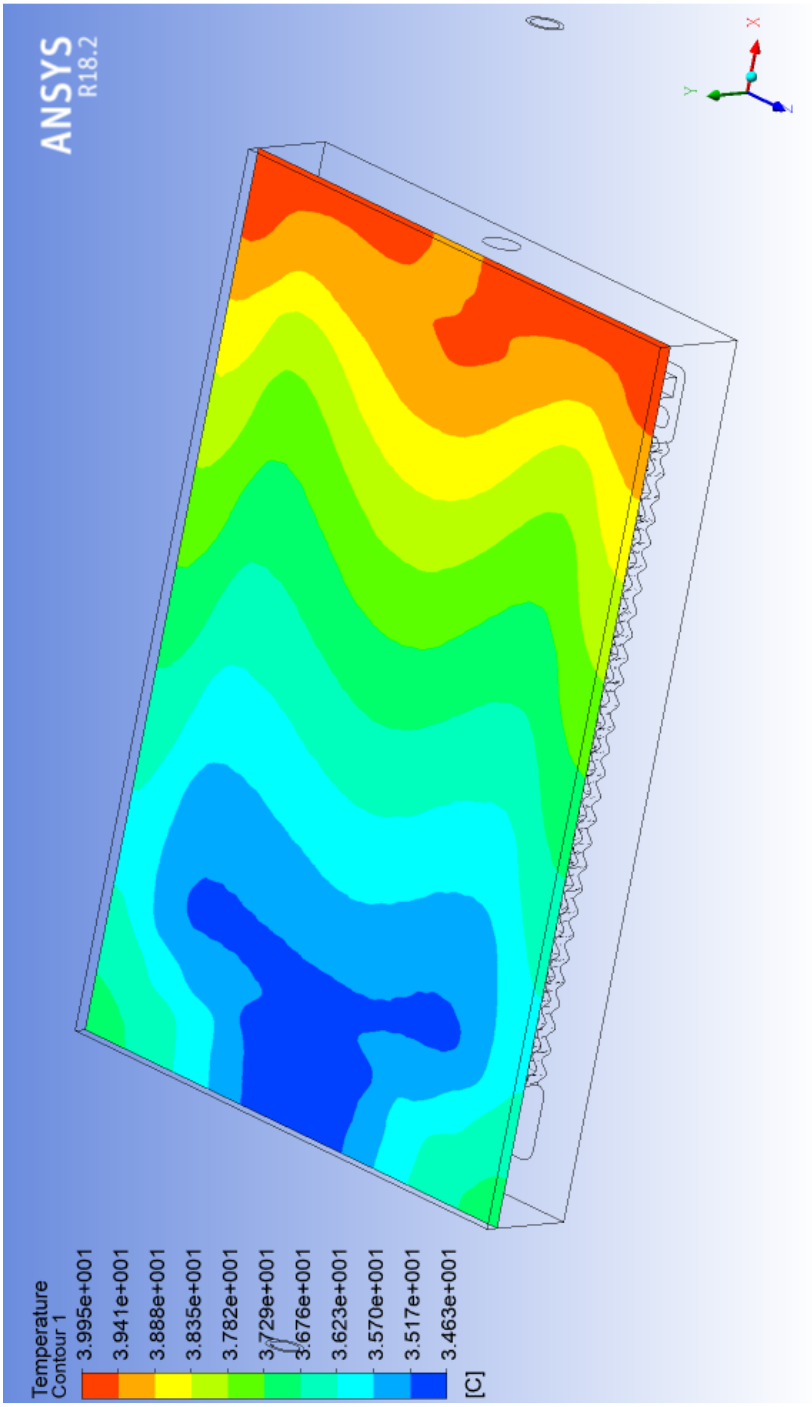

Figure A-9: Temperature Contours at the Heat Source-Cold Plate Interface for Fluid Mass Flow Rate of 50 g/s.

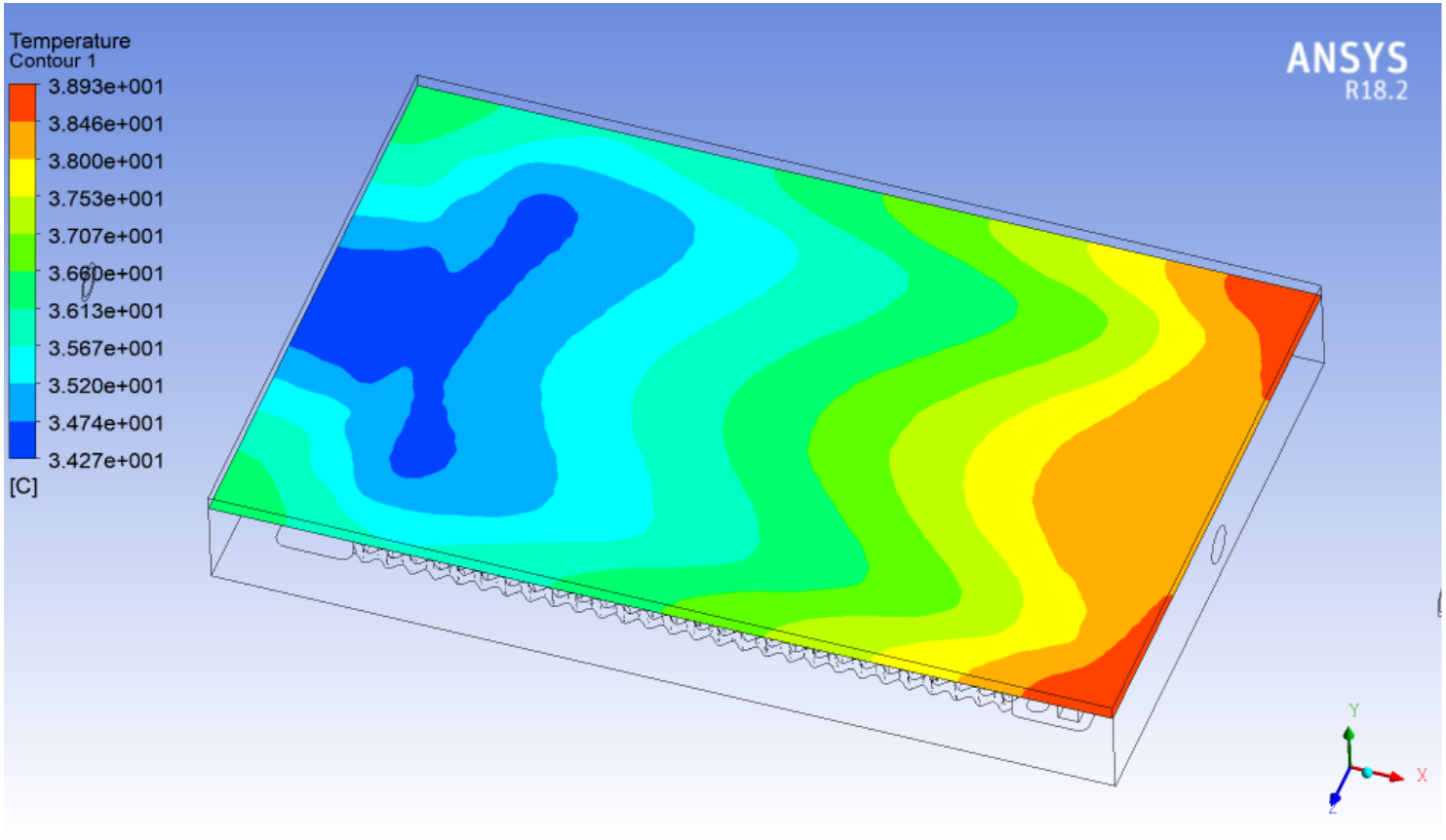

Figure A-10: Temperature Contours at the Heat Source-Cold Plate Interface for Fluid Mass Flow Rate of 60 g/s.

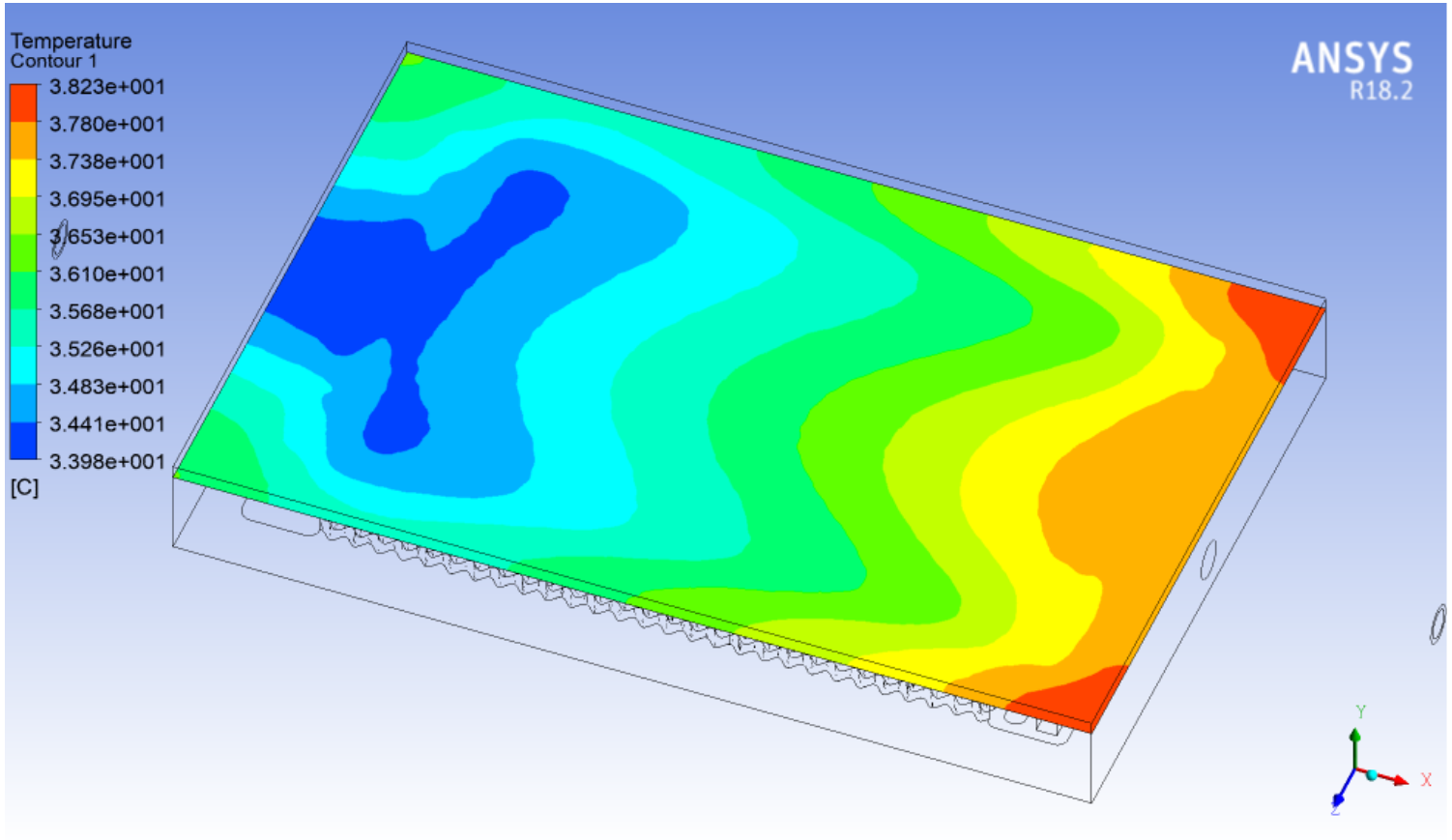

Figure A-11: Temperature Contours at the Heat Source-Cold Plate Interface for Fluid Mass Flow Rate of 70 g/s.

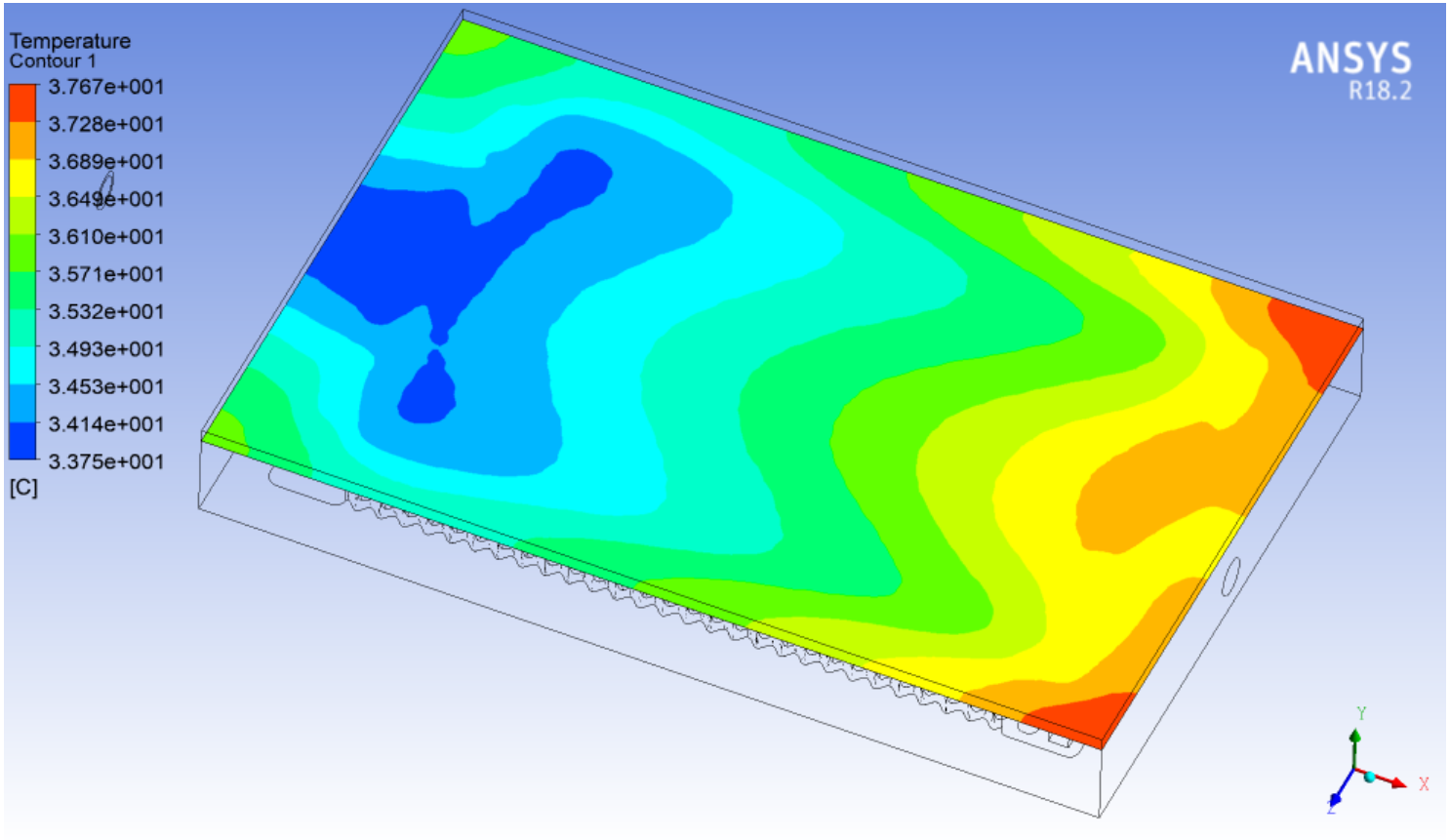

Figure A-12: Temperature Contours at the Heat Source-Cold Plate Interface for Fluid Mass Flow Rate of 80 g/s.

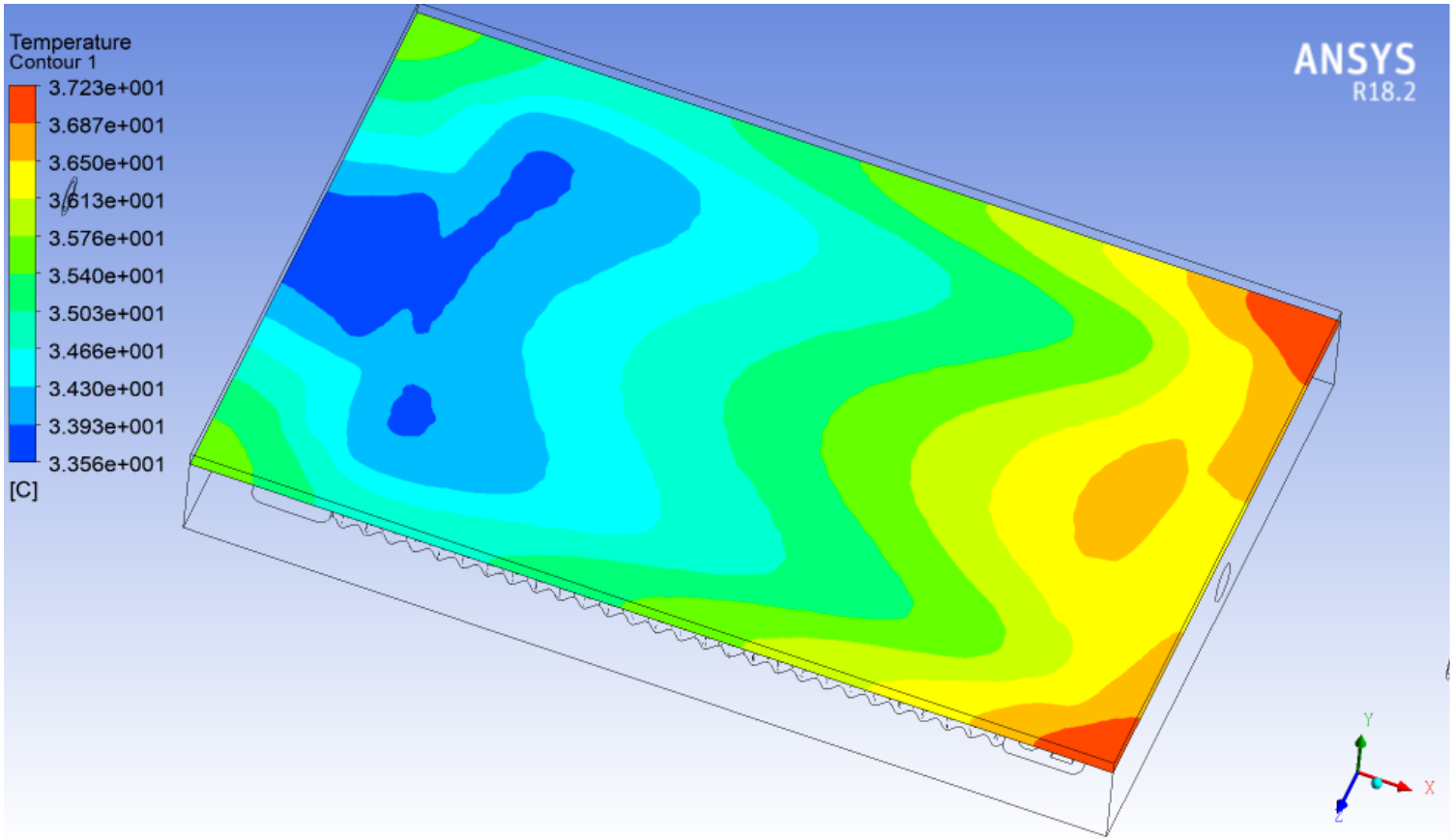

Figure A-13: Temperature Contours at the Heat Source-Cold Plate Interface for Fluid Mass Flow Rate of 90 g/s.

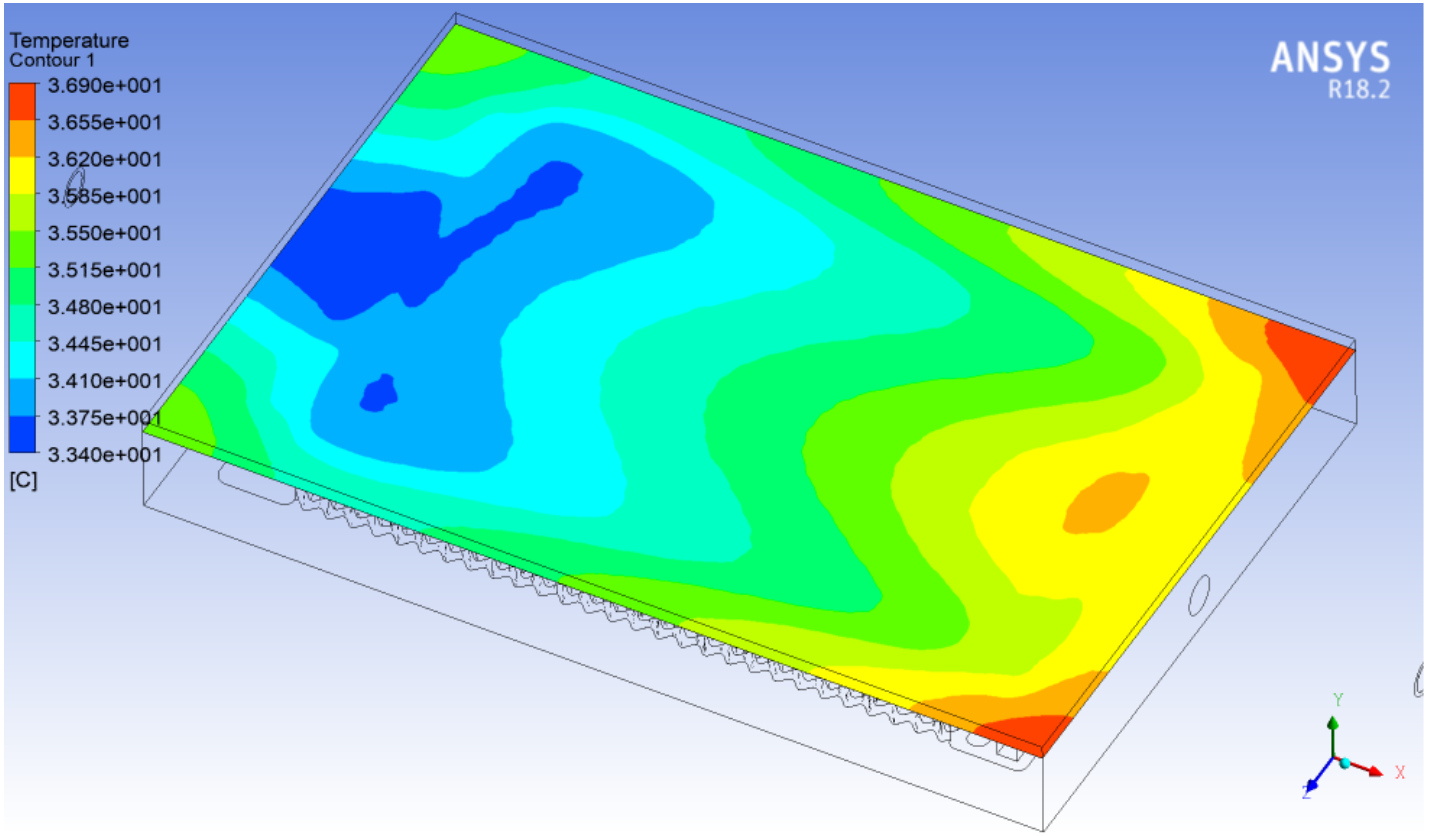

Figure A-14: Temperature Contours at the Heat Source-Cold Plate Interface for Fluid Mass Flow Rate of 100 g/s.

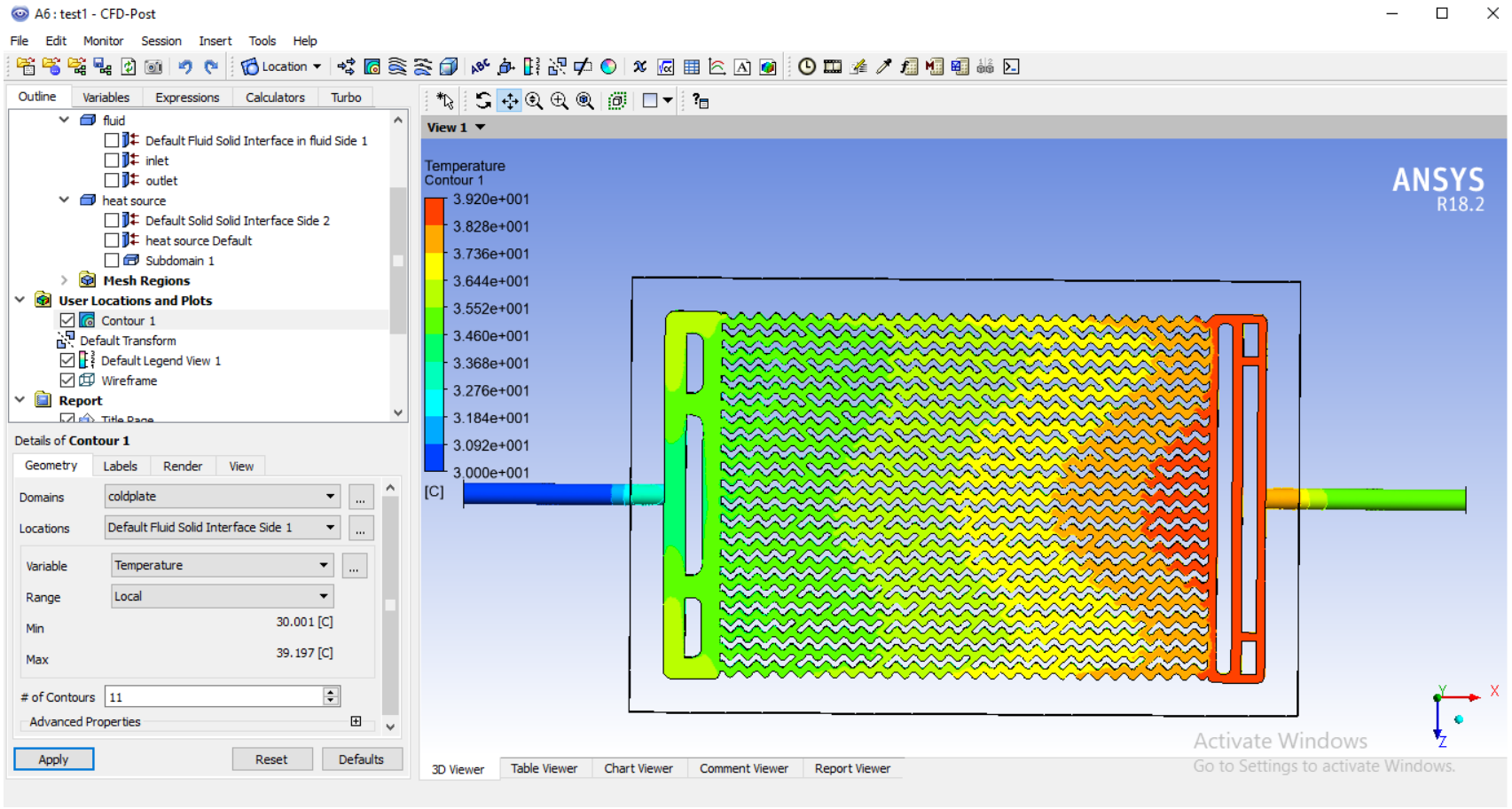

Figure A-15: Temperature Contour at the Fluid-Cold Plate Interface for Fluid Mass Flow Rate of 50 g/s.

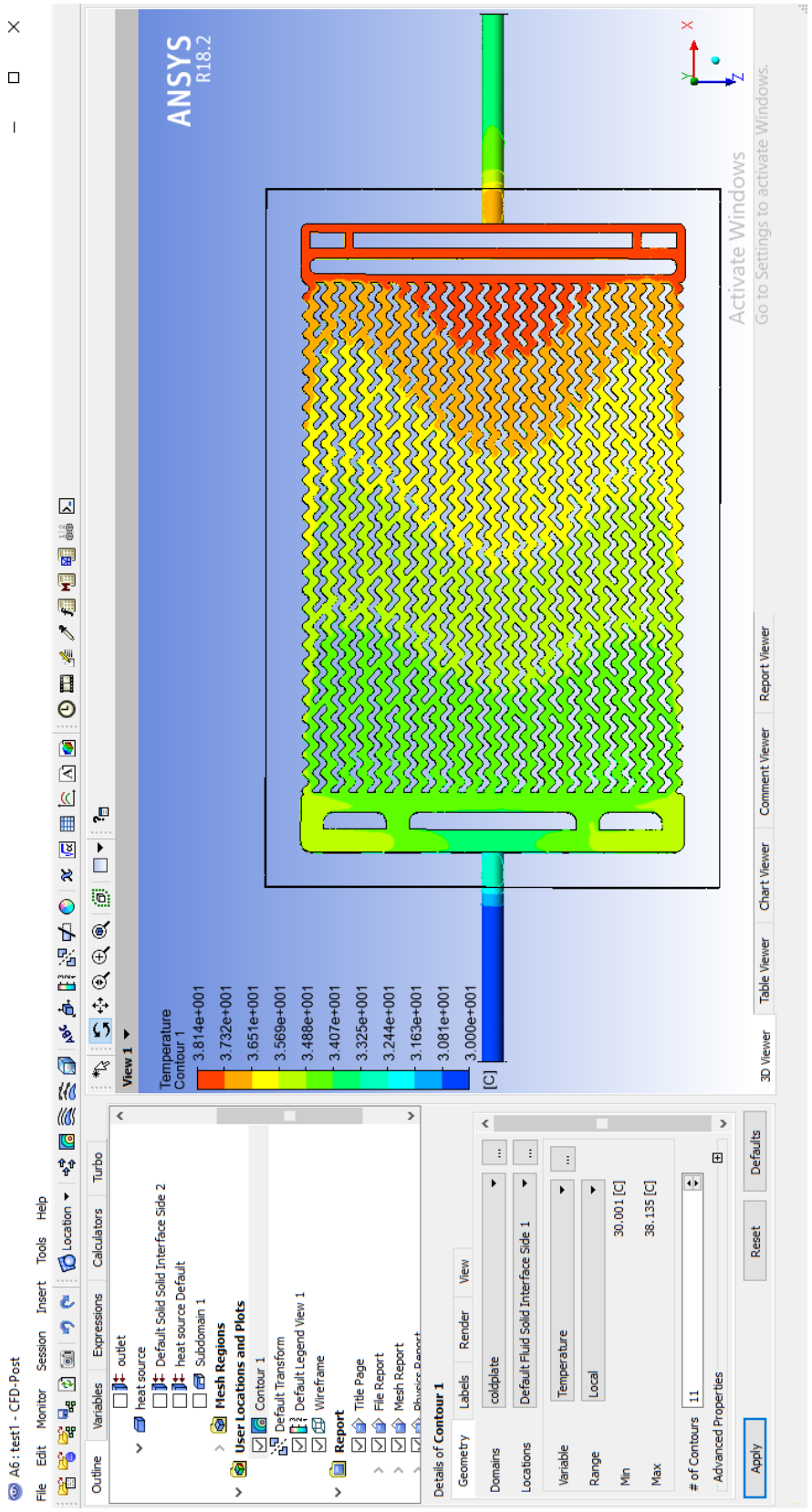

Figure A-16: Temperature Contour at the Fluid-Cold Plate Interface for Fluid Mass Flow Rate of 60 g/s.

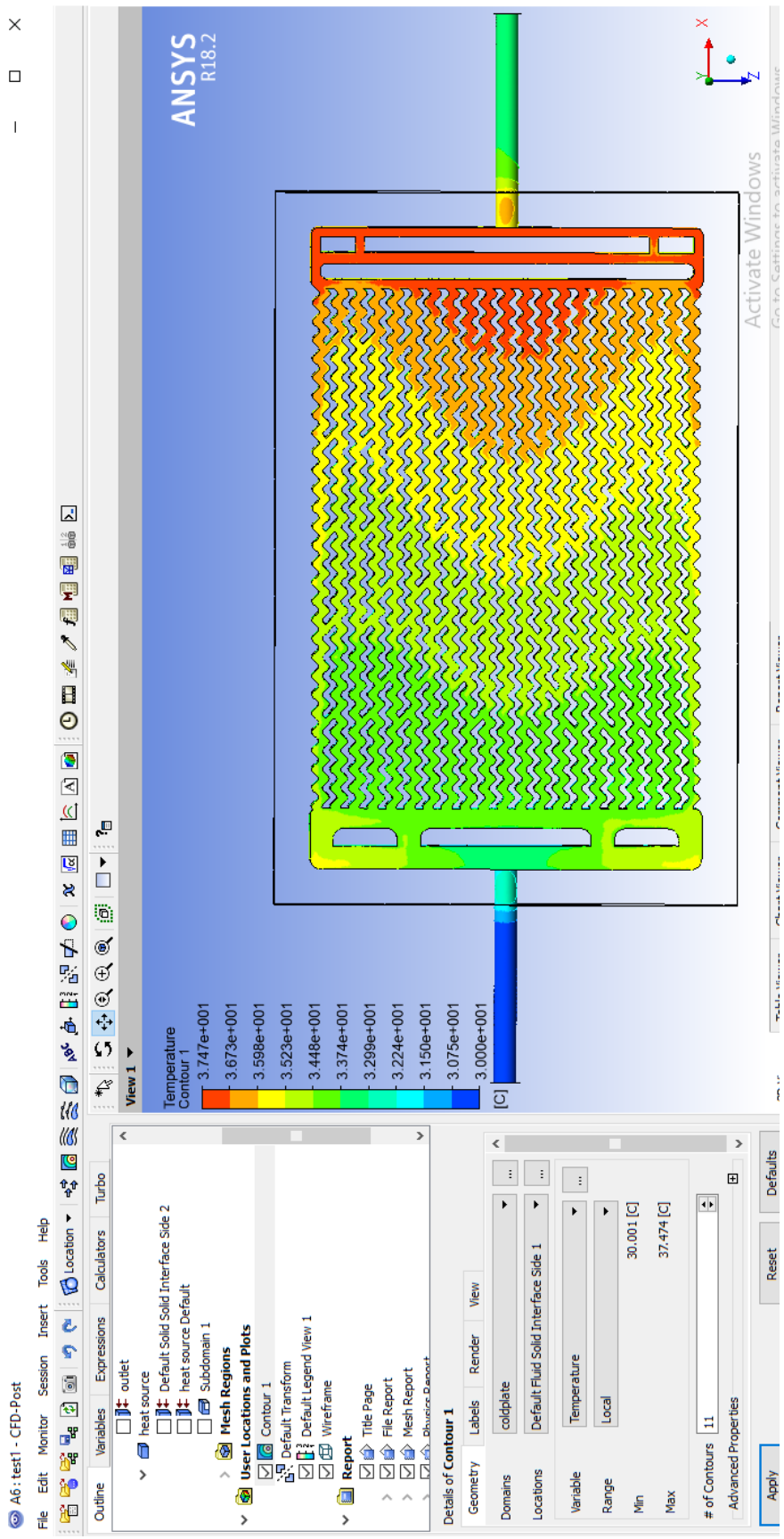

Figure A-17: Temperature Contour at the Fluid-Cold Plate Interface for Fluid Mass Flow Rate of 70 g/s.

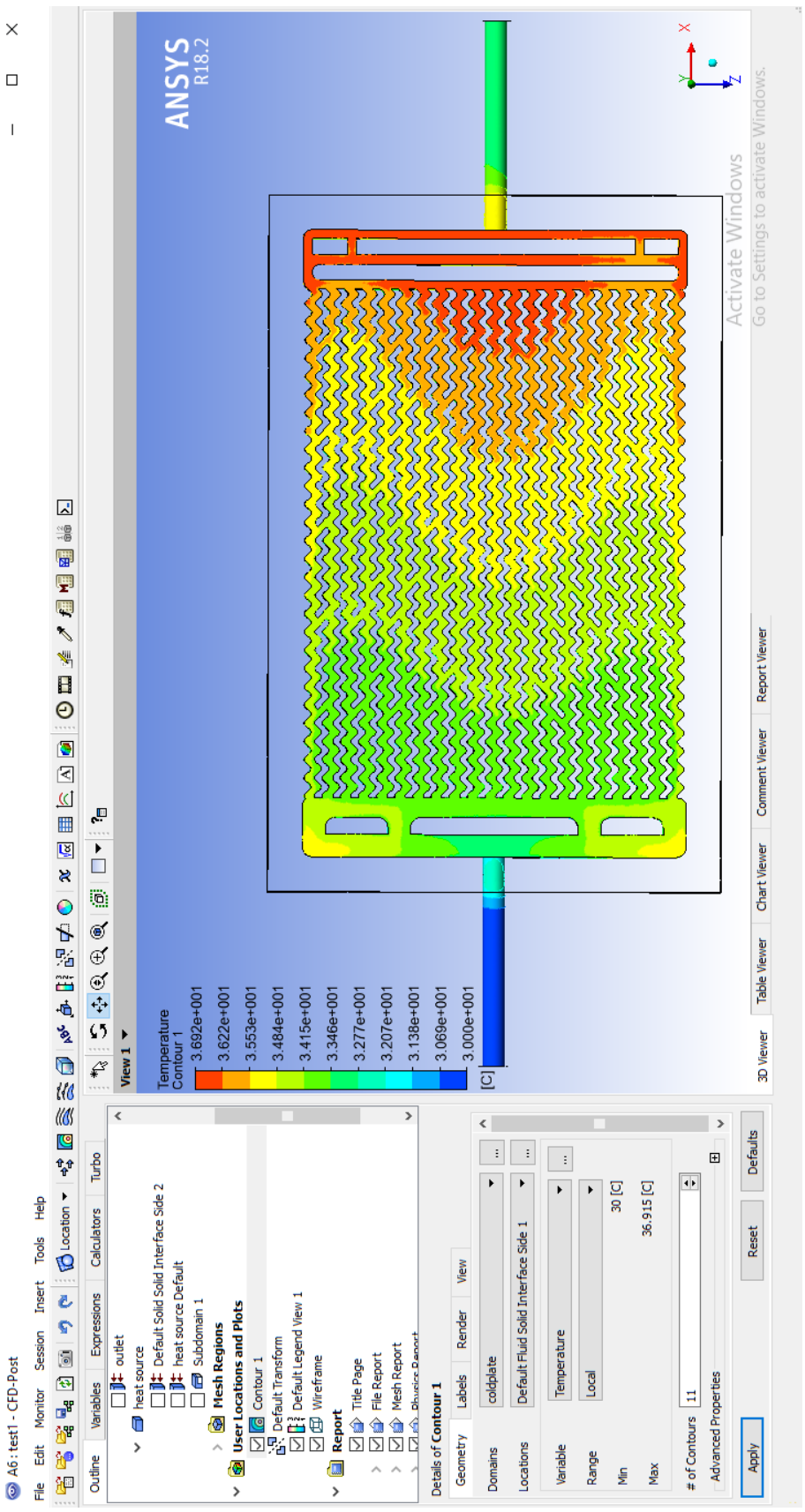

Figure A-18: Temperature Contour at the Fluid-Cold Plate Interface for Fluid Mass Flow Rate of 80 g/s.

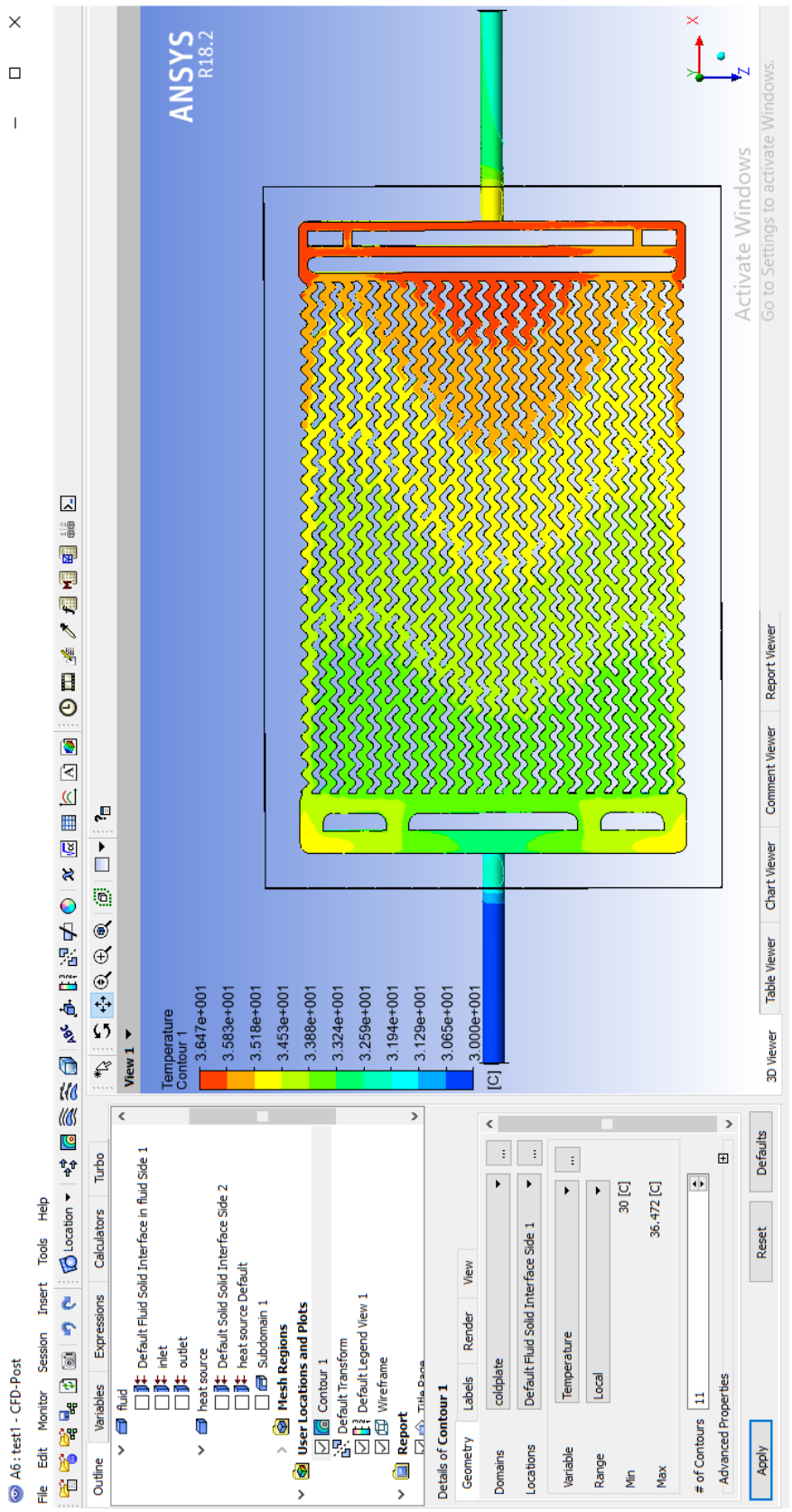

Figure A-19: Temperature Contour at the Fluid-Cold Plate Interface for Fluid Mass Flow Rate of 90 g/s.

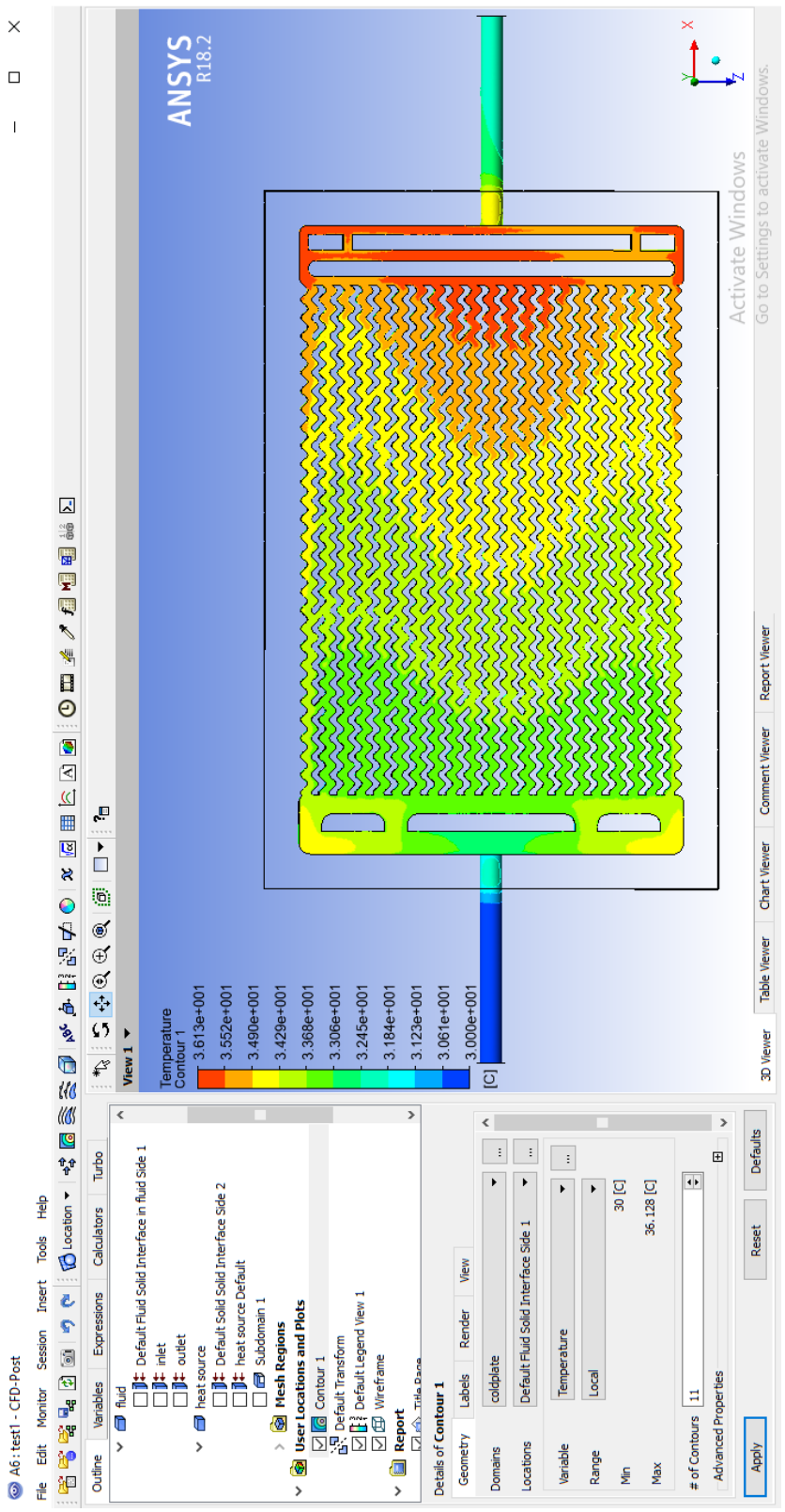

Figure A-20: Temperature Contour at the Fluid-Cold Plate Interface for Fluid Mass Flow Rate of 100 g/s.

APPENDIX D: Milling Toolpaths

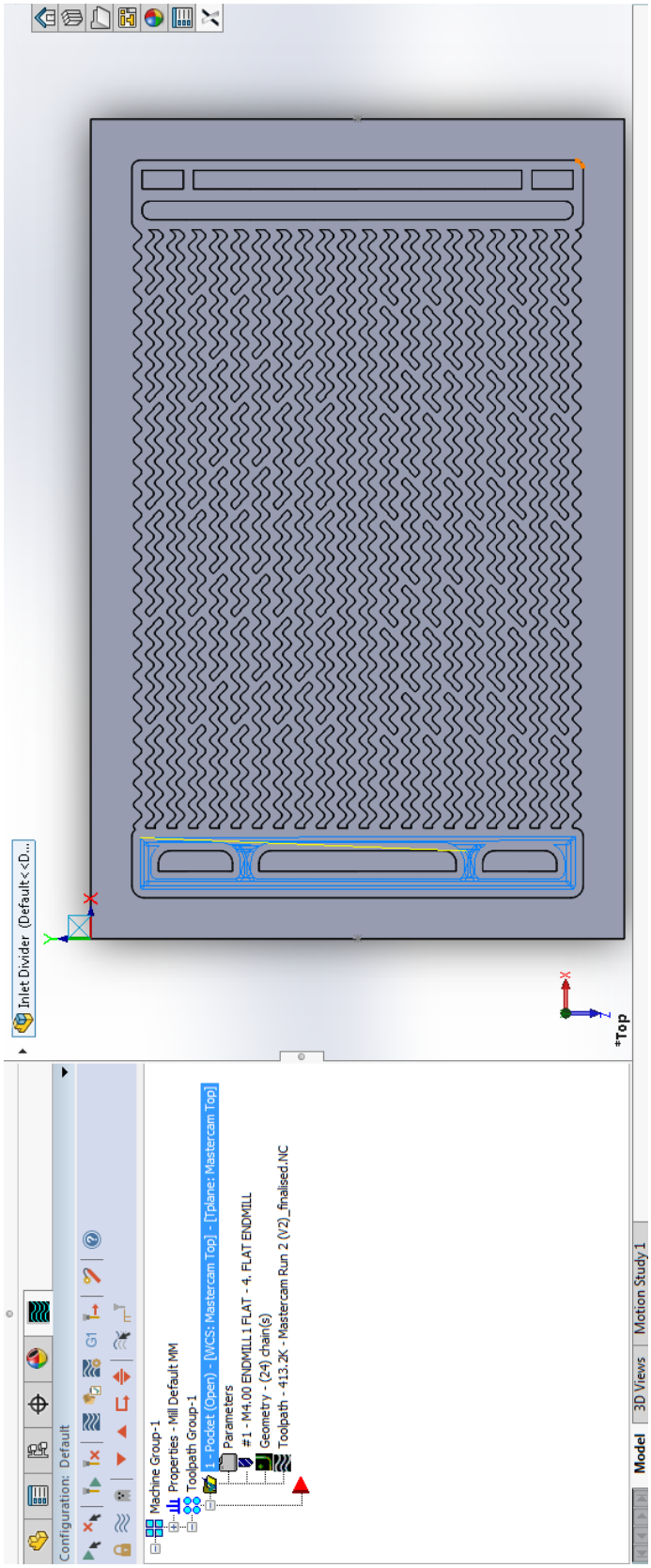

Figure A-21: Milling Toolpaths of Inlet Divider as Generated by MasterCAM.

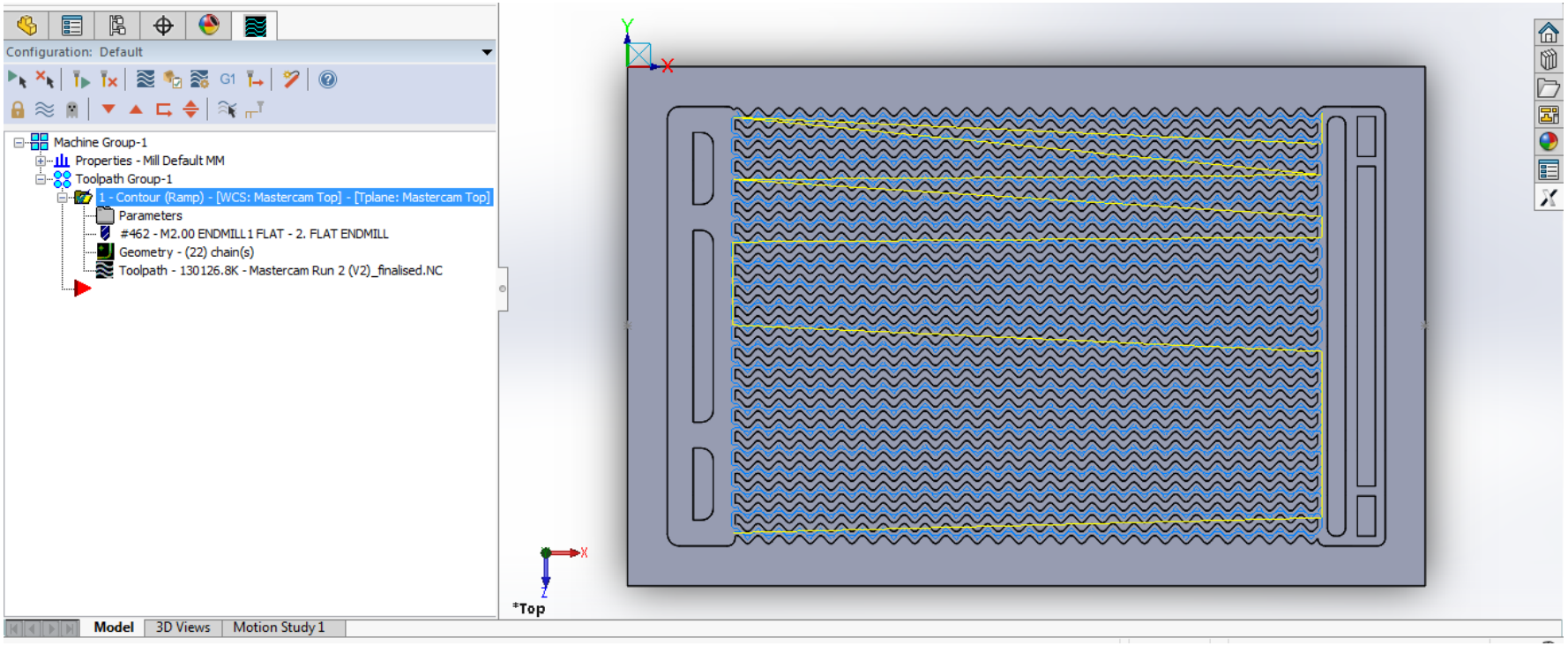

Figure A-22: Milling Toolpaths of Wavy Channels as Generated by MasterCAM.

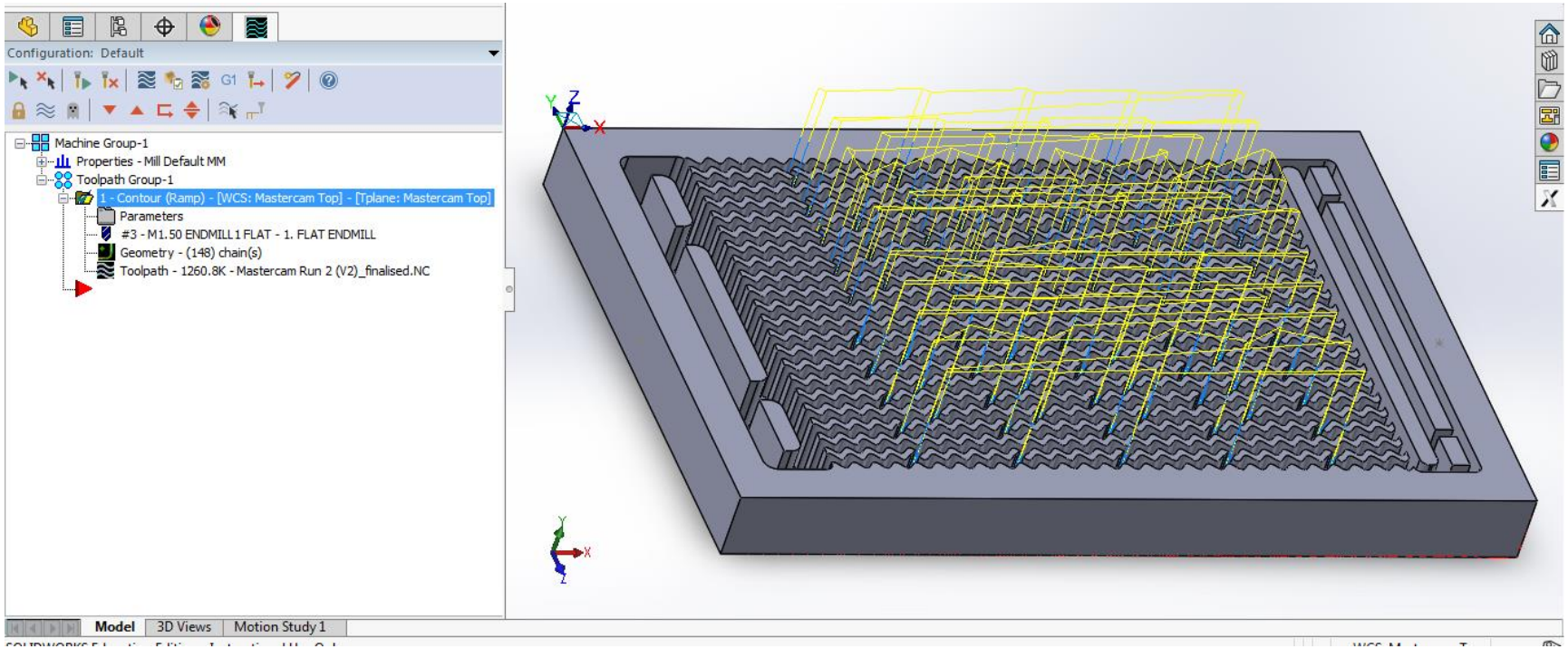

Figure A-23: Milling Toolpaths of Secondary Channels as Generated by MasterCAM.

APPENDIX E: Engineering Drawing

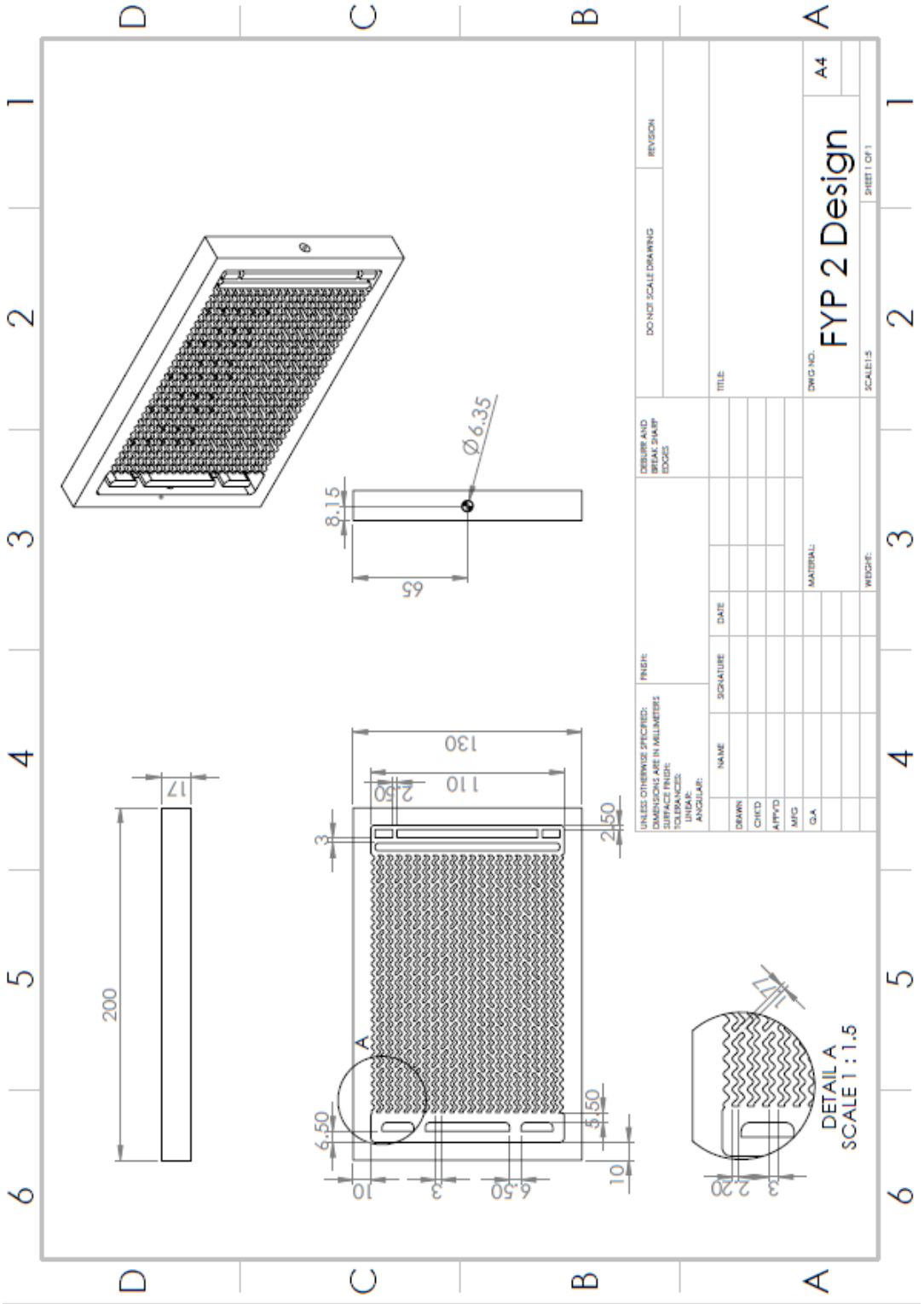

Figure A-24: Engineering Drawing of the Optimised Wavy Channels Cold Plate.

APPENDIX F: Prototype

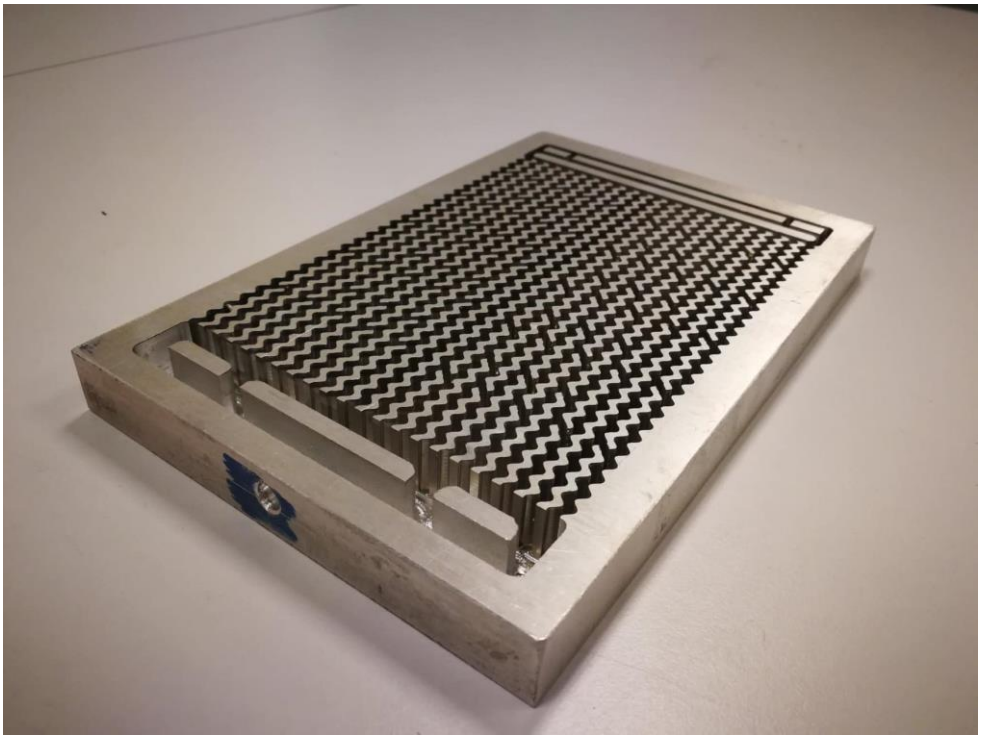

Figure A-25: Fabricated Prototype of Wavy Channels Cold Plate (View 1).

Figure A-26: Fabricated Prototype of Wavy Channels Cold Plate (View 2).